Gravity Studies of Two Silicic Volcanic Complexes

Thesis

UNRESTRICTED

Gravity studies of two silicic volcanic complexes

A thesis presented for the degree of
Master of Philosophy

David Alexander Giles Nowell

B.Sc. (Hons) Liverpool University

Department of Earth Sciences
The Open University
Milton Keynes

November 1994

Date of submission : 7 th November 1994

Date of award : 10 th January 1995

ProQuest LLC.
789 East Eisenhower Parkway
P.O. Box 1346
Ann Arbor, MI 48106 – 1346

Abstract

Gravity data from two silicic volcanic complexes, the Valles Caldera, New Mexico and the Breiddalur central volcano, Iceland, have been modelled and interpreted.

The Rubio Volcano (4 Ma to 1.5 Ma) in the area of the Toledo Embayment in the Jemez Mountains formed the centre of a depression which grew southwestwards and then collapsed to form the Toledo Caldera (1.45 Ma) and then the Valles Caldera (1.12 Ma). Published gravity data covering the Valles Caldera are used to generate three profiles across the caldera. Models in 2½D show a combination of chaotic collapse and a trapdoor caldera up to 3,600 m deep, hinged to the west with some faulted basement blocks. The maximum depth of tuffs filling the caldera are up to 1,000 m less than in previously published models, although in other places the tuffs are found to be over 1,000 m thicker.

Gravity data from Breiddalur in southeastern Iceland indicate that the partly silicic, andesitic volcano was about 2,000 m thick, with a 500 m thick silicic core and that at least two other buried silicic centres may have developed during the volcano's history.

The generation and storage of silicic magmas in these contrasting volcanic provinces is considered. Much more basic material is required at Valles than at Breiddalur to produce the inferred volumes of silicic material. The consequences of this difference are discussed.

Contents

List of Figures

List of Tables

Acknowledgements

This project was initiated by the late Geoff Brown who died when Mount Galeras volcano, Colombia, erupted on 14th of January 1993. He and Hazel Rymer are thanked for their support and encouragement before and during my illness, without them this thesis would not have been possible. Pal Imsland is thanked for helping with the Icelandic fieldwork and gathering the samples of rock from the Breiddalur area. Academic computing services are thanked for helping to sort out my computing problems. I would like to thank the following people for their support in Milton Keynes, Josanne Cutajar, David Stevenson and especially Christopher Pym and Liz Keller. Finally I must thank my parents for their support during this difficult time.

Gravity studies of two silicic volcanic complexes.

1. Introduction

Gravity data from two contrasting silicic volcanoes were analysed using a 2½D forward modelling program GRAVMAG, designed by the British Geological Survey. The first volcano, Valles Caldera in the Jemez Mountains, is situated in rifted continental crust; while the second, Breiddalur central volcano is located on thickened oceanic crust.

Valles Caldera in North America is located on an offset of the Rio Grand Rift in New Mexico and represents the culmination of volcanic activity in the Jemez Mountains. The Rio Grand Rift developed as a result of stresses developed in the western half of the North American plate by the change from eastward subduction of the Farallon and Cocos plates to dextral movement of the over riding plate relative to the Pacific plate. The halting of subduction beneath western North America led to the collapse of mountains and to the development of the Basin and Range and the Rio Grande Rift as the continental crust relaxed and spread out. Within the Rio Grande Rift basic volcanism developed as rifting occurred: the Jemez Mountains formed within the rift and the erupted lavas have become gradually more silicic with time. This final phase led to the development of caldera collapse on at least two occasions, first the Toledo Caldera and then later the Valles Caldera. Data from a gravity survey (Segar 1974) in the Valles Caldera were used to model three 2½D gravity profiles across the area. These show up to 3,600 m thickness of low density silicic rocks filling a trap door caldera.

The location of Iceland on the Mid Atlantic Ridge and its relationship with normal mid ocean-crust is discussed. Iceland can be regarded as an area of over-thickened oceanic crust due to the presence of a hot spot beneath the area. The Breiddalur central volcano developed in this environment and consists of acid, intermediate and basic lavas about 2,000 m thick. Gravity data from the Breiddalur area, collected by G.C. Brown and H. Rymer, were used to develop four 2½D gravity models of profiles across the volcano. These profiles suggest that silicic rocks up to 1,200 m thick may be present in the area and that the volcano had more than one centre during its history.

The question of how basic magmatism results in silicic magmas other than by fractional crystallisation is discussed. The process involves basic magma heating crustal rocks until they melt producing silicic magma which then rises, often to the surface. The inputs of basic magma needed and the temperatures required to produce given volumes of silicic magmas are considered. Apart from fractional crystallisation the melting of crustal rocks by hot basic magma is also an important source of silicic material. The amount of silicic material generated depends on the type of country rock melted; the thickened oceanic crust below Breiddalur results in a far smaller volume of granitic magma than the continental crust below the Valles Caldera. This difference is quantified and considered in the text.

2. The tectonic framework of western North America.

2.1 Introduction.

To devise a tectonic framework, the western half of North America and surrounding offshore waters have been divided into regions, or units (Figure 1). The geological history of western North America in the Cenozoic and more importantly the last 20 million years has been determined by the sequence in which subduction has ended beneath the North American plate. Subduction has gradually been replaced along the western margin of the North American plate by dextral movement between the oceanic Pacific plate and the continental North American plate (Zoback et al. 1981). The timing of these events is important with regard to the collapse of the subduction arc mountain range and development of Basin and Range tectonics along the western margin of this continent. Many aspects of the tectonic evolution of western North America result from relaxation of the Lithosphere after the Farallon plate ceased to be subducted below the southern Rocky Mountains (Park 1988). The Basin and Range province was formed by back-arc spreading and crustal shearing which led to the rapid extension of the Basin and Range areas by over a factor of two, as well as having a wider effect on the whole of western North America. The role of subducted fracture zones and the effects of rotation at the end of subduction beneath the continent in relation to the tectonic and volcanic history of these regions is discussed. The resulting clockwise rotation of the Colorado Plateau (Aldrich and Laughlin, 1984) and its border with the Great Plains to the east is a

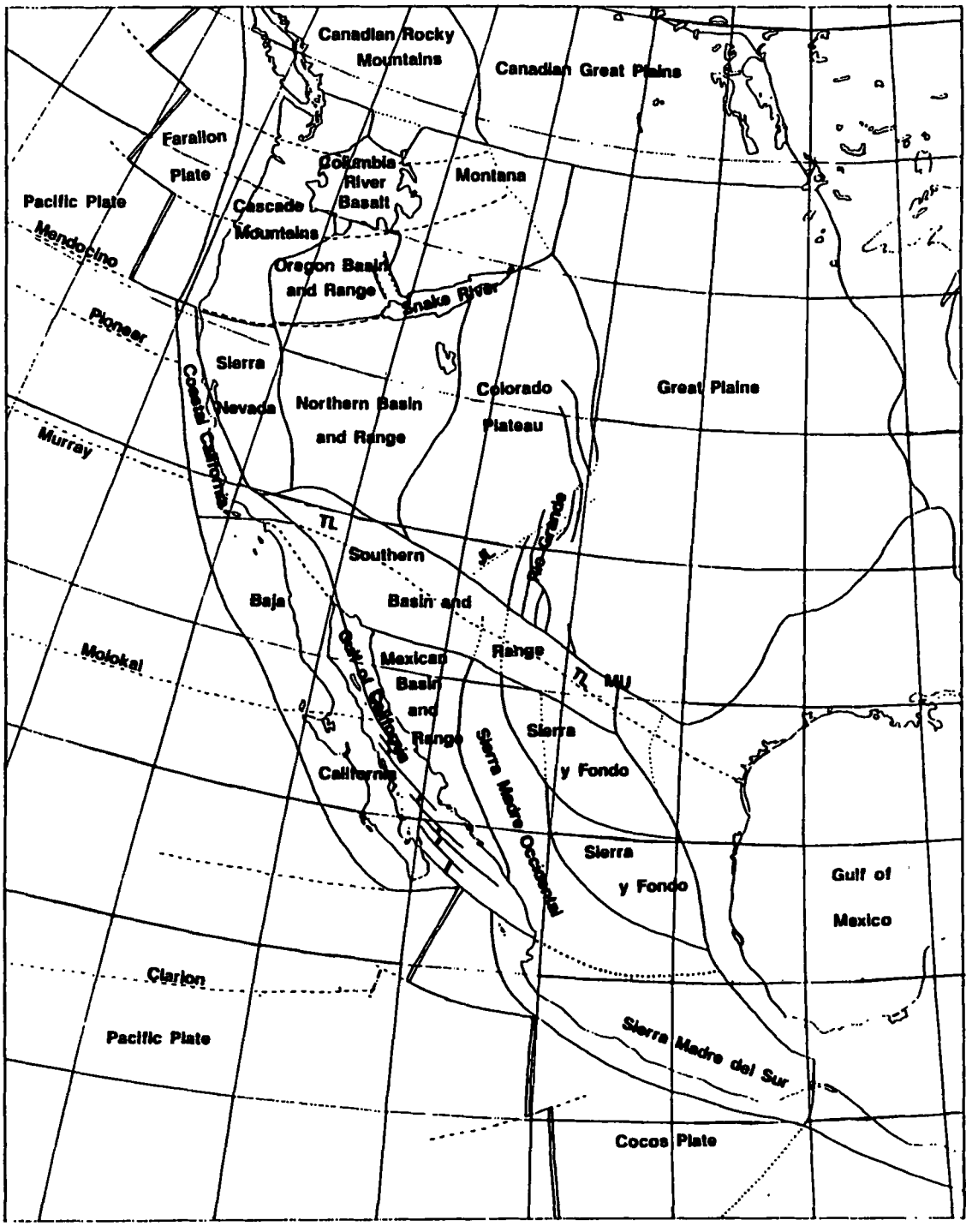

Figure 1. The tectonic framework of western North America. T.L. = Texas Lineament, M.U. = Marathon Uplift, J.L. = Jemez Lineament

central part of this, which has led to the development of the Rio Grande Rift along the southern half of this margin. The development of the Jemez Mountains volcanic field at the rift's intersection and offset along the Jemez Lineament in turn is smaller part of the overall tectonic framework of the Basin and Range area of North America.

2.2 The tectonic framework.

The units into which I have sub-divided the western part of the North American and surrounding plates (Figure 1), are grouped into five main areas which are described in the following paragraphs.

The Colorado Plateau forms a relatively stable area between the Basin and Range provinces to the west and south and the stable Montana area to the north and the Great Plains to the east. The Great Plains form the stable area southwards from Canada to the east of the Rocky Mountains until the Edwards Plateau, Texas, in the south where the Texas Lineament Zone forms its southwestern border and the Gulf of Mexico its southeastern margin, the Mississippi River marks the eastern limit of this vast region.

Between the southern Colorado Plateau and the Great Plains, the Rio Grande Rift has developed. This rift is widest in the south of New Mexico as it runs into the southern Basin and Range region and narrows in a series of grabens and half grabens into Colorado. Along the northern margin of the two regions the Rio Grande Rift is replaced by the compressional features of the Front Range and in Wyoming, to the north, the Laramie Range and Bighorn Mountains.

The Basin and Range is the country between the Colorado Plateau and Sierra Madre Occidental in the east and a narrow (less than 300km wide) coastal strip along the margin of the Pacific Ocean. The northern-most Basin and Range comprises the Oregon region and the Columbia River Basalts region to the north. The Northern Basin and Range is to the south of Oregon and the Snake River Plain, this area of the Northern Basin and Range is also known as the Great Basin. The Southern Basin and Range straddles the Texas Lineament, which runs from near Los Angeles in the west to the Gulf of Mexico in the east. The region is about 200 km to 400 km wide and its southwestern margin may include the northern most part of Baja California along with areas along a line from the northern end of the Gulf of California to the Rio Grande river to the south of the Marathon uplift, Texas, in the east. The Mexican Basin and Range to the south is wedged between the Gulf of California to the west and the Sierra Madre Occidental to the east and runs parallel to Baja California.

For this study the rest of Mexico, can be divided into four regions (Figure 1). The Sierra Madre Occidental runs south from the southern Basin and Range, between the Mexican Basin and Range to the west and the Sierra y Fondo to the east, down to the Trans-Mexican volcanic belt. Between the Sierra del Carmen and Sierra Madre Oriental to the east and the Sierra Madre Occidental lies the country which I have referred to as the Sierra y Fondo. This has been given the Spanish name for Basin and Range because on geological maps of North America the region resembles the Basin and Range to the northwest. It consists of a series of linear fault bounded blocks separated by valleys filled with resent sediments. The Sierra Madre

del Sur runs along the margin of the Middle American Trench as far west as the Gulf of Tehuantepec south of the Trans Mexican volcanic belt. The Gulf of Mexico includes the land to the east of the Sierra Madre Oriental and the land covered by Cenozoic sediments to the southeast of the Great Plains. The Gulf of Mexico is a basin which is centred on the Sigbee Deep (over 4,000 m) between the Mississippi delta and the Yucatan peninsula.

Canada is divided between the Canadian Rocky Mountains to the west, which include a northern part of Washington state down to the Columbia River Basalts region, and the Canadian Great Plains which are a northern extension of the U.S. Great Plains and extend as far west as Lake Winnipeg. The Montana region is comprised of the western half of the state of Montana and neighbouring Idaho north of the Snake River Plain. The Columbia River Basalts region covers large areas of southern Washington state and northern Oregon. The Snake River Plain runs along the Snake River from the southeastern Oregon Basin and Range to Yellowstone National Park in the east.

2.3 The history of subduction beneath western North America.

Along the Pacific Coast of North America the Cascade Mountains run from the Canadian border to Cape Mendocino. This active chain of volcanoes is the result of the subduction of the Farallon Plate beneath North America. To the south subduction has ceased over the last few million years. The Sierra Nevada region extends south to just north of Los Angeles: its western margin is the San Andreas fault. To the west of the dextral San Andreas fault the Coastal

Californian region is part of the Pacific plate which is moving north relative to the rest of North America. South of Los Angeles, Baja California is also part of the Pacific plate and is moving north relative to Mexico. In the southern half of the Gulf of California between Baja California and Mexico the plates are pulling apart and new Oceanic crust is starting to develop. This is due to the dextral movement between the North American and Pacific plates as the Pacific moves northwards relative to North America. Further south the Cocos plate is being subducted under the Sierra Madre del Sur.

In order to gain an understanding of the major tectonic events within the western half of the North American plate, the sequence of events along the western margin of the continent must be considered. A series of cartoons, developed by the author, showing the gradual sequence of events as the Farallon and Cocos plates have been subducted beneath North America, are set out in Figure 2. The Farallon and Cocos plates are considered to be two separate plates which probably had a spreading margin between them, as they are converging on the North American plate at different angles. Though this effect could be due to rotation since a single plate (the former eastern Pacific) was spilt. Once a single plate is split apart due to the subduction of its middle, the two new plates will no longer have the same forces acting upon them and will move independently.

A simple model of the history of the western margin of North America was developed by the author. At the start of the Cenozoic, Figure 2f, there was subduction beneath the western margin of North America from south of Alaska southwards. The Farallon plate extended from along the coast of Canada to southern California and the present

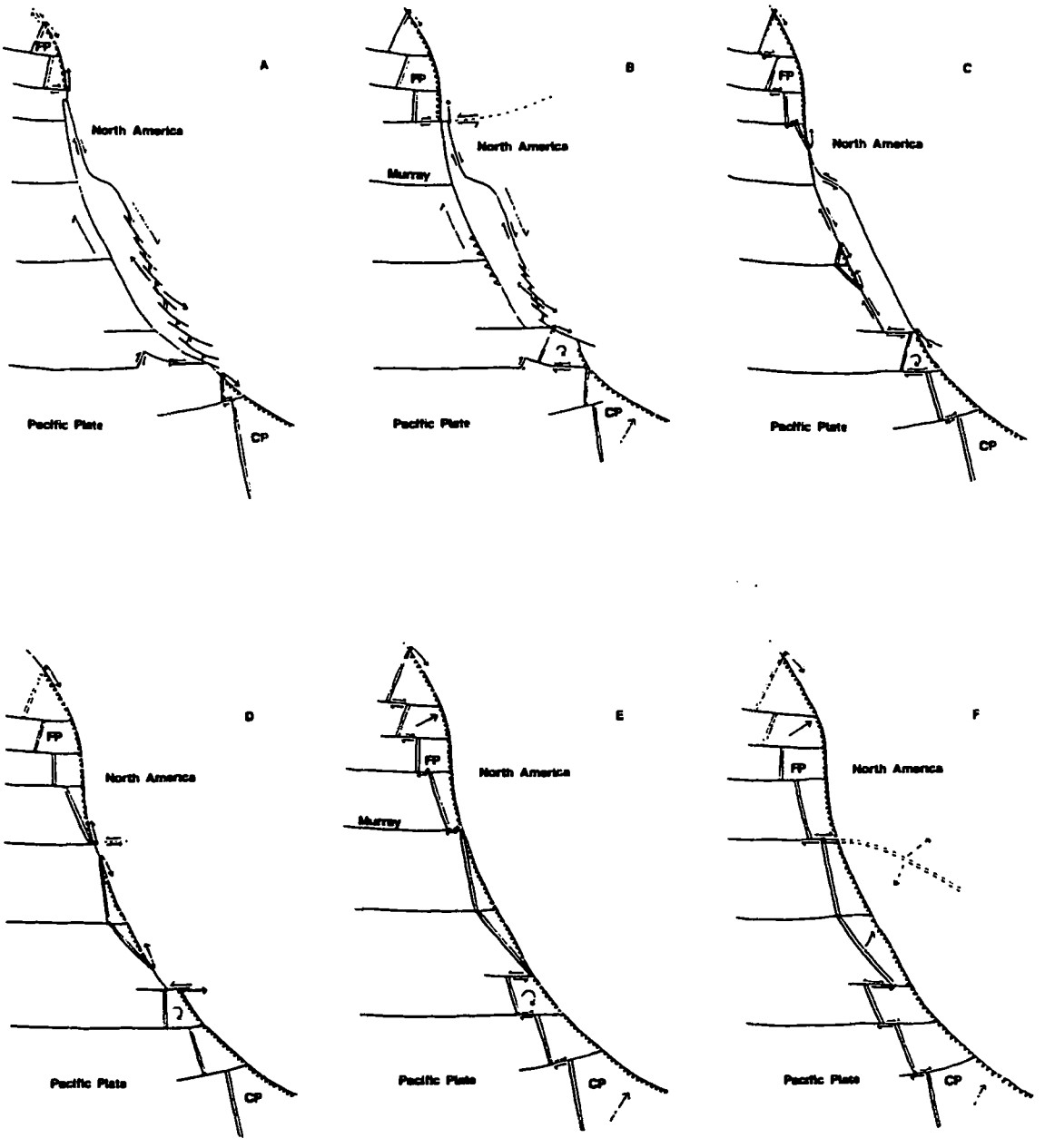

Figure 2. Cartoons of the subduction of the Farallon and Cocos Plates beneath North America. F.P. = Farallon Plate, C.P. = Cocos Plate, saw edge = subduction zone, parallel lines = spreading axis, arrows indicate sense of movement. a 10-20 Ma in the future, b Present day, c 4 Ma ago, d 20 Ma ago, e 30 Ma ago, f 40 to 50 Ma ago at the start of the Cenozoic. Note the saw tooth line marking the subduction margin is on the down going plate away from the margin.

Murray fracture zone where it had a triple spreading junction with the Pacific and Cocos plates. The Cocos Plate extended from this point southwards to the Nazca Plate off South America. The northern triple junction between the North American, Farallon and Pacific plates was and still is moving southward along the margin of North America. The subduction of the spreading margin between the Cocos and Farallon plates led to extension along the Texas Lineament in the continental crust above. In time this led to the formation of the Southern Basin and Range which was initially a zone of north-south tension, and later of east-west tension due to the ending of subduction beneath these parts of North America. In the early Cenozoic the whole of western America was under compression due to the convergence of the Cocos and Farallon plates with North America. So the whole of the area between the Great Plains and the Gulf of Mexico was confined to a strip of mountains probably less than half the width of this region at present. The area of the Rio Grande Rift and the northern and southern Sierra y Fondo were back-arc basins which were undergoing extension, especially in Mexico.

At about 30 Ma ago (Figure 2e) subduction halted to the south of the Murray fracture zone and the triple junction between the Pacific, Farallon and Cocos plates bifurcated into two triple junctions. The northern Farallon, North American and Pacific plates triple junction remained stationary with respect to North America as subduction continued up to the Murray fracture zone. Meanwhile the Cocos, North American and Pacific Plates triple junction started to move southwards and subduction also started to cease southwards along the coast of Baja California. Subduction also ceased at around this time at the

southern end of Baja California. This resulted in the triple plate junction between the northern detachment of the Cocos plate, the Pacific and North American plates moving northwards along the coast of Baja California. In the middle of the Cenozoic the area of the Rio Grande Rift and the Sierra y Fondo country to the south would have been part of the back-arc basin associated with subduction beneath Baja California to the west. This back-arc basin was centred on the northern Sierra y Fondo region as subduction started to cease to the south. Later to the north the back-arc basin developed into rifting as subduction ceased and the Colorado Plateau started to rotate clockwise in the late Miocene. The initial tension within the crust between the southern parts of the Colorado Plateau and the Great Plains was focused into a zone of thinning 70 km to 170 km wide which spread outwards to reach a maximum width of about 275 km at about 20 Ma as a back-arc basin (see section 3.2). The triple junction between the Cocos, Pacific and North American plates moved westwards along a fracture zone into the margin of North America, resulting in the formation of the mouth of the Gulf of California and the clockwise rotation of the fragment of the Cocos plate north of the Clarion fracture zone, Figure 2d. Later, over about the last 20 million years the triple junction of the Farallon, North American and Pacific plates moved northwards along the coast of California as North America has over ridden the Pacific (Zoback et al. 1981) and subduction of the Farallon plate under North America has been replaced by dextral transform motion between the North American and Pacific plates.

In the Northern Basin and Range, the extension vectors rotated clockwise some time after 23 Ma (Aldrich et al. 1986) due to the

subduction of the Farallon Plate under North America being replaced by dextral transform motion between the North American and Pacific plates. Regional extension was at first in an ENE - WSW direction, the same as the axis of the Snake River Basalt region to the Yellowstone hot spot line. This line links to the Mendocino fracture zone along a line that rotates to the present east-west alignment of the Basin and Range extension vectors. This suggests that at the start of the Cenozoic, the Mendocino fracture zone was being subducted in an ENE direction. The volcanism along the Snake River - Yellowstone axis may be due to the difference in the spreading direction of the subducted slabs north and south of the Mendocino fracture zones (Figure 3). This allowed the edge of this section of the subducted plate to overlap with the subducted slab to the north of the Mendocino fracture zone as it was subducted. The result of this was localised thickening of the subduction slab leading to the slab being at a higher level beneath the crust and greater friction with the continental plate above resulting in higher heat flows beneath the Snake River - Yellowstone axis and the generation and eruption of vast amounts of basaltic magma. It is also possible that a gap between subducted sections of slab could also result in a higher heat flow above this line, as compressed material below the slabs escaped upwards into the gap in the subduction slab and decompressed generating large amounts of heat. The Yellowstone hot spot, the author conjectures, is a result of the disturbance at the deepest part of the overlap or gap between sections of the subduction slab having a more permanent effect on the convection patterns within the Mantle. Further north the fracture zones within the Farallon plate have

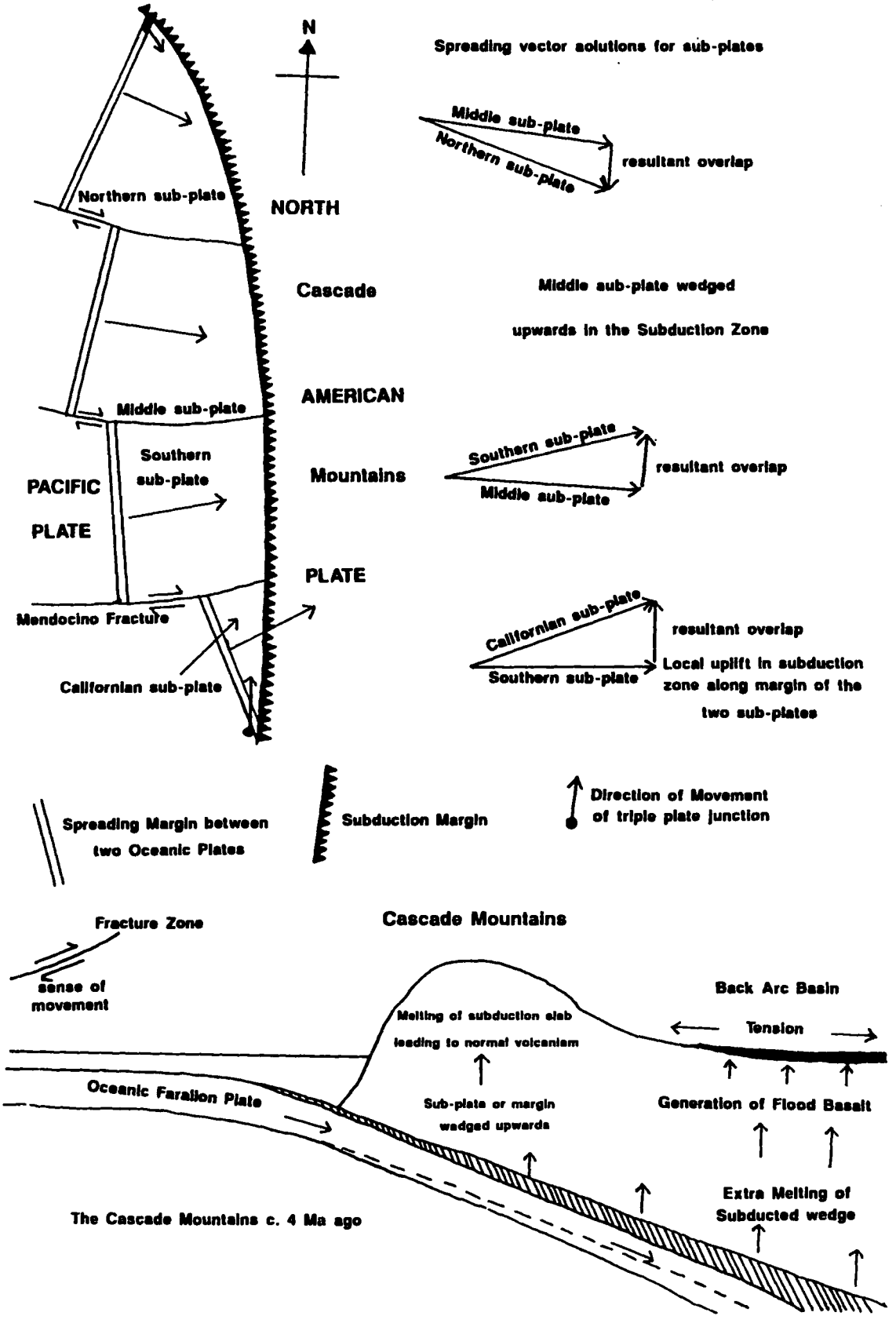

Figure 3. Cartoons of subduction wedging beneath the Cascade Mountains about 4 Ma ago.

resulted in the middle slab of the three parts of the present plate being subducted as a wedge. The wedge has been forced upwards against the North American plate above by the impinging slabs to the north and south (Figure 3). This has resulted in increased friction between the wedged slab which has been subducted at a gentler angle and the continent above also resulting in raised heat flow and the generation of large volumes of basic magma and the eruption of the Columbia River Basalts. The Oregon Basin and Range and the Columbia River Basalts area are the back arc basin of the subducting Farallon plate to the west. Extension parallel to the subducting margin in a back-arc basin is normal and results in similar effects as the extension due to the ending of subduction in the Northern Basin and Range just to the south.

The Colorado Plateau has rotated clockwise by up to 10° since about 9 Million years ago as the southern half of the Northern Basin and Range and the Southern Basin and Range had by this time extended due to the halting of subduction beneath North America. Meanwhile the northern half of the Northern Basin and Range was still undergoing extension, as subduction ceased northwards along the coast of California. This is marked by a period of accelerated rifting within the Rio Grande Rift (Aldrich et al. 1986) between the southern portions of the Colorado Plateau and the Great Plains. The Albuquerque-Belen Basin to the southwest of the Española Basin in the Rio Grande Rift is subsiding at a faster rate (Baldridge et al. 1980). The Española Basin to the north of the Jemez Lineament is offset in the Rio Grande Rift and suggests that the southern rift has been rifting at a faster rate, this would fit in with the clockwise

rotation of the Colorado Plateau away from the Great Plains. The Rio Grande Rift is regarded as a northward embayment of the main Basin and Range stress province to the west which, itself, was the result of relaxation in the Lithosphere after the Farallon plate ceased to be subducted below the southern Rocky Mountains (Park 1988). This fairly uniform zone of thinning fractured during the late Miocene as subduction ceased under the region to form the narrow inter-connected grabens of the Rio Grande Rift as defined by Baldridge et al. (1980). The northern Sierra y Fondo was the last part of the back-arc basin to cease spreading as it is due east of the Molokai fracture zone, the location of the last subduction beneath Baja California. As a result of the clockwise rotation of the Colorado Plateau a series of thrust faults have developed behind the northeastern margin of the plateau, with the result that the Rio Grande Rift to the south is replaced by a series of compressional features, such as the Front and Laramie Ranges and the Bighorn Mountains, along the northern boundary of the Colorado Plateau and the Great Plains.

In the last few million years (Figure 2c), subduction had nearly ceased along the coast of California and Baja California where it was confined to a narrow zone around the Cadros Deep at the end of the Molokai fracture zone, Karig et al. (1978). The halting of subduction led to the collapse and eastward extension of the Northern, Southern and Mexican basin and Range areas.

The build up of dextral tension between the Pacific Plate and the North American Plate led to the formation of the San Andreas fault and the Gulf of California as this motion was displaced inland. The margin of the Southern and Mexican Basin and Range was the weakest

link in the crust of North America. To the north, where subduction had ceased at a later date the coastal strip in front of the Sierra Nevada was weaker, the San Andreas fault developed. The effect of the Murray fracture zone having a sinistral sense of movement due to its past history, as the point at which a spreading triple junction was subducted under North America, was to displace sinistrally the Transverse Ranges and the San Andreas - Gulf of Mexico fault system. The sinistral displacement of the end of Baja California and the clockwise rotation of the northern most part of the present Cocos Plate eventually led to slithers of the spreading ridge between that part of the Cocos and Pacific plates being incorporated into the Gulf of California. Such a series of fault segments joined by small lengths of spreading centre at which new crust originates is termed a leaky transform fault (Thompson and Melson 1972). At present (Figure 2b), the southern half of the Gulf of California is starting to spread apart as sections of the spreading ridge to the south are 'fed' into the Gulf. Due to the clockwise rotation of this fragment of Cocos Plate to the south of Baja California the fracture zone at the spreading ridge is pulling north from the Clarion fracture to form a chain of Volcanic islands, Isle Socorro and Isles Benedicto of the Revilla Gigedo Islands.

In the future (Figure 2a), Baja and Coastal California (part of the Pacific Plate) will move northward up the coast of North America as new oceanic crust is created in the spreading Gulf of California along its southeastern margin. Subduction will be confined to an ever-shrinking part of the margin in the north as the Farallon Plate disappears under North America and the start of the subduction zone in

the south will move southeastward along the coast of Mexico as the Cocos Plate also disappears to be replaced by dextral movement.

2.4 Summary and Conclusion.

The evolution of western North America in the Cenozoic is controlled by the development of dextral movement between the Pacific and North American plates replacing subduction of the Cocos and Farallon plates beneath parts of the continent. Arc-volcanism with its associated compressive stress regime along the continental margin of the subduction zone, with, further away from this margin, tensional back-arc basins, have been replaced by tectonic collapse and the formation of the Basin and Range province. To the east of the Northern Basin and Range region the Colorado Plateau has rotated clockwise as collapse within the neighbouring Basin and Range migrated northwards as subduction ceased to the west off the coast of California (Figure 2c & d). The northern part of the Baja California back-arc basin developed into the Rio Grande Rift as the Colorado Plateau moved away from the Great Plains and subduction ceased. The subduction of a spreading margin between the Farallon and Cocos plates may be one of the Key factors that led to the development of tension in the continental crust above. I suggest that this may explain the north-south spreading along the Texas Lineament of the southern Basin and Range which took place before the onset of the more general east-west Basin and Range spreading.

3. A review and reclassification of the Geology and Structure of the Jemez Mountains, New Mexico

3.1 Introduction

The Valles Caldera lies in the Jemez Mountains of New Mexico (106½°W 36°N), in the southern Rocky Mountains of the western U.S.A.. The Jemez Mountains are located at the intersection of the northeastward trending Jemez Lineament (first defined by Mayo, 1958), with the western margin of the north-south Rio Grande Rift, (Self et al. 1986). To the north the rift is displaced eastwards, and the Valles Caldera is located amid young volcanic strata on the north-western side of this offset (Figure 4). The area was mapped by Smith et al. (1970) who also provided a stratigraphic framework (Bailey et al. 1969). They divided the Jemez volcanic rocks into three main groups which overlap temporally, but are petrologically significant and are from oldest to youngest: the Keres, Polvadera and Tewa groups. Structurally the Jemez Mountains volcanic field is progressively faulted downward to the east by many north-south trending faults (Smith et al. 1961). New radiometric data (Gardner et al. 1986) between 16.5 Ma and the present, have led to the stratigraphic revisions by the author discussed later (Appendix 1). Not all dates referred to in the text are to be found in Appendix 1 as either the data on which they are based are unpublished or they are not determined by the K-Ar method.

The Valles Caldera is a classic example of a resurgent caldera with a high-temperature volcanic geothermal system. Indeed the Jemez

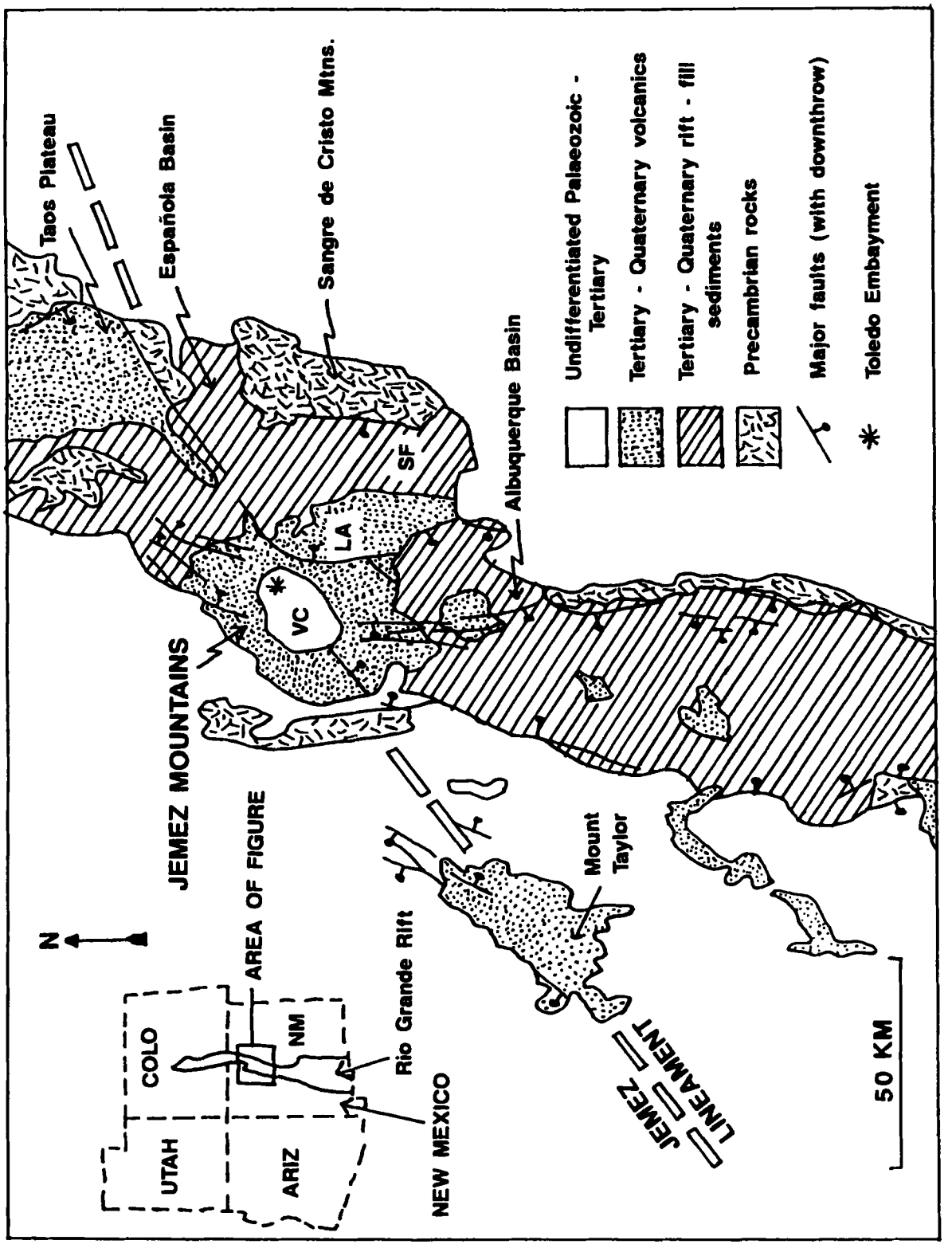

Figure 4. Location map showing the basins of the north-central Rio Grande, Pre-Cambrian rocks, Tertiary-Quaternary volcanic fields and major faults. VC is the Valles Caldera, L.A. is Los Alamos and S.F. Santa Fe. Based on Self et al. (1987)

Mountains have been drilled intensively as part of the Continental Scientific Drilling Program. The present caldera, including the Toledo Embayment to the northeast of the Valles Caldera is approximately 20 km northwest-southeast by 25 km northeast-southwest. The whole depression was formed by a series of catastrophic eruptions that occurred in the middle of the Jemez volcanic field and 600 km^3 (nearly 150 cubic miles) of rhyolitic pyroclastic material was deposited to form most of the Bandelier Tuff (Smith 1979). The Bandelier Tuff is an extremely widespread ash-flow deposit that is found up to 30 km from the centre of the present caldera. At least two major caldera collapse events are recognised; these erupted the Otowi (Lower Bandelier Tuff) (1.45 Ma) and Tshirege (Upper Bandelier Tuff) (1.12 Ma), members of the Bandelier Tuff (Izett et al. 1980). These are thought to have been erupted as a result of the respective collapses of first the Toledo Caldera (1.45 Ma) and then the Valles Caldera (1.12 Ma). Heiken et al. (1986) consider these calderas to be a pair of approximately coincident trap door calderas, hinged to the west. Since the eruption of the Tshirege Tuff, rhyolitic domes have developed to form a series of vents with a circular distribution, which was mapped by Smith et al. (1970) as the Valles Caldera ring fracture; resurgent doming has also occurred in the centre of the caldera; and a complex geothermal system has evolved.

The Jemez Mountains range in height from 1,646 m (5,400 ft) O.D. near San-Felipe to the south of the mountains, to the 3,509 m (11,511 ft) high Chicoma Mountain, just to the northeast of the Toledo Embayment (Figure 5). Drainage from the central caldera is to the southwest, through the Canon de San Diego where the northern San

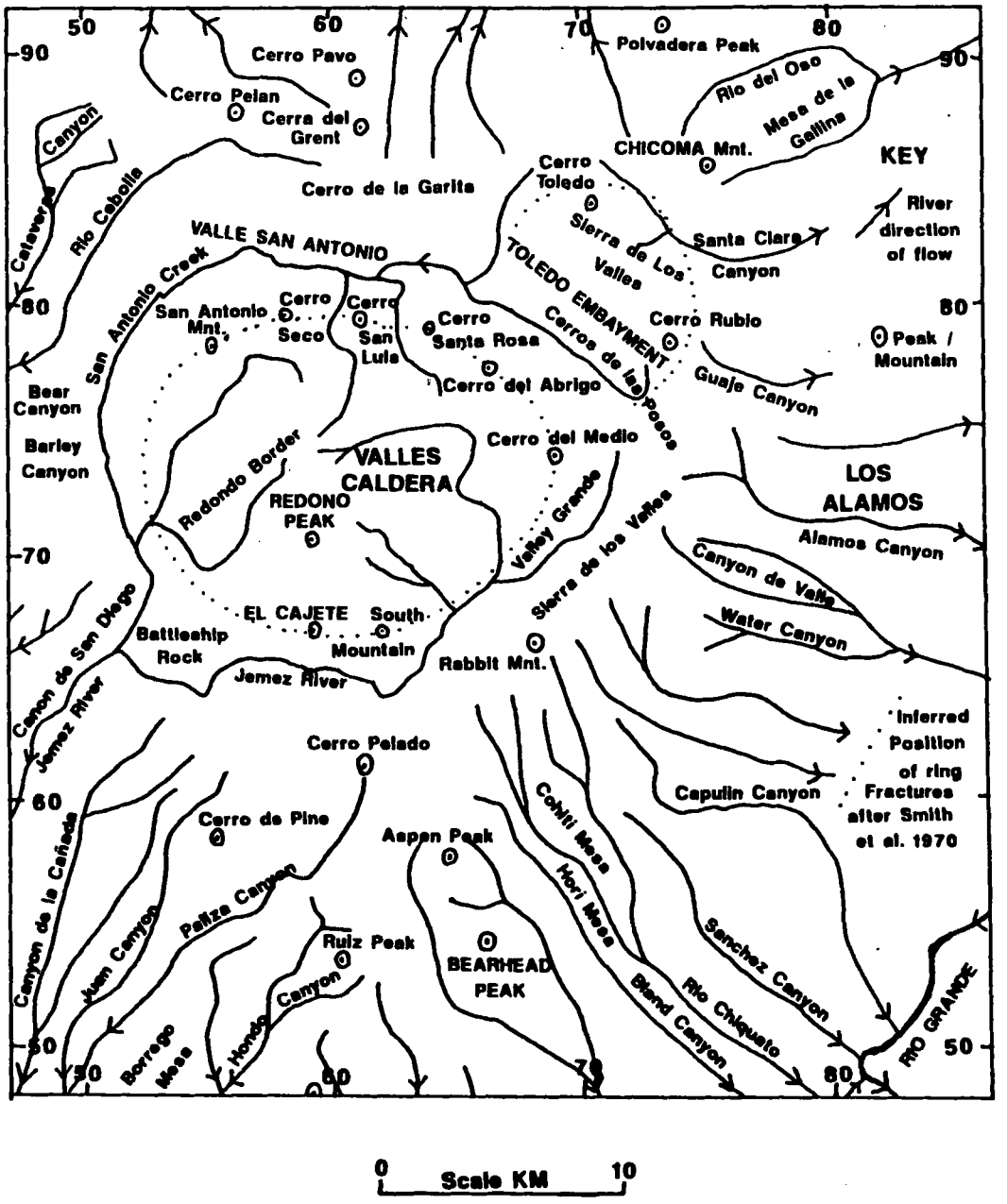

Figure 5. Locations and drainage within and around the Valles Caldera, grid intersections along edges of map are every 10 km.

Antonio Creek and the southern Jemez River meet at Battleship Rock. The drainage pattern off the outer margins of the caldera is radial. Within the Valles Caldera the highest point is Redondo Peak, towards the south of the central area at 3,430 m (11,254 ft). The lowest ground 2,134 m (7,000 ft) is found below Battleship Rock on the south-western edge of the caldera at the head of the Canon de San Diego. Other low points within the caldera are Valle Grande 2,591 m (8,500 ft) in the southeast and Valle San Antonio 2,560 m (8,400 ft) to the north (Figure 5). The main perimeter of the caldera is characterised by ring fracture volcanic vents that range in height from the 3,149 m (10,332 ft) high Cerros del Abrigo in the northeast to the 2,682 m (8,800 ft) high Banco Bonite, which at 0.13 Ma (Marvin and Dobson, 1979) was formed by the most recent eruptive event in the volcanic complex. The rim of the Valles Caldera is between 183 m (600 ft) high at Sierra do Los Valles in the southeast to 549 m (1,800 ft) high at Cerro de la Garita in the north. The Toledo Embayment cross-cuts the topography of the area on the southeastern side, but has a rim between 213-305 m (700-1,000 ft) high on its northern side.

In the following text grid references are quoted in brackets after locations in the text, and are based on the kilometre grid shown on the 1:125,000 Geologic map of the Jemez Mountains (Smith et al., 1970). The eastward location or easting (the vertical grid line to the left of the point in question) is quoted first and then the northward location or northing (the horizontal grid line below the point) is quoted. A location can be given as a four figure reference to within a kilometre, a six figure reference to within 100 meters.

3.2 Tectonic Setting

The Jemez Mountains are located in a region that from 32 Ma onwards has undergone regional extension as part of a back-arc basin, at first in an ENE - WSW direction, and then some time after 23 Ma the extension vectors rotated clockwise to the present east-west or WNW - ESE direction (Aldrich, et al. 1986). This clockwise rotation of the regional extension orientation is probably due to the subduction of the Farallon Plate under North America being replaced by dextral transform motion between the North American and Pacific plates and the consequent movement of the associated triple junction northward as North America has over-ridden the Pacific (Zoback et al. 1981) (Figure 6). However since its inception about 31 Ma the east-west spreading direction of the Rio Grande Rift has been controlled by a pre-existing structural grain (Aldrich et al., 1986). Indeed it is a northward embayment of the main Basin and Range stress province to the west which, itself, was the result of relaxation in the Lithosphere after the Farallon Plate ceased to be subducted below the southern Rocky Mountains (Park, 1988).

The northeast trending Jemez Lineament passes through three regional stress provinces (Aldrich et al. 1986), the Colorado Plateau to the north-west, southern Great Plains to the east and Rio Grande Rift (Figure 7). In the past east-west 'spreading' has not been confined within the present margins of the Rio Grande Rift. In the north of New Mexico the western boundary was located, from 31 Ma, on the Colorado Plateau, in the eastern San Juan Basin, until it moved back east (80-100 km) between 23 Ma and 16 Ma. The eastern boundary

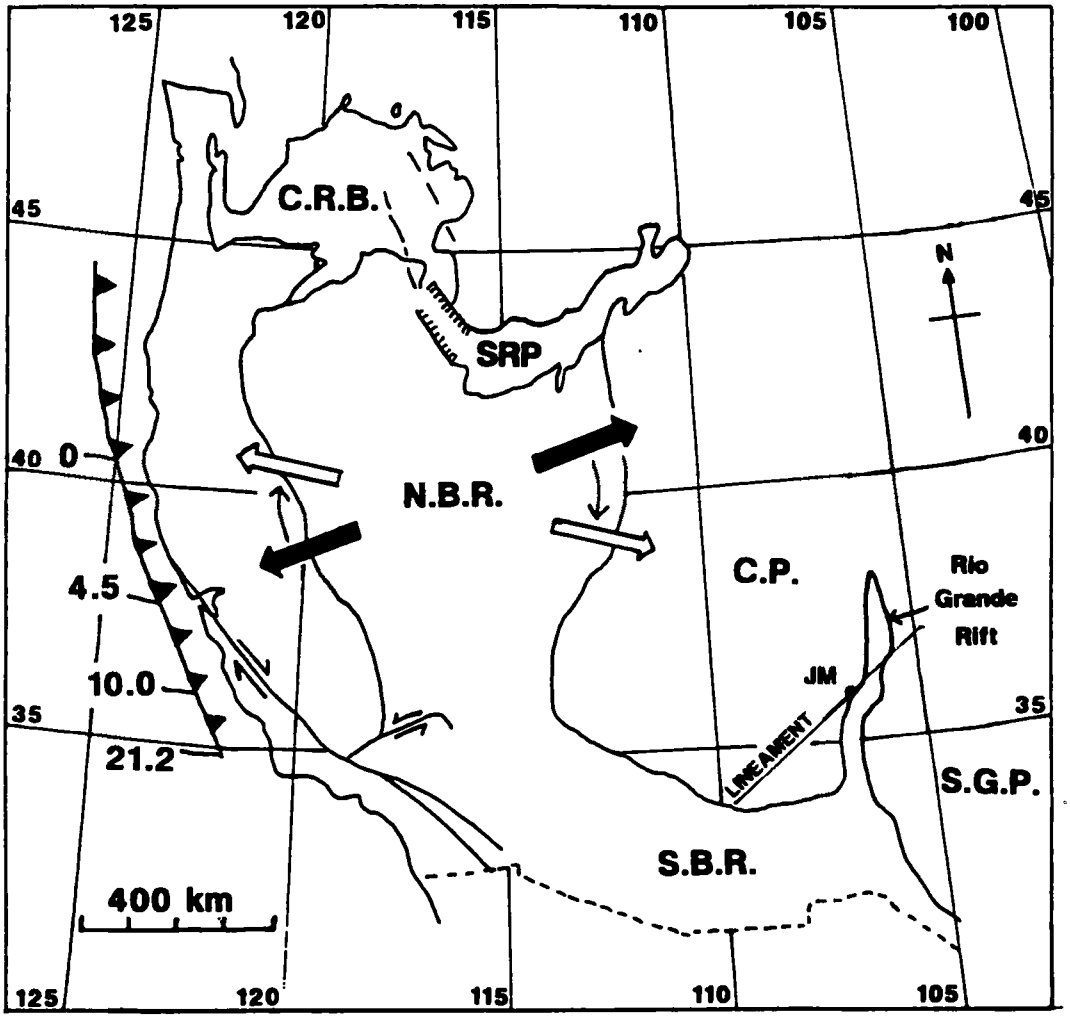

Figure 6. Rotation of least horizontal principal stress in the Northern Basin and Range (N.B.R.), white arrows now, black arrows about 10 Ma ago. This was due to the northward motion of the Farallon, North American and Pacific, triple junction over the last 21 million years when volcanism ceased along this line, the time given by the numbers along the subduction zone (toothed line)(based on Park, 1988, p. 98: regional stress provinces are based on Aldrich et al., 1986). C.R.B. Colorado River Basalts, S.R.P. Snake River Plain, S.B.R. Southern Basin and Range, C.P. Colorado Plateau, S.G.P. Southern Great Plains, J.M. Jemez Mountains and the Jemez Lineament.

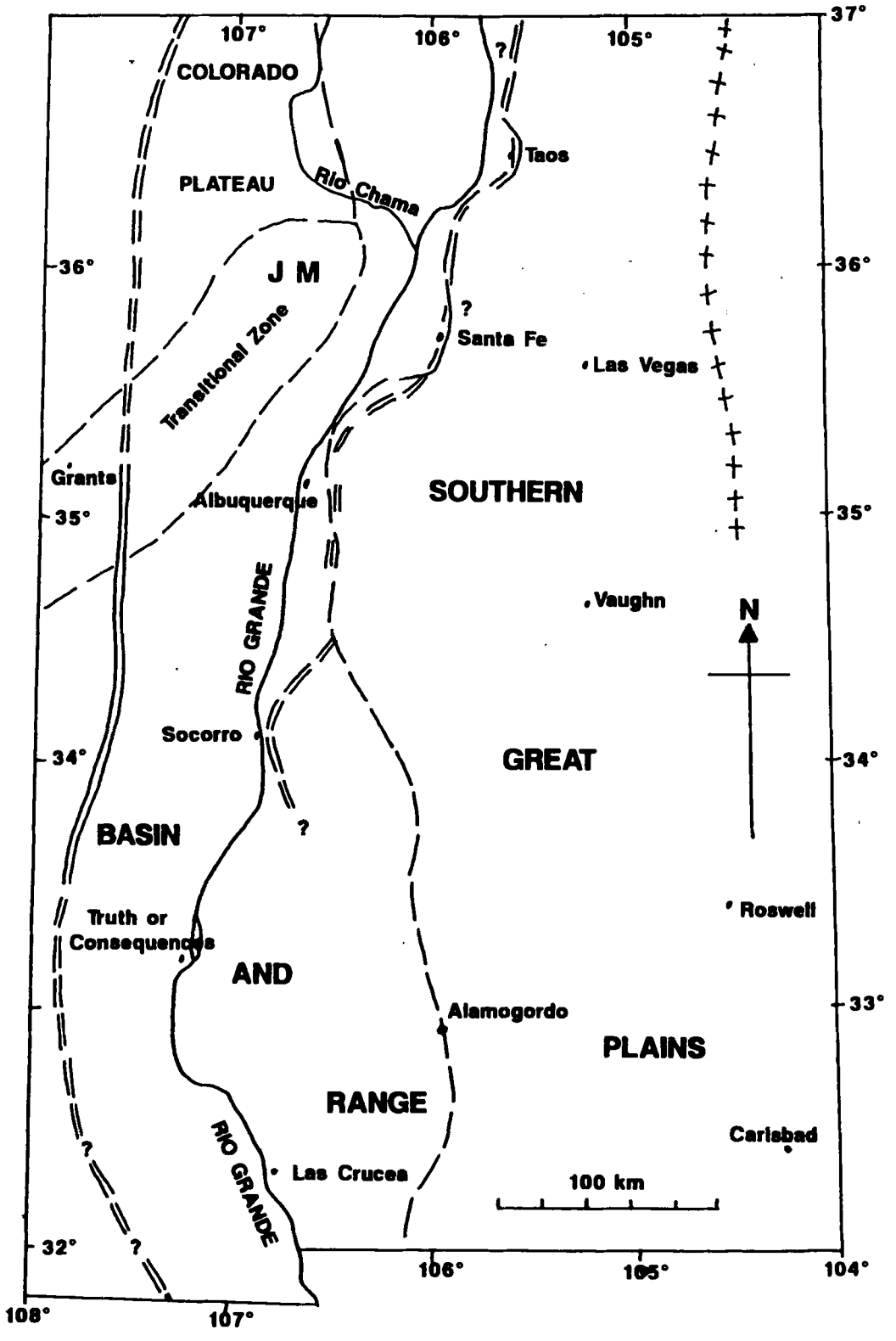

Figure 7. Changes in the boundary of the Rio Grande Rift in New Mexico, based on Aldrich et al. (1986). Key: thick dashed lines, contemporary (0-5 Ma) stress boundaries with named stress provinces; crosses, eastern stress boundary between 20 and 5 Ma; double lines, stress boundaries between 32 and 20 Ma; broken lines indicate uncertainty.

stepped eastward (80-100 km) on to the southern Great Plains some time between 23 Ma and 16 Ma, before moving back to the west, during a period of accelerated rifting that began at about 9 Ma (Aldrich et al. 1986). These effects may be due to the initial tension within the crust between the Colorado Plateau and the southern Great Plains being focused into a zone of thinning 70 km to 170 km wide which over time spread outwards to reach a maximum width of about 275 km. This in turn was a result of the Rio Grande Rift and the Sierra y Fondo country to the south being part of the Cenozoic back-arc basin associated with subduction beneath Baja California to the west. When subduction ceased this fairly uniform zone of thinning fractured during the late Miocene to form the narrow inter-connected grabens of the Rio Grande Rift as defined by Baldridge et al. (1980). The Rio Grande Rift in New Mexico became a through-flowing southward drainage system, spreading northward up the rift, during the late Pliocene (between about 4.5 Ma and 3.0 Ma ago) Bachman and Mehnert (1978). The Jemez Lineament is a northeast trending crustal flaw that, at its intersection with the Rio Grande Rift (Figure 4), has controlled volcanism and tectonism within the rift and has lead to the formation of the Jemez Mountains volcanic field on its western flank (Aldrich, 1986). The northeastward trend of the Valles-Toledo complex is due to this subsurface structural grain, Goff (1983).

The following is a summary of the model developed by Aldrich (1986) (Figure 8). To the west on the Colorado Plateau the Jemez Lineament is a 50 km wide zone of mainly NNE trending faults, which narrows within the Rio Grande Rift to a belt, less than 5 km wide, of northeast to ENE trending fault zones. The deflection of the Jemez

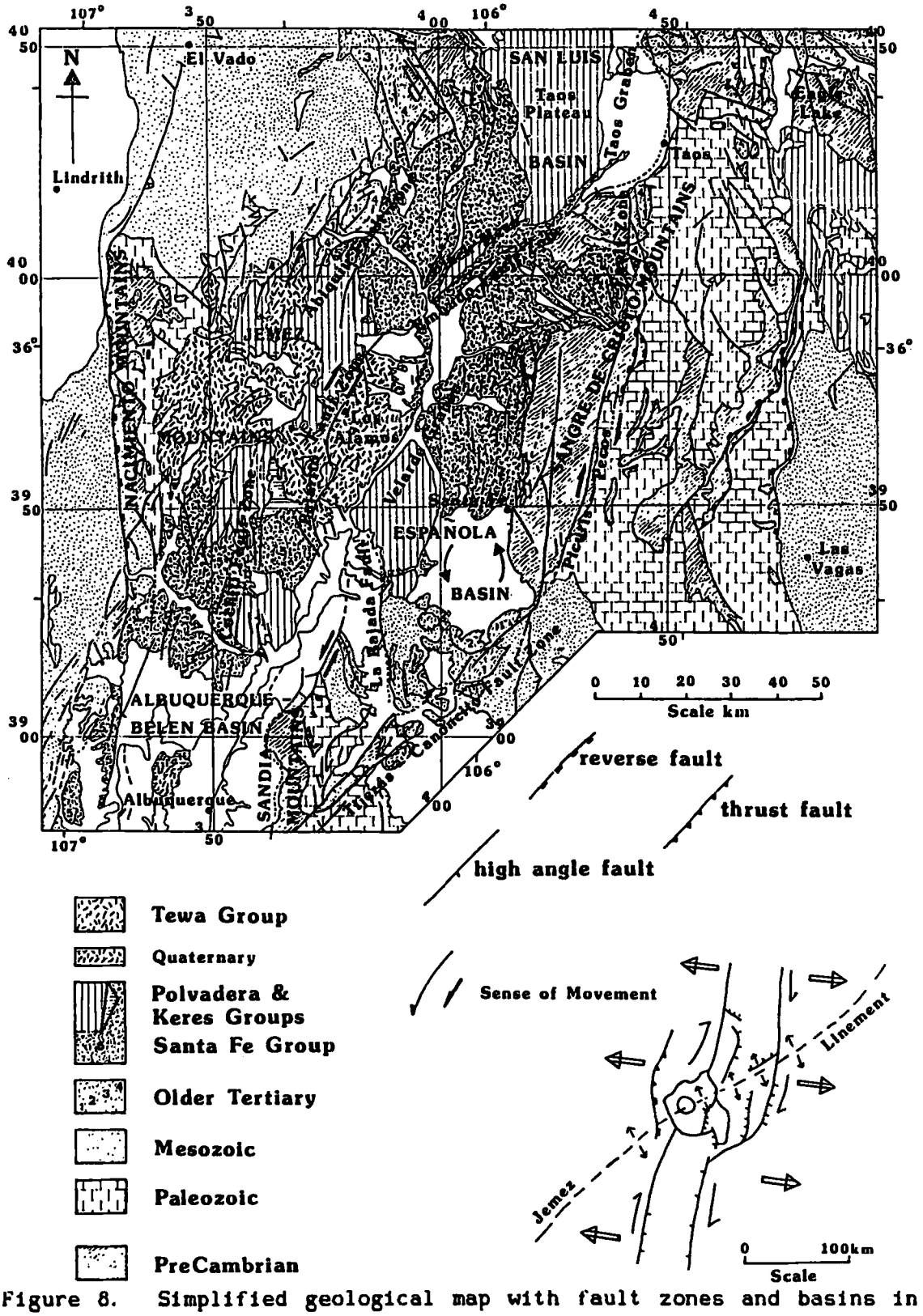

Figure 8. Simplified geological map with fault zones and basins in Rio Grande Rift adjacent to the Jemez mountains, based on New Mexico Geological Map 1:1,000,000, with the rotation and sense of movement of faults bounding the Española Basin (Muehlberger's 1979 suggestion) based on Aldrich (1986).

Cartoon. The Rio Grande Rift, sedimentary basins, volcanic fields and major faults and thrusts: cartoon of extension along the Jemez Lineament and the Rio Grande as a dextral pull-apart basin in the vicinity of the Jemez Mountains, based on the U.S.G.S. 1:5,000,000 Tectonic Map of North America.

Lineament within the vicinity of the Rio Grande Rift towards an east-west direction, normal to the rift axis, is a result of the rifting process pulling apart pre-existing cross-cutting structures. Since its inception the Rio Grande Rift has been dextrally offset along the Jemez Lineament by about 50 km (insert Figure 8).

From at least 15 Ma to 10 Ma the lineament was under extension within the rift, resulting in volcanic vents along its length. Structural studies suggest that the Jemez Lineament in the Jemez Mountains has not moved for at least 5 Ma, while in the eastern Rio Grande Rift, it underwent major movement during the Pliocene (Dungan et al. 1984) which has slowed considerably since about 2.5 Ma. The structure of the Embudo fault zone (the eastern Jemez Lineament in the Rio Grande Rift) may be the result of the rapid spreading in the Española Basin to the south of the fault zone compared with the San Luis Basin to the north (Figure 8). Muehlberger's (1979) suggestion that the diamond-shaped block (Española Basin) bounded by the Pajarito-La Bajada, Embudo, Picuris-Pecos and Tijeras-Cañoncito fault zones is rotating anticlockwise (Figure 8), is supported by evidence that the Pajarito fault zone has undergone dextral movement for at least the past 1.1 Ma.

While most of the movement along the Rio Grande Rift has been east-west extension, the evidence for north-south extension along the Jemez Lineament suggests that in the Jemez Mountain-Española Basin area the rift has in part acted as a dextral pull-apart basin (insert Figure 8). This would explain the anticlockwise rotation of the Española basin, suggested by Muehlberger (1979), compression of the Velarde Graben, the differential spreading rates between the Española

Basin and San Luis (Abiquiu) Basin to the north and the location of the Jemez Mountain volcanic field. The Española Basin has been uplifted relative to the Albuquerque-Belen Basin to the southwest, which is subsiding at a faster rate (Baldridge et al. 1980), reflecting a greater rate of rifting south of the Rio Grande Rift offset. The interaction of the Jemez Lineament and the Rio Grande Rift tectonics, must play a significant part in the evolution of the Jemez Mountains volcanic field. However, this issue has not been fully addressed in the literature.

3.3 Pre Caldera geology

The Jemez Mountains are underlain by Pre-Cambrian rocks which have been encountered in geothermal wells and are described as "fresh" to hydro-thermally altered granitic rocks, gneisses and schists (Goff et al., 1989). These Pre-Cambrian rocks are exposed in the Nacimiento Mountains to the west of the Jemez Mountains. The pre-Cambrian rocks penetrated by a Hot Dry Rock well just to the west of the Valles Caldera topographic rim have been investigated by Brookins and Laughlin (1983), who concluded from Rb-Sr ratios that a major metamorphic event occurred at 1,620±40 Ma. They also reported a younger intrusive igneous event at 1,500±120 Ma which continued with minor dike emplacement until 1,440±30 Ma. Harrison et al. (1986) suggested from $^{40}Ar/^{39}Ar$ analyses on microcline that additional metamorphic events occurred at about 1,030 Ma and 870 Ma. The depth to the Pre-Cambrian basement increases dramatically from west to east across the caldera and pre-caldera Rio Grande faults (Goff et al 1989;

Figure 9). These pre-caldera faults may link up with the Cochiti and Abiquiu fault zones, to the south and northwest of the present Valles Caldera (Figure 8). The pre-rifting Phanerozoic rocks in the Jemez Mountains area prior to Eocene and possibly Oligocene pre-rifting volcanism, are all sediments (Smith et al. 1970).

The **Abiquiu Tuff**, mapped by Smith et al. (1970), are tuffaceous sediments which range in age from at least 22 Ma to 19 Ma. Dates are obtained from igneous rocks that interdigitate with these sediments near Ojo Caliente some 40 km northeast of the Jemez Mountains (Baldridge et al. 1980). May (1980) suggested from field evidence that the base of the Abliquiu Tuff (Formation) correlates with the older Los Piños Formation, about 20 km further north in the Rio Grande Rift, which has also been dated on the basis of the age of an volcanic flow interfingering these sediments at between 25 Ma to 26 Ma (Baldridge et al. 1980). They are similar to the younger Cochiti and Puye formations of the Keres and Polvadera groups respectively, of Miocene age (see below). These tuffs crop out to the west and north of the Valles Caldera (Figure 12), and have a southwest to northeast trend that is probably related to the early rifting pattern of the Rio Grande.

The inception of volcanic activity in the Jemez mountains has been a much-debated problem; however, by 16.5±1.4 Ma alkali basalts are inter-bedded with the early Miocene **Santa Fe Formation** sediments near St. Peter's Dome (77 57, location uncertain), in the southeastern Jemez Mountains. Gardner (1985) suggested that their petrogenesis was separate from that of the Keres Group, but that they marked the onset of the tectonic events that led to the formation of the Jemez

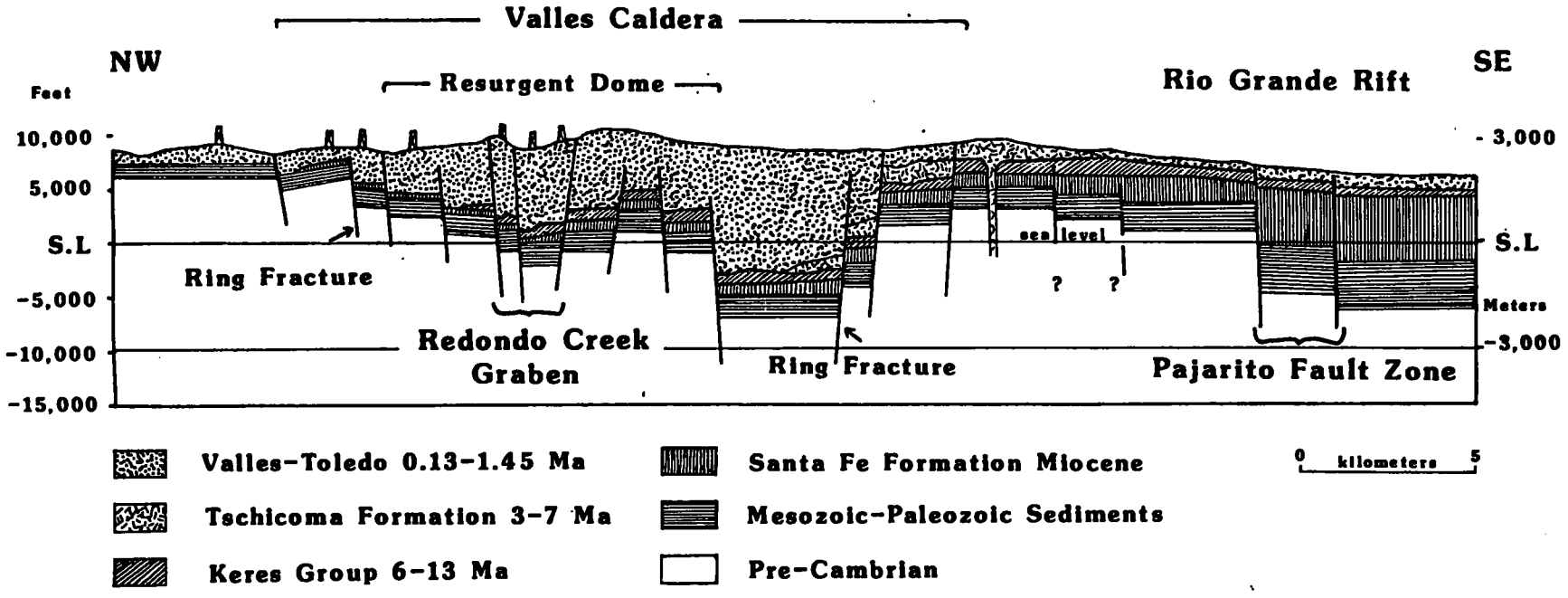

Figure 9. Schematic northwest-southeast cross section across the Valles Caldera based on geothermal well data and the gravity interpretation of Segar (1974) (see later discussion). Intra-caldera volcanic rocks are omitted for clarity. The structure between the Valles Caldera and Pajarito fault zone is poorly constrained (Goff et al. 1989).

volcanic field. Geochemical data for the alkali basalts and Keres group point to the derivation of mafic magmas for both suites from similar upper mantle sources (Gardner et al. 1986). The Lobato Basalt is also interbedded with Santa Fe Group sediments and has been dated by Aldrich (1986) at 14.05±1.4 Ma. Gardner et al. (1986) concluded that the inception of "Jemez volcanism" is a semantical problem and that volcanism in the area had begun by about 16.5 Ma ago. Olivine tholeiites and differentiates were being erupted by this time and by about 13 Ma ago, volcanic sequence formation far exceeded the sedimentation rate of the local Santa Fe Group (Gardner et al. 1986).

The pre-caldera volcanic rocks of the Jemez Mountains were divided by Bailey et al. (1969) into two main stratigraphic groups which, in part, overlap and are the older Keres Group (pre 13 Ma to 6 Ma) and younger Polvadera Group (7 Ma to 1.5 Ma). Often, subdivions of a given rock type within a group are based on geographical occurance rather than stratigraphic criteria. Gardner et al. (1986) reviewed the radiometric dates for the Jemez Mountains volcanic field but at that stage did not reassign units to the temporally-compatible stratigraphic groups. When the area was mapped by Smith et al. (1970), radiometric data were sparse and often age relationships had to be based on less than ideal field evidence. Unfortunately, many units in the Jemez Mountains do not cross cut or overlie each other. I attempt here to revise the stratigraphy of the Jemez volcanic field using the new radiometric dates. The Lobato Basalt was assigned to the Polvadera Group by Bailey et al. (1969), but it has been dated at between 14 Ma and 7 Ma and so I have put it into the older Keres Group. The Cerro Rubio Quartz Latite and Cerro Toledo Rhyolite were

part of the more resent Tewa Group (Smith et al. 1970) but their radiometric dates mean that I consider them as part of the Polvadera Group. The original mapping by Smith et al. (1970) has been used in drawing up the figures for my revised groups. In the following text dates from Gardner et al. (1986) have been quoted in brackets after stratigraphic names. The main stratigraphic groups in this review are based, where possible on temporal divisions (Figure 10), and are summarized below.

3.4 Keres Group

The **Keres Group** (pre 13 Ma to 6 Ma), makes up half the volume of the entire volcanic field (1,000 km^3), and is dominated by the andesites of Paliza canyon. However, the main rock types range from tholeiite basalt to high silica rhyolite (75%+ SiO_2). The group is subdivided into four units, the **Canovas Canyon Rhyolite, Paliza Canyon Formation, Lobato Basalt** and the younger **Bearhead Rhyolite** (Figure 11): **they are interbedded with the volcaniclastic Cochiti Formation.**

The **Canovas Canyon Rhyolite** (>13-7 Ma) was derived from several eruptive centres which lie on the Cañada de Cochiti fault zone; the rhyolites are interbedded with or intrude into the Paliza Canyon Formation. Gardner (1985) suggested that they were derived from partial melts of lower crustal granulite rocks; this is questionable as granulites do not melt easily, unless substantial heating occurred in the lower crust when the geothermal gradient was substantially elevated due to the thinning of the crust during the rapid early stages of rifting under the Rio Grande. The **Paliza Canyon Formation**

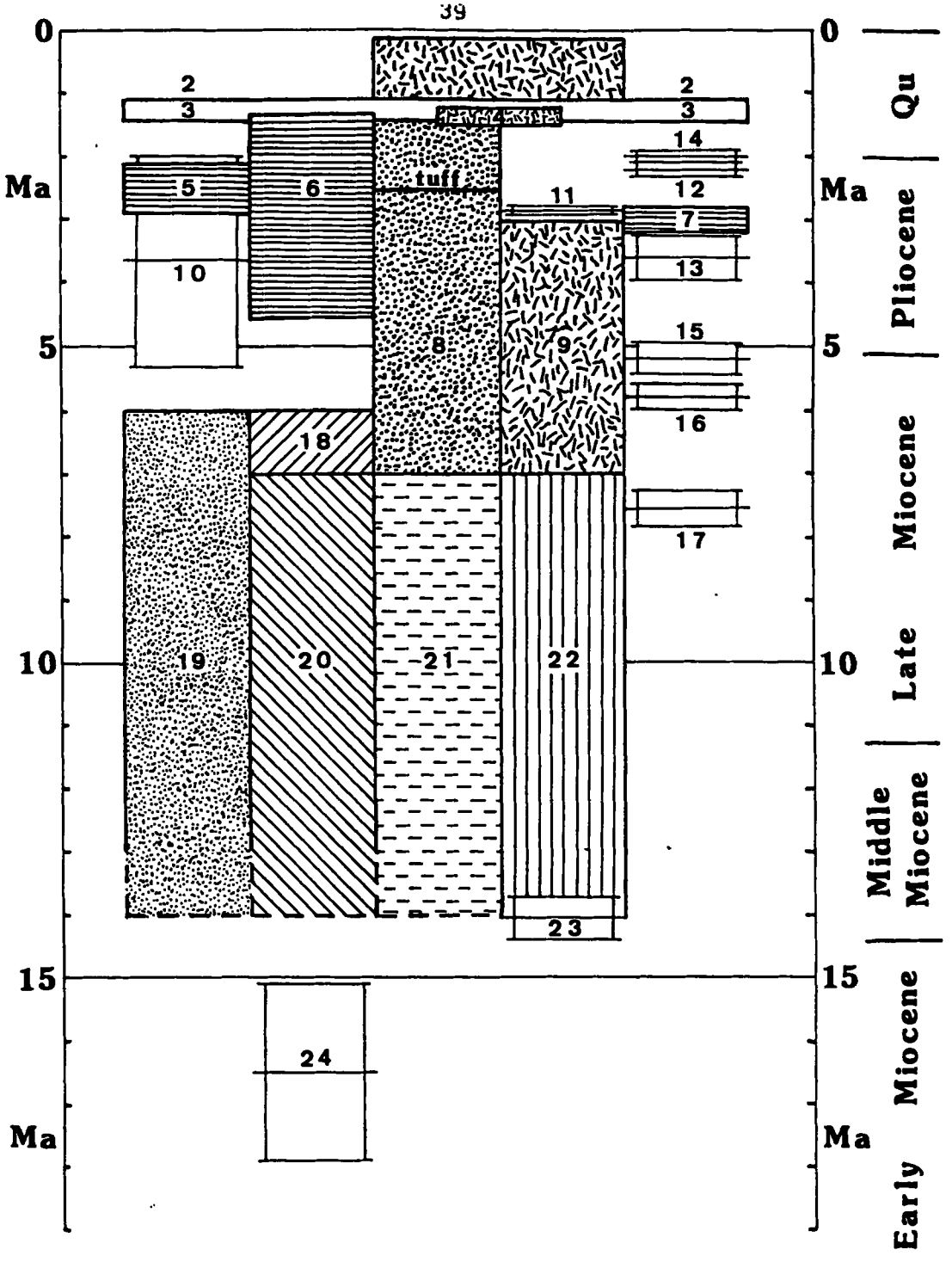

Figure 10. The revised stratigraphy of the Jemez volcanic field, (in the style of Gardner et al. 1986). 1, Valles Rhyolite 2, Tshirege Tuff 3, Otowi Tuff (2 & 3 collectively known as the Bandelier Tuff) 4, Cerro Toledo Rhyolite 5, Basalt of Santa Ana Mesa 6, Basalt of Cerros del Rio 7, El Alto Basalt 8, Puye Formation 9, Tschicoma Formation 10, ignimbrite (A) 11, ignimbrite (B) (10 & 11 San Diego Canyon) 12, Cerro Toledo intrusion 13, Cerro Rubio Quartz Latite 14, El Rechuelos Rhyolite 15, El Rechuelos pumice ring 16, El Rechuelos intermediate Rhyolite 17, El Rechuelos older Rhyolite 18, Bearhead Rhyolite 19, Cochiti Formation 20, Canovas Canyon Rhyolite 21, Paliza Canyon Formation 22, Lobato Basalt 23, basal Lobato Basalt interbedded with Santa Fe sediments 24, Alkali Basalts interbedded with Santa Fe sediments. Unshaded units are shown as the error ranges for their radiometric K-Ar age determinations (see Appendix 1); time downwards in millions of years. Geological Epochs and time scale based on Harland et al. 1982.

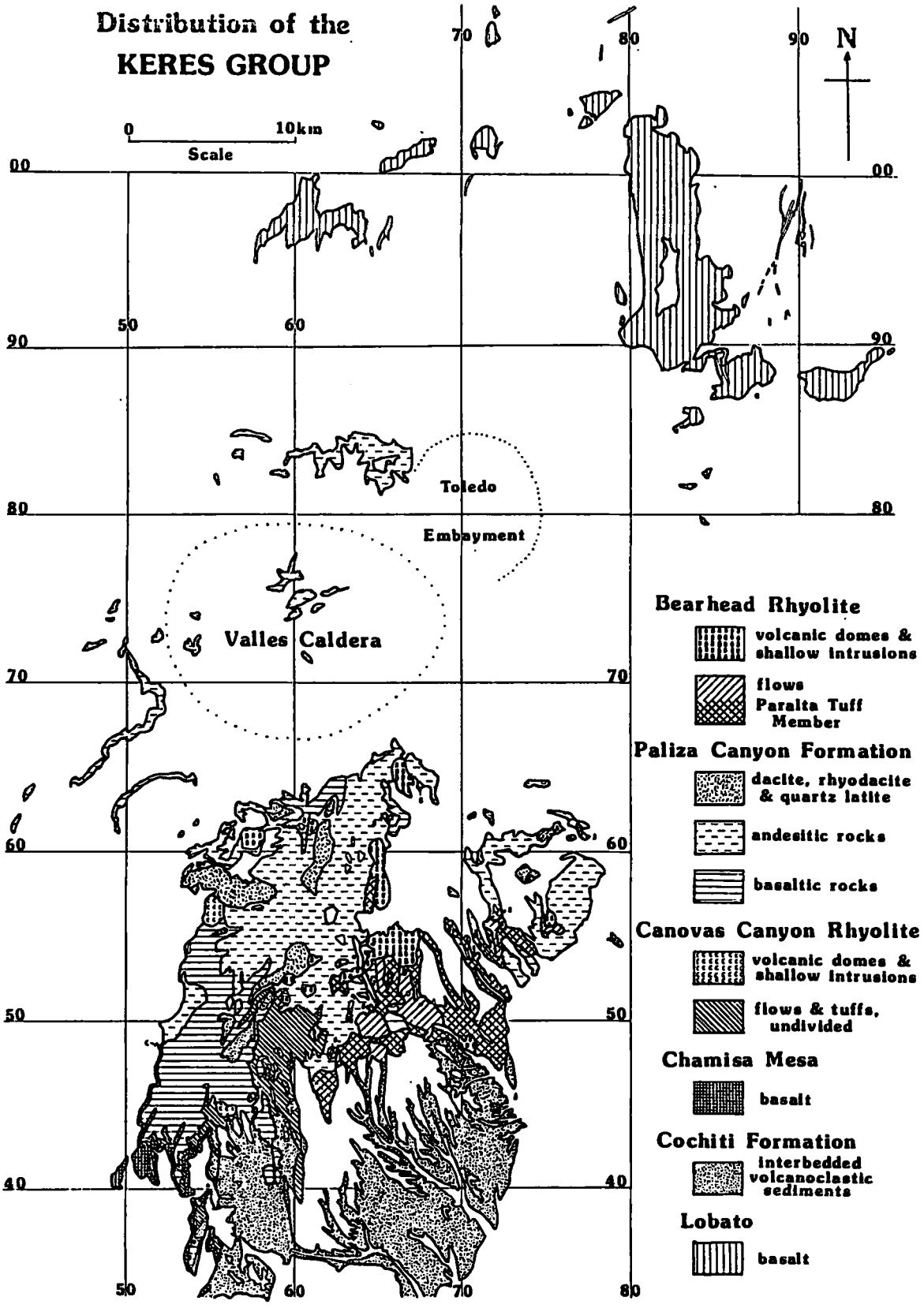

Figure 11. The distribution of the Keres Group, based on mapping from the 1:125,000 Geological Map of the Jemez Mountains (Smith et al. 1970).

(>13-7 Ma) is divided into lower basalts, andesites and upper dacites. The basalts are multiple flows of olivine tholeiite, derived from upper mantle peridotite, (Gardner 1985), that show evidence of fractionation of primarily olivine and clinopyroxene. These basalts give way upwards to more evolved andesites and dacites which overlap into the Canovas Canyon unit and are identical to the **Basalts of Chamisa Mesa** (see Figure 11). The andesites occur as flows and domes of hypersthene-augite andesite and hornblende dacite which are interbedded with the upper Canovas Canyon Rhyolite and Paliza Canyon Basalt. Field relationships within the Canovas Canyon Rhyolite suggest that intermediate composition volcanism began by 12 Ma and accompanied intense faulting. The Paliza Canyon Andesites are the most voluminous and widespread unit in the Keres Group (Figure 11) and are composed of multiple flows of andesite with minor pyroclastic deposits, which pass upwards into domes and dacitic flows. The Paliza Canyon Dacites ($\simeq$9-7 Ma) intrude and overlie all the Keres Group apart from the Bearhead Rhyolite. They tend to be coarsely porphyritic with plagioclase, two pyroxenes and hornblende $\pm$ biotite and often contain up to 10% vesicular clots of Ca-plagioclase and acicular hornblende; they are petrographically similar to the younger Tschicoma formation in the Polvadera Group.

Hydrothermally altered volcanic and hypabyssal rocks of the Cochiti district (about 20 km south of Valles) are the altered and eroded cores of Keres Group andesitic volcanoes intruded by acid rocks similar to the Bearhead rhyolite and later cut by epithermal quartz veins; these events have been dated by various workers at between 11.2 Ma and 5.6 Ma (Stein, 1983; Goff et al. 1989).

The **Lobato Basalt** (≃14-7 Ma) is a series of multiple flows of olivine basalt which have a similar petrology, chemistry and petrogensis to the Paliza Canyon Basalts. The distinction between them is for reasons of geographic distribution, rather than age and they were considered to be part of the Polvadera Group by Bailey et al. (1969). An early Tschicoma dacite flow, from the younger Polvadera Group, is interbedded with the basalts, which for the most part are comformably overlain by them.

The **Bearhead Rhyolite** (≃7-6 Ma) is a series of high silica (75%+ SiO_2) rhyolites, which are chemically and petrographically identical to the Canovas Canyon Rhyolite. Gardner (1985) suggested that they were similarly derived from partial melts of lower custal granulitic rocks. The Bearhead Rhyolite postdates the Paliza Canyon Formation, and a local horizon, the Peralta Tuff, is taken as the approximate boundary between them.

The **Cochiti Formation** consists of volcanic detritus that was derived from and interbedded with the Keres Group and is composed of lahars, vent breccias and gravels that pinch out in the western Jemez Mountains as detritus was washed east and then southwards into the developing Rio Grande rift. The geometry of the formation suggests that the Cochiti (Cañada de Cochiti) fault zone (see Figure 8) was in effect a zone of growth faults bounding the western side of the Rio Grande Rift and is indicative of the intense rifting at the start of volcanic field development.

3.5 Polvadera Group

The **Polvadera Group**, (7 Ma to 1.45 Ma), contains a large spectrum of compositions and is dominated volumetrically by 500 km^3 of Tschicoma Dacite. The same level of stratigraphic detail as within the Keres group is not available; however, the group is subdivided into six units, from oldest to youngest: the **older El Rechuelos Rhyolite, Tschicoma Formation,** the **intermediate El Rechuelos Rhyolite, Cerro Rubio Quartz Latite, Cerro Toledo Intrusion** and **El Rechuelos Rhyolite** (Figure 12). The Tschicoma Formation is interbedded with the volcaniclastic **Puye Formation.**

The **Tschicoma Formation** ($\simeq$7-3 Ma) consists of voluminous dacite domes and flows with subordinate andesites similar to those in the Paliza Canyon Formation. From the data of Smith et al. (1970) and Loeffler (1984), most Tschicoma andesites are considered to be a younger generation of basalt differentiates than the Keres Group that possibly have been contaminated with upper crustal material, similar to the Paliza Canyon Andesites. The dacites are commonly coarsely porphyritic with plagioclase, augite, hypersthene and hornblende $\pm$ biotite; they appear to have been generated by mixing and homogenization of magmas similar to those of the Paliza Canyon (Keres Group) andesites and high-silica rhyolites. Conformable and unconformable contacts exist with both the Lobato Basalt and Paliza Canyon Formation, because the Tschicoma volcanism overlapped the waning Keres volcanism.

The **older** and **intermediate El Rechuelos Rhyolite** have been K-Ar dated by Loeffler et al. (1988). The oldest rhyolite centre along

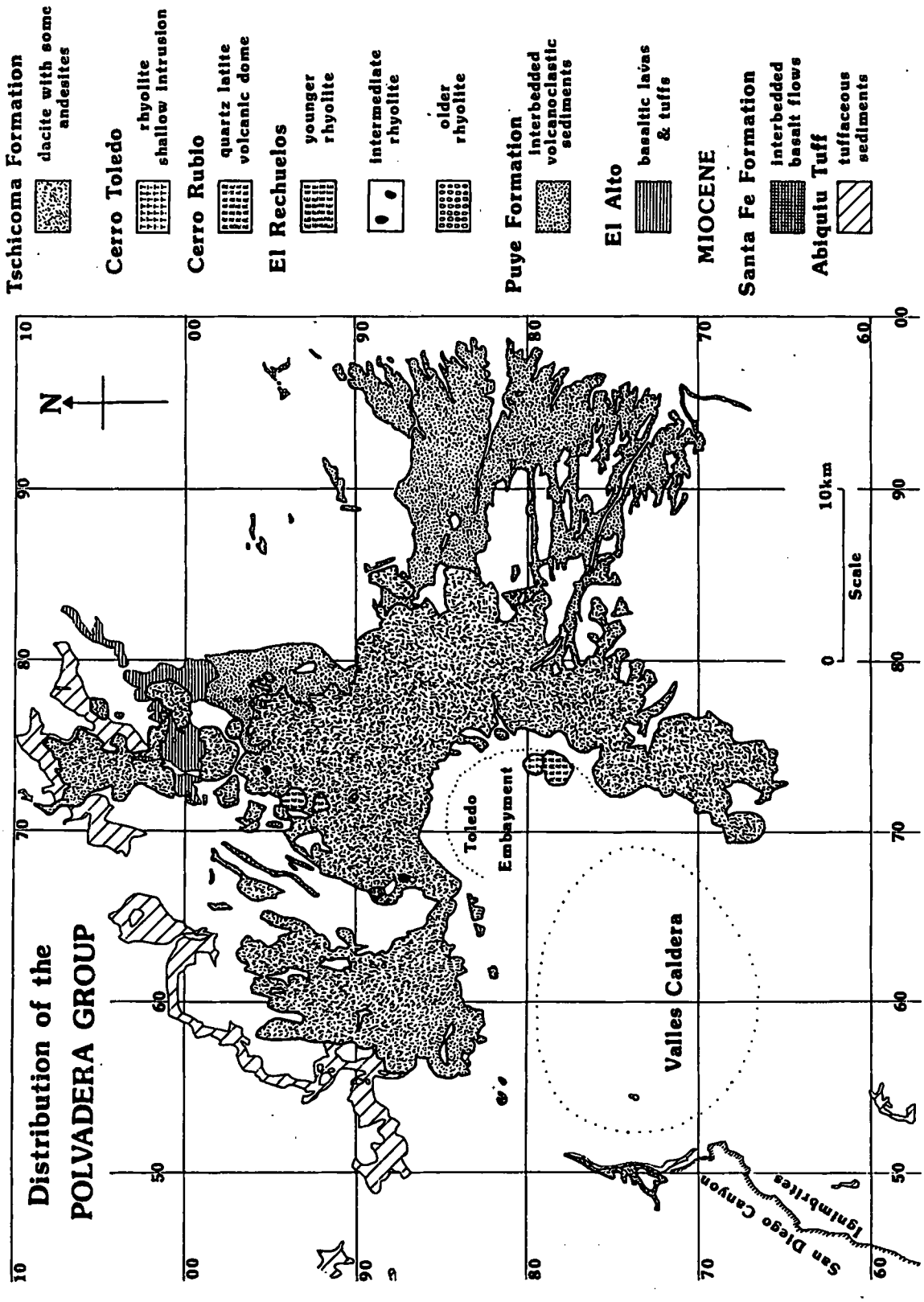

Figure 12. The distribution of the Polvadera Group, based on mapping from the 1:125,000 Geological Map of the Jemez Mountains (Smith et al 1970).

Canonite Seco, (66 88) recognized by Bailey et al. (1969), is a flow banded biotite rhyolite, dated at 7.54±0.28 Ma (Appendix 1). This is pre-Polvadera in age by about half a million years, but is included within the group as it is unrelated to any unit in the older Keres Group, but is the same age as the late Canovas Canyon rhyolites. An intermediate rhyolite along Canonite Seco (67 87) has silicifcation and myrmekitic textures which suggests that this centre may have been a volcanic neck; this material is 5.80±0.20 Ma in age. A pumice ring 4 km north of Polvadera Peak (73 95) contains phenocrysts: zoned plagioclase with high calcium cores; plagioclase; rounded and embayed quartz; biotite and hornblende; in a matrix of microlites and glass. This phenocryst assemblage is similar to the Tschicoma Dacites and the date of 5.21±0.25 Ma suggests that the Polvadera pumice ring may have been the site of a volcanic vent during the eruption of the Tschicoma Formation. The pumice ring has a high 69.75% SiO_2 content and so has been included with the intermediate age rhyolite. The rhyolites may be petrogenetically related to Keres Group rhyolites but have either been contaminated with, or undergone less fractionation from, a more mafic magma (Loeffler et al. 1988).

The **Cerro Rubio Quartz Latite,** is mineralogically and chemically similar to the Tschicoma dacites and has been dated at 3.59±0.36 Ma (Heiken et al. 1986).

The **Cerro Toledo Intrusion** of rhyolite, intrudes Cerro Rubio to the north and has been dated at 2.18±0.09 Ma (Heiken et al. 1986).

Both these units form part of what the author proposes calling the Rubio Volcanics, which were a volcanic edifice that formed in the Toledo Embayment (see end of Section 3.9). Smith et al. (1970)

assigned them to the more recent Tewa Group but their radiometric ages clearly put these units into the Polvadera Group..

The **El Rechuelos Rhyolite** forms three domes of aphyric, pumiceous rhyolite with obsidian, along Polvadera Creek (≃71 92) to the west of Polvadera Peak (Loeffler et al. 1988), and have yielded a date of 2.01±0.06 Ma. Loeffler et al. (1988) consider that the El Rechuelos Rhyolite was derived from the lower crust, in a separate magma chamber from the Cerro Toledo Rhyolite which is related to the Bandelier chamber in the upper crust.

The **Puye Formation** (≃7-1.45 Ma) consists of volcanic detritus that was derived from and interbedded with the Polvadera Group and is composed of lahars, conglomerates and tuffs. These rocks form a broad alluvial fan (McPherson et al. 1984) that extends for 15 km southsouthwest of the nearest exposures below the Bandelier Tuff (Dransfield and Gardner, 1985). The contrast in geometry with the Cochiti Formation may indicate that the Puye Formation was deposited in a period of relative tectonic inactivity.

The **El Alto Basalt** (3.2-2.8 Ma) in the northern Jemez Mountains, is contemporaneous with the Tschicoma Formation and probably they have a close petrological relationship (Goff et al. 1989). However this basalt was not included in the Polvadera Group by Smith et al. (1970).

The **San Diego Ignimbrites** were deposited before the collapse of the Toledo Caldera. These deposits are up to 80 m thick below the Otowi Tuff in San Diego Canyon, to the southwest of the Valles Caldera (Turbeville and Self, 1988; see Figure 12). The ignimbrites have been K-Ar dated: the older (A) is 3.64±1.64 Ma in age (unreliable, only 4% ^{40}Ar, see Appendix 1), lithic-rich and non-welded, while the younger

(B) is 2.84±0.07 Ma in age, partly welded and pumiceous (Self et al. 1986). A 3.2 m thick rhyolitic plinan pumice deposit in the upper portion of the Puye Formation has been K-Ar dated at 2.53±0.1 Ma (Turbeville 1986). The lower part of this deposit contains pumice which is similar to that in the younger (B) ignimbrites; the trace element compositions in these two deposits are indistinguishable. These ignimbrites may be deposits from the Rubio Volcano 20 km to the northeast, as they have the same age range and the younger Bandelier Tuff travelled similar distances. If this is the case it would suggest that the Rubio Volcanics form a thin layer about 100 m thick at the base of the Valles Caldera complex, below the Otowi Tuff and that eruptions of the Rubio Volcano were explosive.

3.6 Caldera-forming and Post-caldera events

The **Tewa Group** (1.5 Ma to 0.13 Ma) blankets or intrudes most of the older volcanic units in the Jemez Mountains and is best exposed within the Valles Caldera and Toledo Embayment and on the flanks of the Jemez Mountains (Gardner et al. 1986; Figure 13a). The group represents the events that lead to the formation, collapse and resurgence of first the Toledo Caldera and then the Valles Caldera (Figure 13b). Formations included in the Tewa Group by Griggs (1964), Bailey et al. (1969) and Smith et al. (1970) which have been dated radiometrically as pre-Tewa, 1.5 Ma, have not been included in the Tewa Group here. The Tewa Group consists of the **Bandelier Tuff, Cerro Toledo Rhyolite** and **Valles Rhyolite.** It is almost entirely rhyolite and volumetrically dominated by the 600 cubic kilometres (Smith 1979) of the Bandelier Tuff.

The **Otowi Tuff** (300 km^3) was deposited by the collapse of the **Toledo Caldera** at 1.45±0.06 Ma (Izett et al. 1981) and **Tshirege Tuff** (300 km^3) was deposited by the later collapse of the **Valles Caldera** at 1.1±0.1 Ma (Baldridge et al. 1980). The two tuffs are collectively known as the **Bandelier Tuff.** The Otowi Tuff has a much smaller outcrop than the Tshirege Tuff, below which it subcrops. Both members have prominent ash-fall beds at the base, the Guaje Pumice (Otowi) and Tsankawi Pumice (Tshirege). Both tuffs form thick composite ash-flow sheets with increased welding towards their source, the Tshirege Tuff is more densely welded. The tuffs contain lithic fragments of pre-caldera volcanic rocks, Palaeozoic sediments and rare Pre-Cambrian rocks: the older Otowi Tuff contains more of these lithic

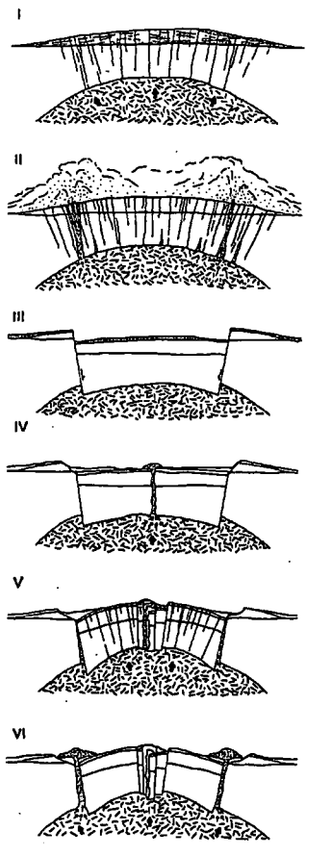

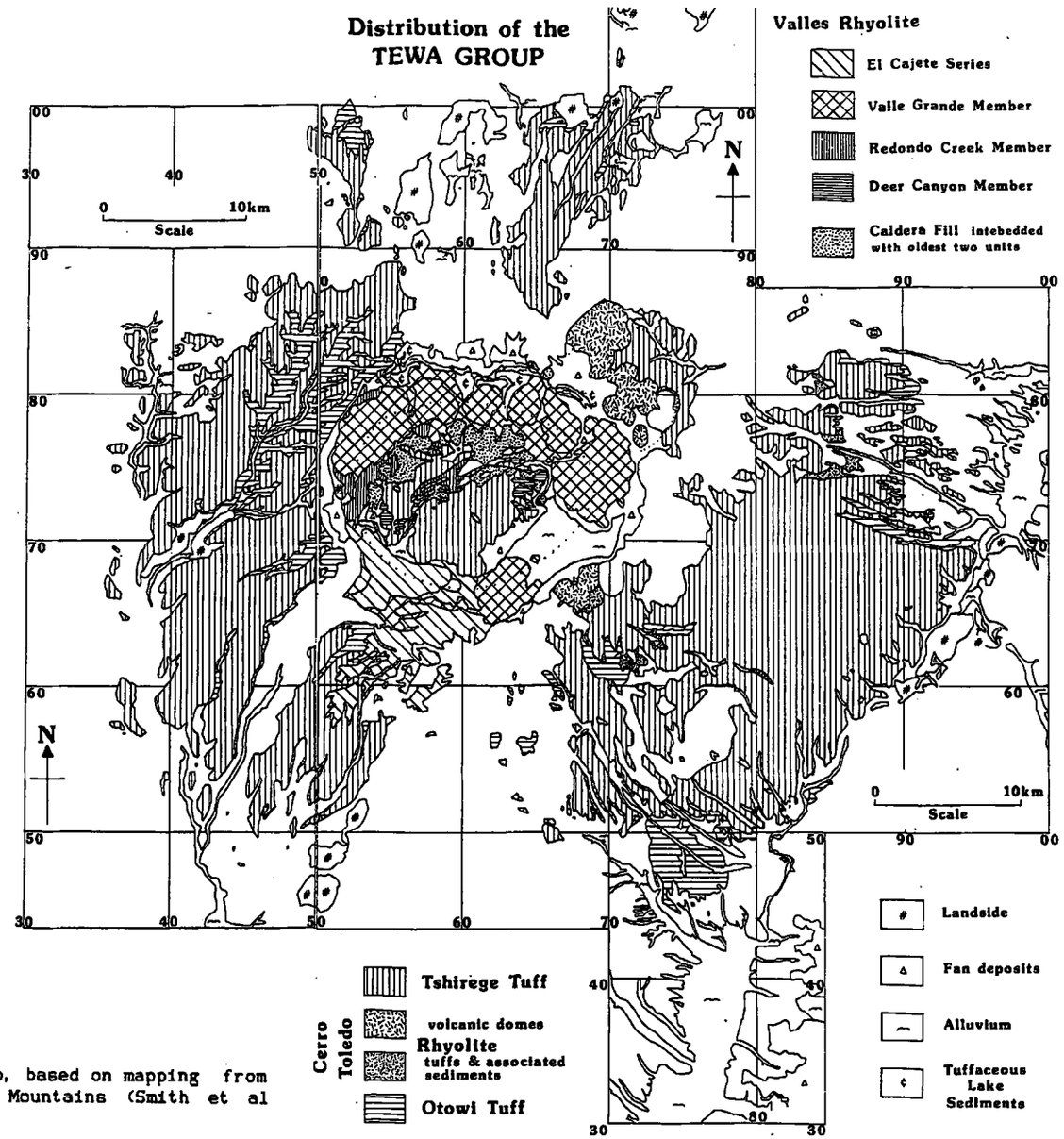

Figure 13a. The distribution of the Tewa Group, based on mapping from the 1:125,000 Geological Map of the Jemez Mountains (Smith et al 1970).

Figure 13b. Six stages of caldera formation and resurgence according to the Smith and Bailey (1968) model: (I) Regional tumescence and generation of ring fractures; (II) caldera forming eruptions; (III) Caldera collapse; (IV) Pre-resurgence volcanism and sedimentation; (V) Resurgent doming; (VI) Major ring-fracture volcanism (Goff et al. 1989).

fragments. The tuffs include abundant quartz and sanidine phenocrysts with sparse mafic minerals in a eutaxitic groundmass. The uppermost part of the younger Tshirege Tuff contains anorthoclase and hypersthene, while the base of the member contains sanidine and fayalite. Chemically the Bandelier Tuff consists of rhyolite with small variable amounts of CaO, K_2O and Na_2O.

The Toledo Caldera was originally considered to be confined to the Toledo Embayment, on the north-eastern margin of the Valles Caldera (Goff et al. 1984). However, Nielson and Hulen (1984) found an average thickness of 400 m of intra-caldera Otowi Tuff under the northwestern Valles Caldera, indicating that the Toledo Caldera had a far larger extent, than had been previously supposed. Kite (1985) showed that the distribution of the Otowi Tuff was symmetrical about the Valles Caldera, and Potter (1983) using pyroclastic-flow directions in the Otowi Tuff, demonstrated that the earlier Toledo Caldera had roughly the same size, shape and location as the later Valles Caldera. Radiometric dating of domes within the Valles Caldera, by Heiken et al. (1986), also suggested that the Toledo Caldera was of similar dimensions and nearly coincident with the Valles Caldera. These latter authors interpreted the Toledo-Valles complex as a pair of nearly coincident trapdoor calderas hinged to the west, with thicker inter-caldera fill in the east of the complex, see Figure 9.

The following origins for the Toledo Embayment have been suggested by Heiken et al. (1986): (i) the site of an earlier but smaller caldera that developed in the Toledo Embayment and erupted silicic tuffs (4 Ma to 1.5 Ma) that are found inter-bedded within the

Puye Formation (Self et al. 1986); the distribution and volume of these Tuffs would support this. (ii) As a scallop-shaped slump formed on the edge of the main Valles-Toledo complex, analogous with the faulting in the Cerro de la Graita area on the northern side of the present Valles Caldera, which is a mass of large slide blocks (Smith et al. 1970). (iii) As a part of the earlier Toledo Caldera, that collapsed beyond the main Valles-Toledo complex. (iv) A collapse that resulted from the pyroclastic eruptions which were followed by the extrusion of the large Cerro Toledo Rhyolite domes. Heiken et al. (1986) considered that a combination of the suggested origins would best explain the origin of the Toledo Embayment, with the possibility that the Jemez Lineament, which passes through it and the Valles Caldera from southwest to the northeast, also exerted some control on its development (Figure 4).

The Toledo Embayment is probably the site of a rhyolite vent that was initially similar to those found in the older volcanic units of the Jemez Mountains. Weakened crust at the intersection of the Jemez Lineament and faults on the western flank of the Rio Grande Rift allowed the Rubio Volcano (4 Ma to 1.5 Ma) to form in the area of the Toledo Embayment. The centre of this depression migrated south-westwards as it grew, until its western margin hit a major rift fault, with thicker crust to the west (Figure 14). At its maximum, it was an area of downwarped country about 24 km in diameter, bounded by the Cerro de la Graita, Toledo Embayment, Rabbit Mountain and the main western ring fracture of the later Valles Caldera. The centre of this topographic depression collapsed about 1.45 Ma ago to form the Toledo Caldera, about 20 km east-west by 15 km north-south, slightly

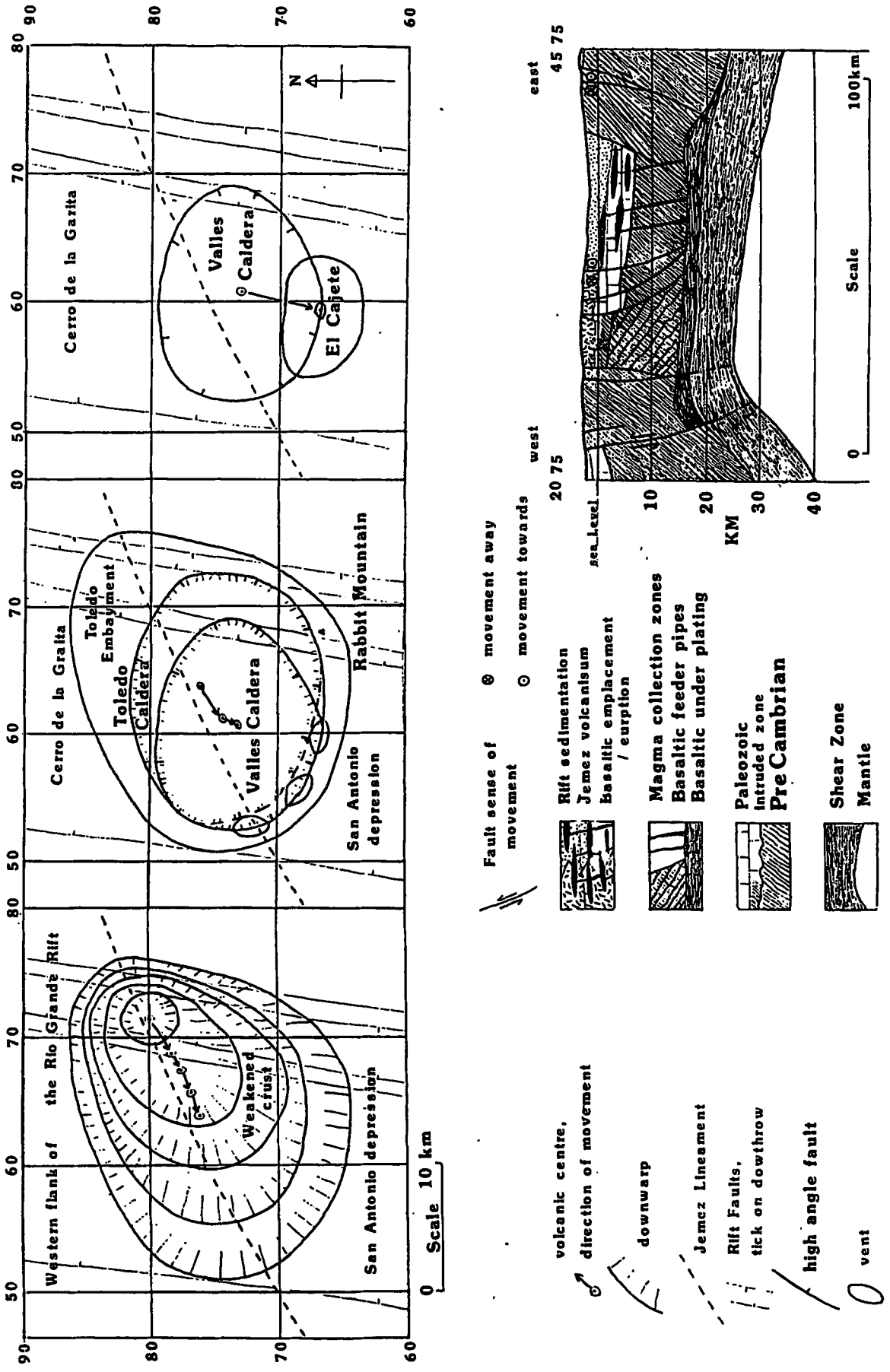

Figure 14. Development of the Rubio Volcano / San Antonio depression (4 Ma to 2 Ma) into the Toledo Caldera (1.45 Ma), Valles Caldera (1.1 Ma) and finally the El Cajete vent (0.13 Ma), time series from left to right. Schematic cross section through the Rio Grande Rift and the Valles Caldera based in part on Ankeny et al. (1986).

larger with less well developed ring fractures than those of the Valles Caldera (16 km by 13 km). The Warm Springs, Cerro Traquilar and Los Poses domes may represent volcanism along one of the main Toledo caldera ring fractures. This sequence of events would help to explain the formation of the faulted and slumped ground in the Cerro de la Graita area and the northeastward location of the Toledo Embayment.

The **Otowi Tuff**, deposited by the collapse of the Toledo Caldera (1.45 Ma), has at its base a plinian deposit known as the Guaje pumice bed (Griggs 1964). This is one of the five widespread fall units at the base of the Otowi tuff that each have a different dispersal pattern, which is consistent with changes in wind direction between plinian phases of the eruption. As the deposits do not contain large lithic volcanic bombs, the material must have fallen some distance from the source vent. the dispersal patterns obtained from maximum lithic size (isopleth) maps and thickness distribution (isopach) maps are good vent location indicators (Walker 1980,1981). The distribution of relatively dense lithic material is least affected by eruption column turbulence and the wind; therefore the isopleths have a symmetrical and restricted distribution around the vent. For the Otowi fall units all this evidence suggests that eruption was from a vent or vents in the centre of the centre of the present Valles caldera.

In the Jemez Mountains a lower unwelded Otowi unit (Kite 1985), is found on the basis of clast orientation to have flow directions that indicate pyroclastic flows moved out from the centre of the present caldera (Potter 1983). Over 60 m of densely welded, lithic

rich ignimbrite was intersected in the VC-1 corehole (53 67) in the southwest of the caldera. This is interpreted as intra-caldera fill, from its thickness and the degree of welding which again suggests that the Toledo Caldera must have been extended that far west.

In the upper part of the Otowi tuff there are prominent lithic lag fall and other proximal lithic breccias (Walker 1985). These are found on the southwestern side of the Valles Caldera topographic wall and are either poorly exposed or absent from sections in other parts of the caldera rim. Individual lag breccias are a maximum of 5 m thick and contain large blocks up to 2 m in size. There are three types: (i) Laterally continuous outcrops restricted to the caldera rim with a lenticular bed form, which is in part matrix supported and thought to represent a lithic lag-fall deposit (Wright and Walker 1977) that has had some lateral transport. (ii) Pods and lenses of matrix-supported lithic fragments set in a matrix of coarse pumiceous ignimbrite. (iii) Flow units with a much greater proportion of large lithic fragments at their base similar to those from Santorini (Druitt and Sparks 1984). These lithic breccias suggest that during the later part of the Otowi eruption, when the Toledo Caldera collapsed, vents opened in the southwest, roughly in the area between Battleship Rock and Redondo Peak (55 77). These vents may have been above the growing Toledo Caldera ring fracture, only three to five kilometres from these deposits, which would be consistent with deposits from the proximal deflation zone of an erupting column. The Toledo collapse burst through at this point due to a combination of the following factors: (i) The western side of the caldera is relatively uplifted and as a result probably has a thinner Pre-Tewa volcanic pile. (ii)

Faster erosion above the major rift fault below the western margin of the present Valles Caldera and the San Diego Canyon fault. (iii) The general southward slope of the Rio Grande Rift resulted in greater erosion in the southwest of the caldera. Thus this part of the collapsing structure was weakest and the eruption blew off the remaining material in places to form vents.

The following is an account of the inter-caldera resurgent volcanic activity, based on Heiken et al. (1986), for details of the K-Ar radiometric dates see Appendix 1. The first stage occurred before the collapse of the Valles Caldera and as a result is discussed here before the Tshirege Tuff.

The **Cerro Toledo Rhyolite** was formed after the collapse of the Toledo Caldera (1.45 Ma), when there was a period of resurgent volcanic activity before the collapse of the Valles Caldera (1.12 Ma). An arcuate line of four domes located along the northeastern side of the present Valles Caldera had previously been mapped as part of the Valles Rhyolite by Smith et al.(1970) and has now been designated as part of the Cerro Toledo Rhyolite, Heiken et al. (1986). Radiometric dates indicate that the two western domes, to the north of the Valles Caldera, Warm Springs (59 81) and Cerro Trasquilar (65 81), were formed at about 1.26 Ma. The Los Posos domes, western (70 78) and eastern (72 77) have been dated at about 1.49 Ma. They are to the northeast of the Valles Caldera, on the boundary of the Toledo Embayment; significantly, mapping has revealed small outcrops of Tshirege Tuff on top of these domes. Apart from the older Cerro Rubio complex (2.18 Ma to 3.59 Ma), domes within the Toledo Embayment have been dated at between 1.20 Ma and 1.62 Ma. Ash fall deposits

from these domes, the Cerro Toledo Rhyolitic Tuffs, have been dated at 1.23 Ma for the upper unit and 1.47 Ma (two fission track ages give 1.43±0.11 Ma) for the lower unit. Thus these ash fall deposits are contemporaneous with or younger than the Otowi eruption and pre date the Tshirege Tuff. The Rabbit Mountain dome (68 67) just to the southeast of the Valles Caldera, has been dated at between 1.52±0.06 Ma and 1.43±0.04 Ma. Along most of Obsidian Ridge, Rabbit Mountain deposits are overlain by the Tshirege Tuff; Thus, they are of inter-caldera age and contemporaneous with the Cerro Toledo Rhyolitic domes, which they resemble petrographically and geochemically. The Rabbit Mountain dome has associated pyroclastic deposits interbedded with rhyolite flows, which trend southeast for 7 km, away from the rim of the Valles Caldera.

Sanidine from the basal Guaje pumice bed of the Otowi tuff has been used to K-Ar date the formation of the Otowi Tuff at about 1.45 Ma ago. This is younger than some dates obtained from intra-caldera deposits, which are up to 1.62 Ma old, while field relationships suggest that the Otowi Tuff is older. This implies that the far more voluminous Otowi Tuff either cooled far more slowly than some of the smaller domes that followed it, or Argon was lost from the glass in some samples, as it devitrified (crystalised), and the date was reset (pers. comm. S Kelley). In general groundmass glass and mesostasis minerals are highly susceptible to alteration and Argon loss (Baldridge et al. 1980) In cases where there is no subsequent Argon loss, the closure temperature is defined as the temperature at which a sample had its apparent age. The K-Ar system has a range of closure temperatures for different minerals which depend on effective grain

size and fracturing. A range of approximate closure temperatures are as follows: 550° C for hornblende; 350° C for muscovite; 300° C for biotite; 250° C for Sanidine; and 230° C for feldspar.

The following description of the Tshirege Tuff is based on Self et al. (1986).

The **Tshirege Tuff**, deposited by the collapse of the Valles Caldera (1.1 Ma), has at its base an extensive plinian deposit, the Tsankawi pumice bed, which represents the first stage of a series of plinian eruptions that led to the collapse of the Valles Caldera. The pumice beds deposited during these eruptions consist of four coarse pumice fall units and two finer ash fall units. The second unit is most wide-spread and has some ultraplinian characteristics (Walker 1980), it is thicker 20 km downwind of the supposed vent and has seven times the normal Tshirege Tuff phenocryst content. The dispersal patterns are similar to basal units of the Otowi Tuff, with a centrally located vent or vents. This is borne out by the distribution of the third unit a fine pyroclastic flow all around the present caldera. In places the last unit grades into a ground surge pyroclastic flow deposit, which represents an irreversible change in the eruption from fall to pyroclastic flow.

Above this unit ignimbrites are widely distributed around the Jemez Mountains and almost all areas, except perhaps the highest peaks, must have been covered, with the thicker deposits ponded in valleys. Kite (1985) recognized a similar sequence all around the caldera, which suggests that these events took place at the same time and were from a central source. The lack of well developed proximal lithic breccias around the central caldera implies a lack of ring

fracture vents. This is not conclusive, as proximal lithic deposits associated with the ignimbrites may have been removed by subsequent erosion. A likely site for such a vent could be the intersection of the Jemez fault zone and the ring fractures on the south-western side of the caldera rim. Evidence for this is found in the older Otowi Tuff (Walker 1985) and it is suggested that this pathway would have, most probably, been choked with material from the earlier eruption.

The **Valles Rhyolite** was erupted after the collapse of the Valles Caldera (1.12 Ma), when there was a period of resurgent volcanic activity, which although extended in time and space, gradually died down and became quiescent (0.13 Ma), apart from continued hydrothermal activity. The rhyolite consists of domes, flows and tuffs erupted inside the Valles Caldera. Lavas within the formation were erupted and similar material was intruded during the growth of the resurgent dome and later 'moat' rhyolites; that postdate and surround the central resurgent dome (Figure 13b). This resurgent dome is faulted and has an apical graben (Smith and Bailey 1961), which trends northeast-southwest and is about two to three km wide. Nielson and Hulen (1984) suggested these dome faults were influenced by older faults associated with the northeast trending Jemez lineament. They developed a numerical model for the formation of the Redondo Dome which suggests that the top of the causative magma body is located at a depth of about 4,700 m or 2,200 m below sea level. This is 1,460 m below the deepest geothermal well in the dome, so no intrusions related to this magma have been penetrated. The bounding faults were active early in the uplift history (post Valles) of the dome and account for many of the structural differences between hypothetical

and real dome development.

Smith et al. (1970) divided the **Valles Rhyolite** into six members, from oldest to youngest: the **Deer Canyon, Redondo Creek, Valle Grande, Battleship Rock, El Cajete** and **Banco Bonito** members; these are the youngest volcanic rocks in the Jemez Mountains. Dates obtained for the Valles Rhyolite range from 1.04 Ma to 0.13 Ma (Gardner et al. 1986; Appendix 1). Determinations for the two oldest members have been unsuccessful, due to extensive hydrothermal alteration, though field relationships suggest that these deposits post date the Tshirege Tuff. The three youngest members, the El Cajete Series of Self et al. (1988), flowed through a breach in the southwestern caldera wall and as a result overlie substantially older formations (Smith et al. 1970; see Figure 13a). The formation is petrographically very heterogeneous (Bailey et al. 1969) varying from aphyric to coarsely prophyritic, with an absence of quartz in the Redondo Creek member. Chemically the three oldest members are high-silica rhyolites, while the younger members are a lower-silica type that contains more FeO, MgO, CaO, TiO_2 and P_2O_5 than the older high-silica rhyolites. The youngest units of the Valles Rhyolite are only found in the southwestern moat zone of the Valles Caldera (Gardner et al. 1986).

It should be noted that the Toledo Embayment and the El Cajete area, which is the site of the most resent volcanism (0.13 Ma) in the Jemez Mountains, look strikingly similar on satellite images (Chapin 1989; New Mexico Geol. Soc. 1982). It is possible that the major Rio Grande Rift boundary fault coincident with the western boundary of the Valles-Toledo complex, has channelled the most recent magmatism

southward after progressively shifting southwest ward for the last few million years (Figure 14).

3.7 The Geothermal history and system in the Valles Caldera

The Jemez Mountains have been and are the site of phyllic and argillic hydrothermal alteration due to the waning phases of several volcanic episodes within the volcanic field (Woldegabriel 1990). The present Valles Caldera is the site of a high-temperature geothermal system, with a probable shallow magmatic heat source and convecting hydrothermal fluids which are dominantly meteoric-water (Dondanville, 1978; Goff and Grigsby, 1982).

The results of work on hydrothermally altered clays by Woldegabriel (1990), from the Jemez Mountains, are summarized below.

Both acid-sulfate (kaolinite-alunite) and neutral-chloride (sericite-chlorite) alterations are present in clays <2 m separated from hydro-thermally altered rocks in the volcanic field. As is typical for most volcanic hydrothermal systems, the acid-sulfate alteration occurred at low temperatures (< 100° C) under near-surface conditions due to the oxidation of hydrogen sulphide escaping from deep neutral-chloride fluids. Sericite-chlorite alteration has been found down the VC-1 (53 67) and VC-2A (54 75) bore-holes, in the Redondo Creek area, and in the intensely altered Keres Group rocks of the Cochiti district (to the south of the Valles Caldera). The latter is associated with the typical high temperature (> 100° C) of neutral-chloride waters of a liquid-dominated geothermal reservoir.

Hydrothermally altered clays show that there were three major

hydrothermal events in the Jemez Volcanic Field which formed hydrothermal mineral assemblages. These are represented by Mid-Miocene (17 Ma to 11 Ma) clays found at the bottom of the VC-1 core-hole; Late Miocene (8.2 Ma and 6.96 Ma) clays formed in the waning stages of the Keres Group volcanism; and Pleistocene (1.34 Ma to 1.0 Ma) alteration of Palaeozoic rocks in the VC-1 core-hole. This alteration will have affected the densities of formations in the Valles hydrothermal system, in some places reducing it by removing material and in others (usually at higher temperatures and pressure) increasing it by depositing denser metallic mineral phases or filling pores with secondary mineralisation such as quartz. The last thermal event is probably related to the eruption of the Toledo and Valles calderas and base-metal sulphide ore minerals found in the same borehole were deposited at this time. Quartz veins in the Cochiti district containing gold and silver are late Miocene in age (5.6 Ma to 6.0 Ma), which is later than the mid-Miocene hydrothermal episode in the caldera area.

The thermal regime of the Jemez Mountains and conductive heat flux in borehole VC-1, outlined by Sass and Morgan (1988), is summarized below.

The heat flows associated with the Valles Caldera are about an order of magnitude above the continental mean, in excess of 500 mWm^{-2}, and are thought to be associated with a magmatic heat source. The conductive heat flow in VC-1 Phanerozoic sediments and 'moat' volcanics is 463 ± 15 $mW\ m^{-2}$. This is very similar to the peak heat flow in the coeval Long Valley Caldera in eastern California (Lachenbruch et al. 1976 a,b) and about half that of the younger

Yellowstone Caldera in northwestern Wyoming (Morgan et al. 1977). Kolstad and McGetchin (1978) interpreted the thermal gradient down to three kilometres at the Fenton Hill hot dry rock drilling site (49 71) (about one kilometre from the western rim of the caldera), to be consistent with the conductive cooling of a major magma chamber. They proposed that this chamber was larger in area than the caldera, with its top just three kilometres below sea level, about 5½ km below ground level. It was emplaced (Kolstad and McGetchin, 1978) during the formation of the Valles Caldera (1.0-1.1 Ma ago). Recent geothermal data from this site, Harrison et al (1986), have shown that the heating is probably a very recent event, less than 40,000 years ago and the distribution of surface heat-flow in the caldera is asymmetric (Figure 15). This suggests that either the heat source is asymmetric, or heat transfer is in part convective (this is confirmed by deeper boreholes). Heat flow data from VC-1 indicate higher near surface heat flow on the southwestern margin of the caldera; the water table results in a break in the geothermal system with a conductive heat flow of 463 mW m^{-2} below this between 335 m and 737 m.

The main surface and subsurface drainage from the Valles Caldera follows the topography to the southwest, in the vicinity of the VC-1 core-hole (Figures 5 & 16). Dates from the travertine deposits at Soda Dam, about two kilometres downstream of VC-1 (Goff and Shevenell, 1987), indicate a continuous subsurface hydrothermal flow during the past million years that has resulted in these deposits. Dzurisin et al. (1990), have shown that heat input from basaltic intrusions is required to maintain Yellowstone's silicic magmatic system and shallow hydrothermal system over periods longer than about 100,000 years, this

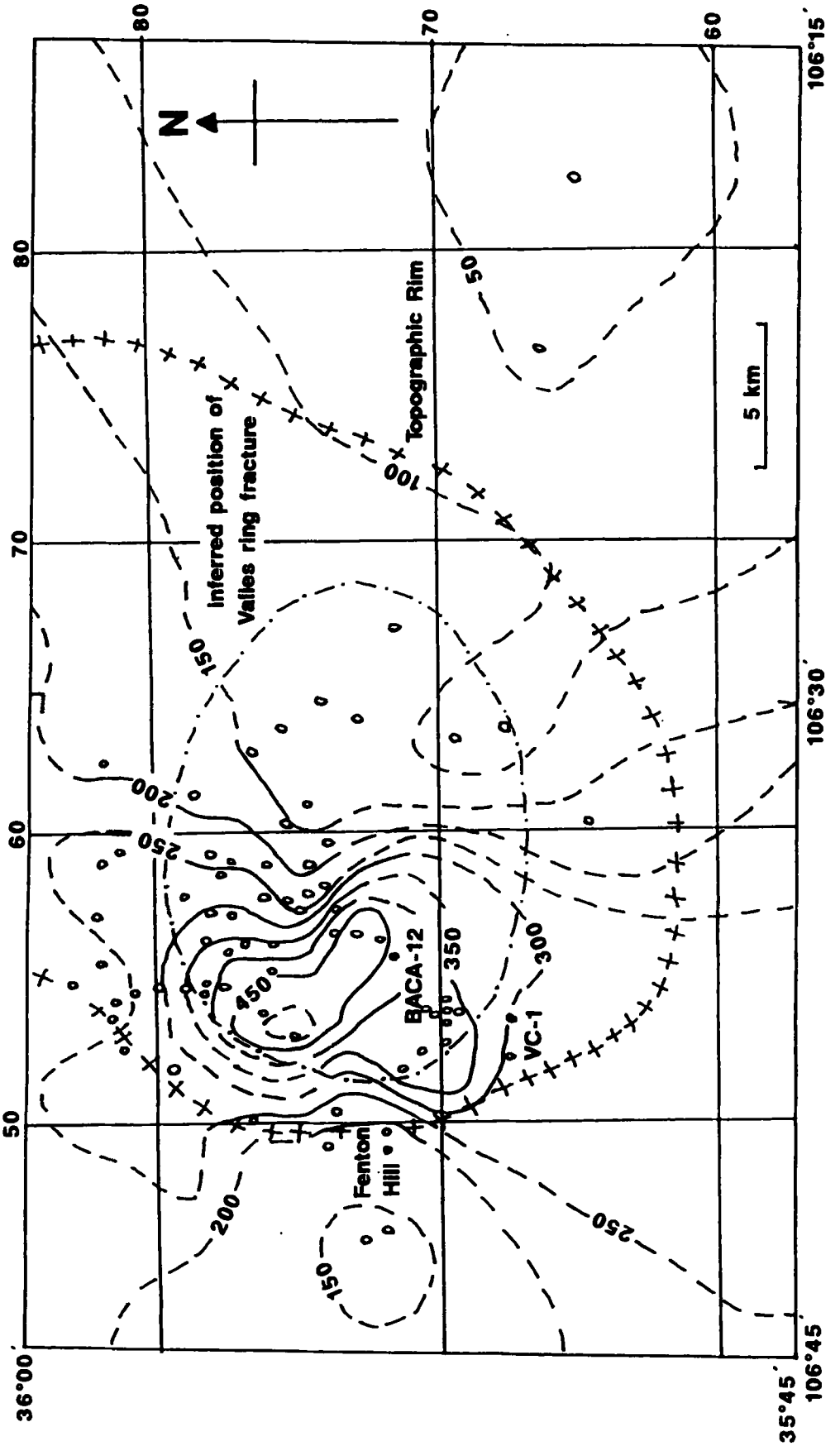

Figure 15. Near surface heat flow (mW m^{-2}) in and around the Valles Caldera. Circles show location of the data points, grid added (Sass and Morgan 1988).

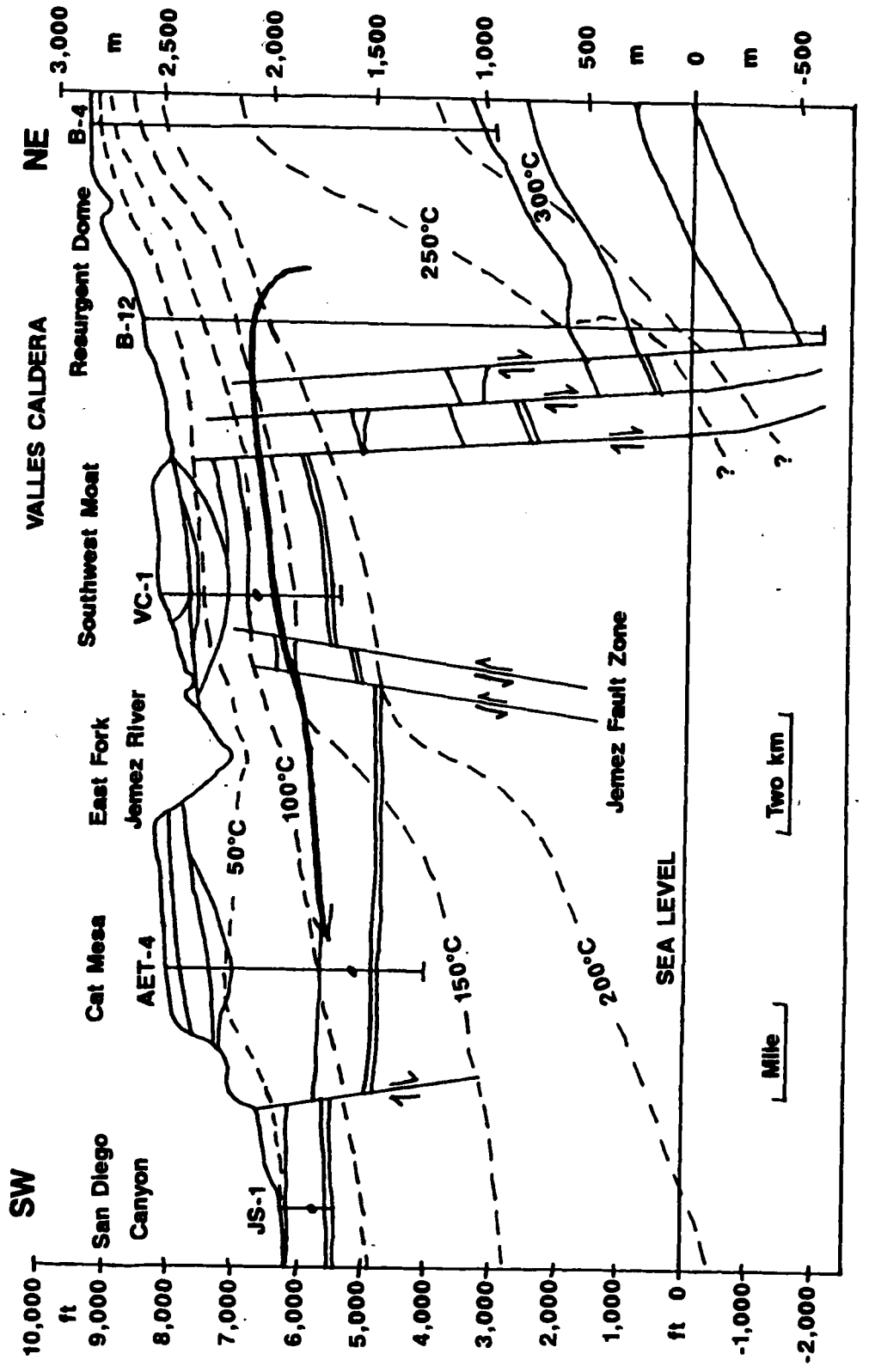

Figure 16. Cross section showing structure and isotherms through the southwestern edge of the Valles Caldera (vertical exaggeration x3·5). Dots along boreholes indicate thermal aquifers, the line and arrow show a possible thermal fluid flow out of the caldera, lithology omitted for clarity (from Goff et al. 1988).

is also likely for the Valles Caldera Hydrothermal system. Homogenization temperatures from secondary fluid inclusions in VC-1 show that the present temperatures were established as the inclusions were formed and support a continuous heat source over an extended period of time (Sasada 1988). Drainage from the caldera must transfer heat laterally to the southwest and must be a factor in the asymmetric near-surface heat flow distribution. In the eastern caldera stable isotope data indicate that heat flow may be suppressed by meteoric water recharging the deep hydrothermal system (Vuataţaz and Goff, 1986). Subsurface drainage to the east, outside the caldera, complements this and may contribute heat from the caldera downflow to geothermal groundwater anomalies in Rio Grande Rift basins (Morgan et al. 1986). Recent resurgent volcanism in the southwestern part of the Valles Caldera is also likely to have contributed to the present heat flow pattern.

3.8 Geophysical work on the Jemez Mountains area

Shallow crustal seismic refraction studies of the Jemez mountains show that the structure beneath the area is complex (Olsen et al. 1986; Ankeny et al. 1986).

The following is a summary of the seismic results obtained by Olsen et al. (1986) and a comparison of these results with Bouguer gravity data (Cordell et al., 1982; Cordell and Keller 1984).

The time for seismic waves either to reach the first refractor from a shot, or return to a receiver at the surface as a head wave from the refractor is called the time term. The total travel time for a refracted seismic wave is composed of the time terms, to and from the surface along with the time spent travelling along the refractor. Time term contours for the Jemez mountains show an increase eastward from values near to zero along the Nacimiento uplift to values of nearly a second along the axis of the Rio Grande Rift (Figure 17). The overburden thickness as shown by the term time contours increases to the east into the Rio Grange Rift. Time terms can in effect be used to remove the overburden by calculating a thickness based on the near surface velocity allowing the refractor P wave velocity to be determined more precisely. Olsen et al. (1986) found that the average refractor velocity below the Jemez Mountains was 5.86 0.01 km/s. This is within the standard deviation for their result from a reversed refraction line along the Nacimiento uplift (5.89±0.07 km/s) to the west of the Jemez Mountains where the Pre-Cambrian basement outcrops or is near to the surface. Time terms can be converted to depths giving a rough estimate of the basement

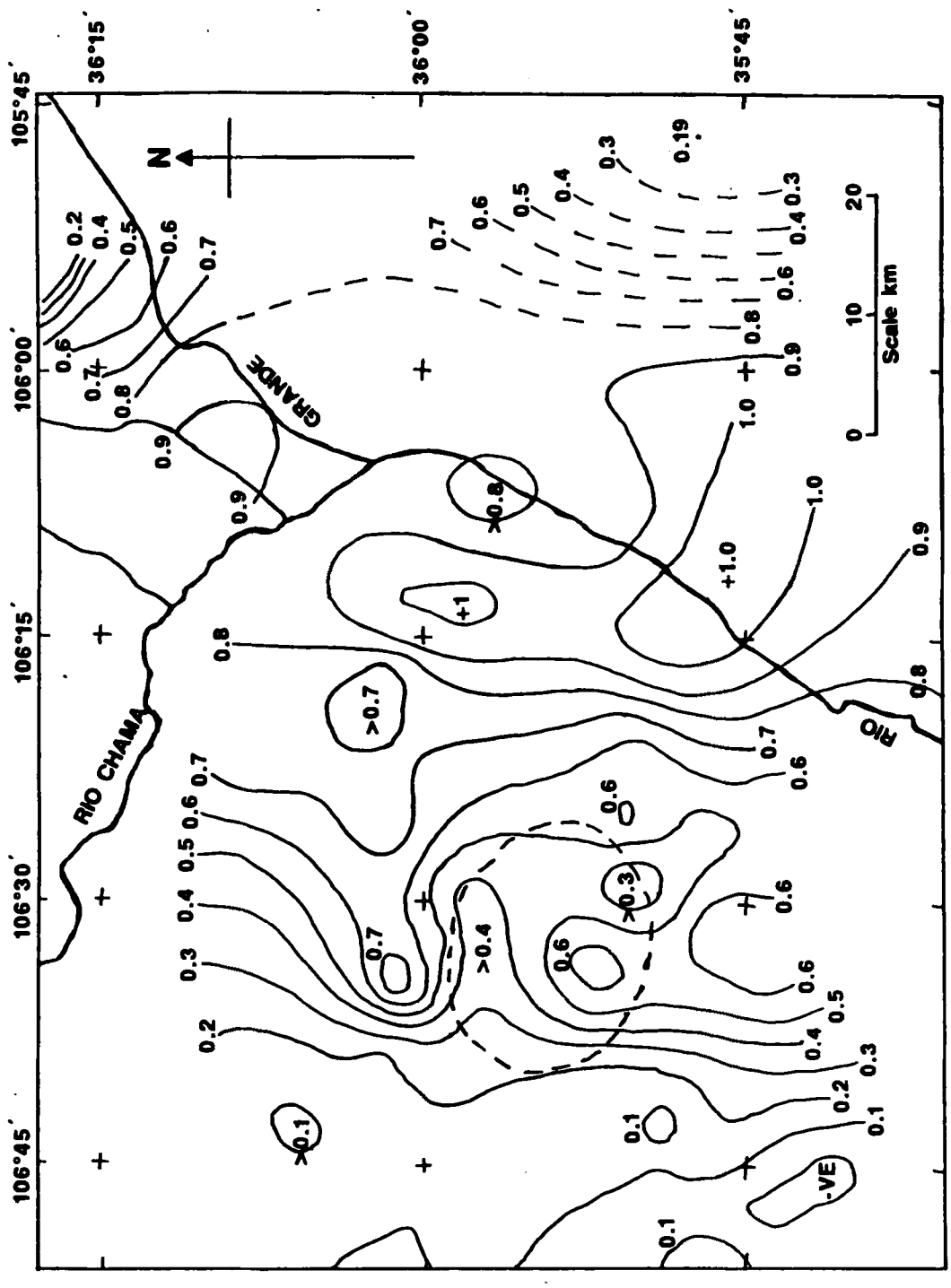

Figure 17. Term Time contours (in seconds) derived from the CARDEX experiment, dashed lines indicate uncertainty (from Olsen et al. 1986)

topography, if a near surface velocity of about 3.0 km/s, observed close to some shot points is assumed. These estimates fit reasonably with those based on gravity (Cordell, 1976) and electromagnetic techniques (Williston et al. 1979) as will be shown below. Gravity data are based on the Rio Grande Rift maps of Cordell et al. (1982) and Cordell and Keller (1984); regional trends were not removed. With a reduction density of 2.2 g/cm^3 Olsen et al. (1986), produced a Bouguer anomaly map (Figure 18). This reduction density was used for two reasons: first, they thought that this was about the same as the water-saturated density of the Santa Fe Formation, the dominant unit in the Rio Grande Rift (Cordell 1976); second, this density was considered a good average for volcanic formations of the Jemez Mountains volcanic field. In fact this reduction density is too low as the material within the Valles Caldera has a density of about 2.35 g/cm^3, in the surrounding Jemez Mountains densities are up to 2.8 g/cm^3 for the Tschicoma formation (Appendix 2) and Williams (1979) suggested that the density of the Santa Fe Formation was 2.4 g/cm^3. Thus a reduction density of between at least 2.4g/cm^3 and 2.5g/cm^3 would have been more suitable. Too low a reduction density will result in Bouguer corrected gravity anomalies correlated with topography and not subsurface density variations (Nettleton 1939).

The Bouguer anomaly map produced by Olsen et al. (1986) shows the following features: highs over the Nacimiento uplift and Sangre de Cristo range where denser Pre-Cambrian rocks are at or near the surface; a high to the south of the Valles Caldera due to the relatively dense Keres Group volcanic rocks; a relatively high spur along the Pajarito fault between the Valles-Toledo complex and the

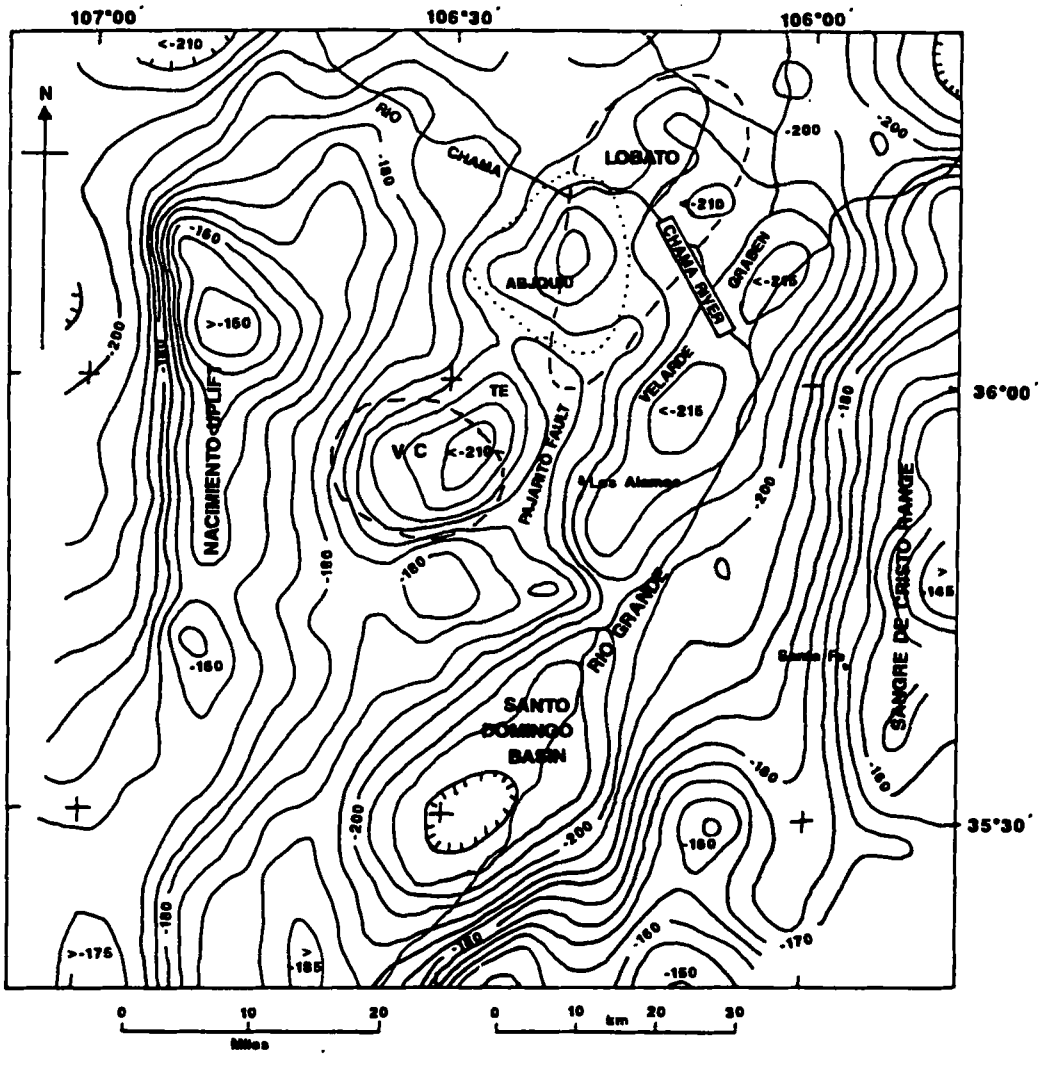

Figure 18. Bouguer anomaly map of the Jemez Mountains and Española basin area, reduction density 2·2 g/cm³ with 5 mGal contours (Olsen et al. 1986). Chama river (box) route of 1930-35 levelling surveys which suggest continued subsidence of the Rio Grande Rift (Reilinger and York, 1979).

Española Basin; a low in the Valles Caldera offset into the Toledo Embayment indicating thick low density volcanic deposits; lows over the relatively lower density sedimentary basins of Española, San Luis (partly volcanic), Abiquiu and San Domingo; and a relatively low anomaly over the area of the Lobato seismic swarm.

Ankeny et al.(1986) modelled the velocity structure beneath the Jemez Mountains and Rio Grande Rift directly to the east by simultaneous three-dimensional (3D) travel-time inversion of earthquake and refraction survey data. They found a good correlation with known geological structures, such as the major uplifted Pre-Cambrian blocks and sedimentary basins associated with the Rio Grande Rift. Below the southern part of the Valles Caldera they found an approximately cylindrical low-velocity body from about 1½ km down to 10 km below sea level. This may be the result of material being intruded into, and partial melting of, the upper crust during the formation of the Jemez Mountain volcanic field and would be consistent with a conductive cooling magmatic heat source 3 km below sea level at Fenton Hill (49 71; 5½ km below the surface). The resulting solidified body (there is no S-wave attenuation) may have a significantly different composition and velocity (5.6-5.8 km/s) from that of the Pre-Cambrian basement rocks (>5.9 km/s), resulting in the observed anomaly. Raised geotherms in the vicinity of the caldera and the heating of the basement rocks could also give rise to such an anomaly.

Segar (1974) conducted a gravity survey in the Valles Caldera; 730 stations were surveyed and a density of 2.45 g/cm^3 was used for Bouguer and terrain corrections. The survey was tied to the U.S.G.S.

gravity network with two loops (return trips between a network station and the new base station, so that the value of gravity at the base station can be found) and values were computed using the International Gravity Formula. Regional gravity effects due to isostatic conditions were removed by approximating them to an increasingly negative regional field of about one milligal per 3.2 km (two miles) towards the NNW with an overall value of between about -220 milligals and -230 milligals. Fifteen milligals were subtracted from all readings taken in areas of Palaeozoic outcrop, as most of this area had a value of about +15 milligals. As no geological control was available in the east of the area, no further adjustments were made. High frequency components of less than 10,000 ft (3,050 m) wavelength in the data, due to local near-surface density changes, were removed. A profile across the centre of the caldera was modelled to estimate the density contrast. The data were then iteratively modelled in 3D with a simple single 0.35 g/cm^3 density contrast. The resulting plot of depth to basement (Figure 19) shows that the caldera is asymmetrical, with only 760 m of low density caldera fill in the extreme west and over 4,570 m under Valle Grande (1,525 m below sea level) in the east. Similar results were obtained by Wilt and Vonder Haar (1986) with two 2D gravity profiles using the densities of 2.12 g/cm^3 for near surface caldera fill, 2.40 g/cm^3 for the underlying volcanics and 2.65 g/cm^3 for basement rocks, though the maximum depth to the basement is 1,000 m less than in Segar's (1974) model. These models are limited because in a 2D gravity profile the half strike (thickness of the body at right angles to the profile) is assumed to be infinite unlike a 2½D gravity profile where the half strike of each body can be adjusted.

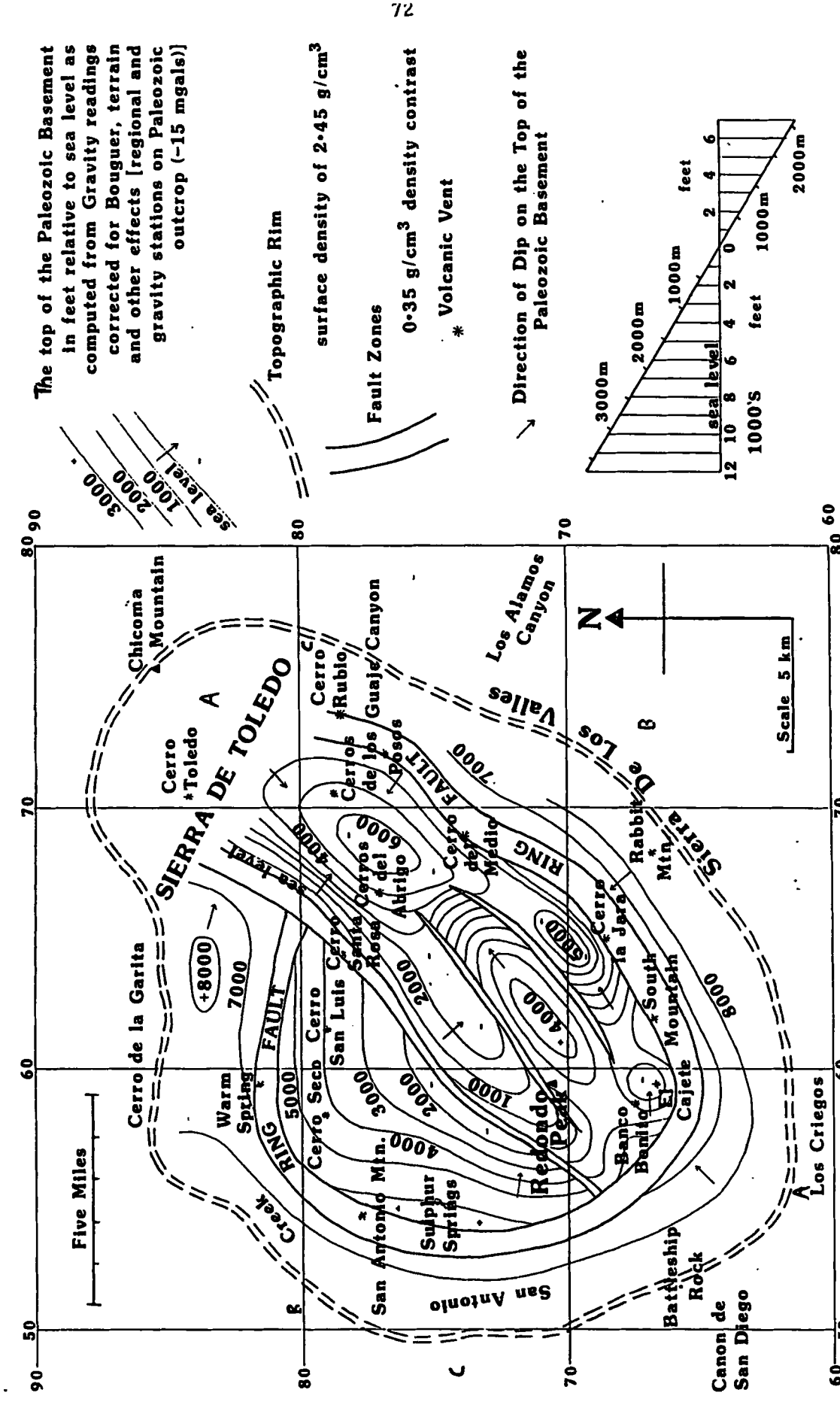

Figure 19. Plot of depth to Valles basement based on Seger (1974)

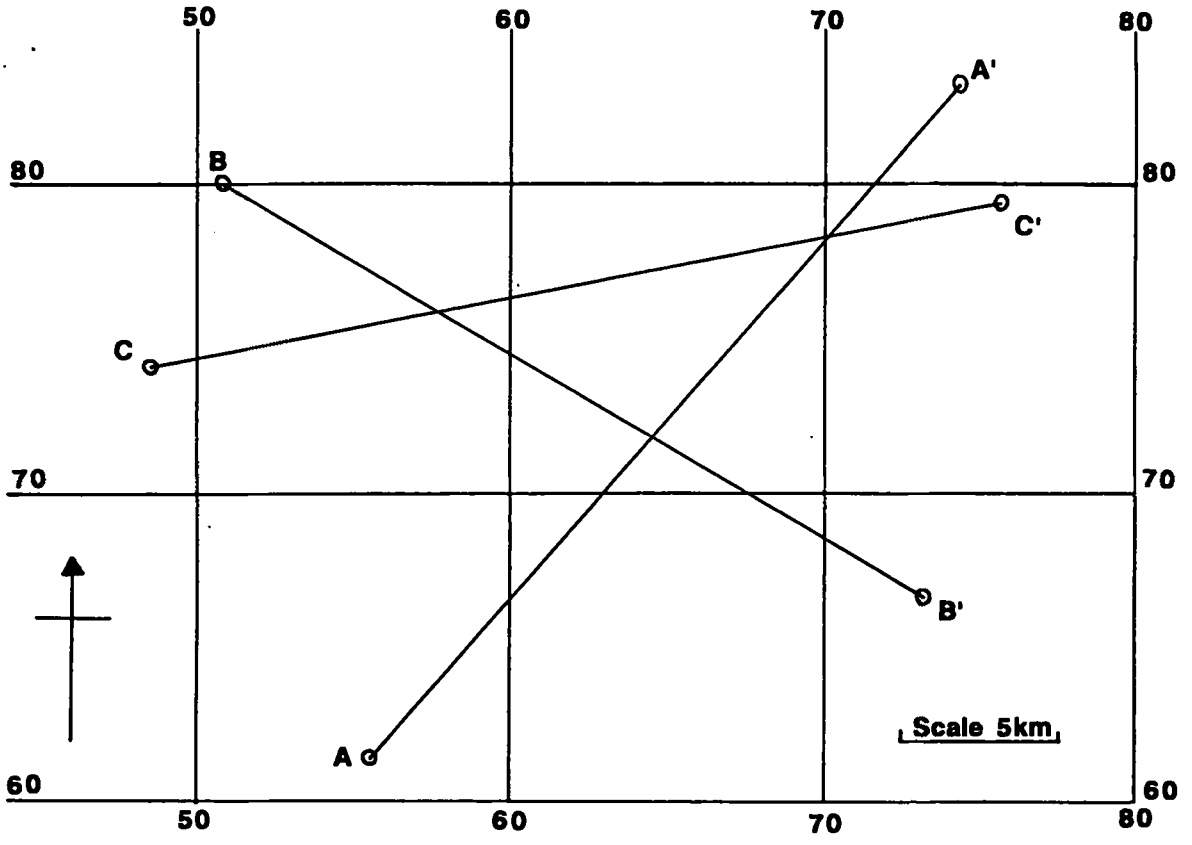

Figure 20. Location of Profiles A-A' , B-B' and C-C' in the Valles Caldera area.

Also the Palaeozoic rocks below the Valles Caldera were not modelled and the two profile have a 25% or 850 m difference in thickness at their intersection not the 10% stated by Wilt and Vonder Haar (1986). It will be shown below that Segar's (1974) model gives a better fit for the basement structure and that a reinterpretation of the shallow subsurface structure has been necessary. Later geothermal boreholes in the east of the caldera have helped to constrain the depth to basement. Heiken et al. (1986) have proposed, on the basis of this asymmetry in fill thickness, that the Valles Caldera is a "trap-door" caldera. The existing data have been remodelled here using more sophisticated software than was available in 1974.

3.9 2½D gravity profiles across the Valles Caldera

Three 2½D gravity profiles were modelled for this work using GRAVMAG (Pedley, 1991) across the Valles Caldera, New Mexico (Figure 20). The gravity values were derived from published maps of Segar (1974). The densities used to produce the plot of depth to the Palaeozoic basement (Figure 19) by Segar (1974) were 2.10 g/cm^3 for the Caldera infill and 2.45 g/cm^3 for normal surface densities, a density contrast of 0.35 g/cm^3. Compared to other densities obtained for rocks in the Valles Caldera (Appendix 2) these are rather low and so higher densities were used for the 2½D gravity profiles. In the 2½D gravity profiles not only was the density contrast with the background density modelled but the half strike or the thickness of the body at right angles to the profile modelled. A model was constructed from a series of user-defined interlocking

polygons, each with a unique density and half strike length. As the height of each gravity value along a profile is entered the terrain is defined. GRAVMAG models the polygons in terms of their density contrast with a chosen background density and is a highly interactive program, allowing the shape, density and half-strike of individual polygons, and thus the calculated gravity, to be changed easily. As GRAVMAG only permits one half strike length for both strike directions on a body an average value must be used if there is a difference in the thickness of the body in both directions. The best fitting values for the main bodies in the profiles were as follows : 2.2 g/cm^3 with a half strike of 2km for alluvium and fan deposits; 2.35 g/cm^3 with a half strike of 10km for caldera tuffs and rhyolites; 2.55 g/cm^3 with a half strike of 10km for Palaeozoic rocks such as the Madera Limestone and Sandia Formation; and a background density of 2.65 g/cm^3 for PreCambrian rocks beneath the caldera. This is 0.20 g/cm^3 higher than the density at which the data were originally reduced, but since it is applied to all the data, makes no difference to the final model and is more consistent with the known basement density. Segar (1974) had removed the regional gradient on his map and for all three profiles a further constant regional anomaly of 17 milligals was also removed from the data before modelling. As the western end of the profile C-C' was constrained by boreholes it was modelled first and then the other two profiles A-A' and B-B' were modelled so that they were in agreement to within 100m at intersections between them. They can be compared with profiles based on Segar's (1974) model, in which suitable half strikes have been added for 2½D modelling (see Figures 21b, 23b and 24b). Segar's (1974) model of the Valles Caldera

(Figure 19) showed the following: a ring fault running 3 km to 5 km inside the topographic rim with a downthrow of between 1,000 ft (305 m) in the northwest and 10,000 ft (3,050 m) in the southeast; three northeast to southwest trending faults about 3 km apart centred on Redondo Peak (59 70) with downthrows of between 1,000 ft (305 m) and 5,000 ft (1,525 m); a maximum basement dip of 37° northeastward (66 74) and 48° southeastwards (67 79); and a maximum depth of 6,000 ft (1,830 m) below sea level near Cerros del Abrigo (68 77) (see profiles A and C, Figures 21b and 24b), or 14,000 ft (4,270 m) below the surface.

The first profile A-A' (Figure 21) runs from the southwest 555 614 near Los Criegos to the Northeast 743 832 near Chicoma Mountain in the Toledo embayment. The Palaeozoic sediments below the caldera were modelled as a 1,000 m thick and without them the fill of the caldera tuffs and rhyolites would have to be 330 m thicker. The profile shows that the caldera is shallow in the southwest and drops in a series of fault blocks down to a depth of 3 km some 500 m below sea level. The maximum depth to the base of the caldera tuffs and rhyolites 3,600 m is over 1000 m shallower than in Segar's (1974) model (Figure 21b). The largest fault, in a similar position to Segar's (1974) ring fault has a downthrow to the northeast of 1,000 m compared to 1,500 m for the ring fault. The other faults have downthrows of between 200 m and 600 m and could be replaced by a slope with an average dip of 9°. At the northeastern end a 100 m high 3 km wide fault block was modelled, without this the calculated profile would be a further 3 milligals below the observed values. The top of this fault block may mark the base of the earlier Rubio Volcano which did not collapse

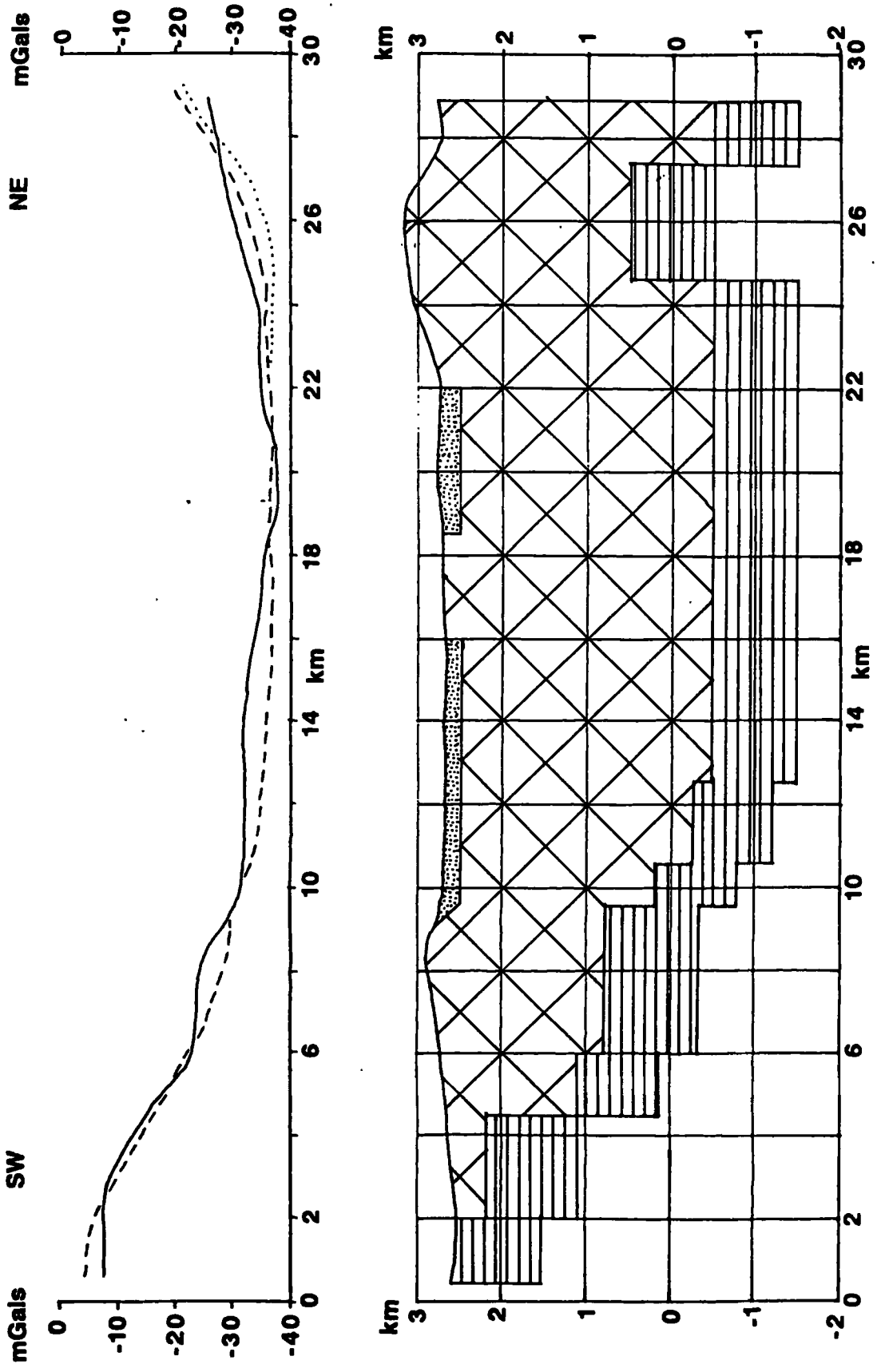

Figure 21. Profile A-A' SW 555 614 to NE 743 832. Solid line is observed profile, Dashes are calculated profile, Dots are calculated profile with no upward step in the formations, horizontal and vertical scales in km. Dots density 2·20 g/cm³ half strike 2 km; Cross-hatching 2·35 g/cm³ half strike 10 km; Horizontal lines 2·55 g/cm³ half strike 10 km; Background density 2·65 g/cm³

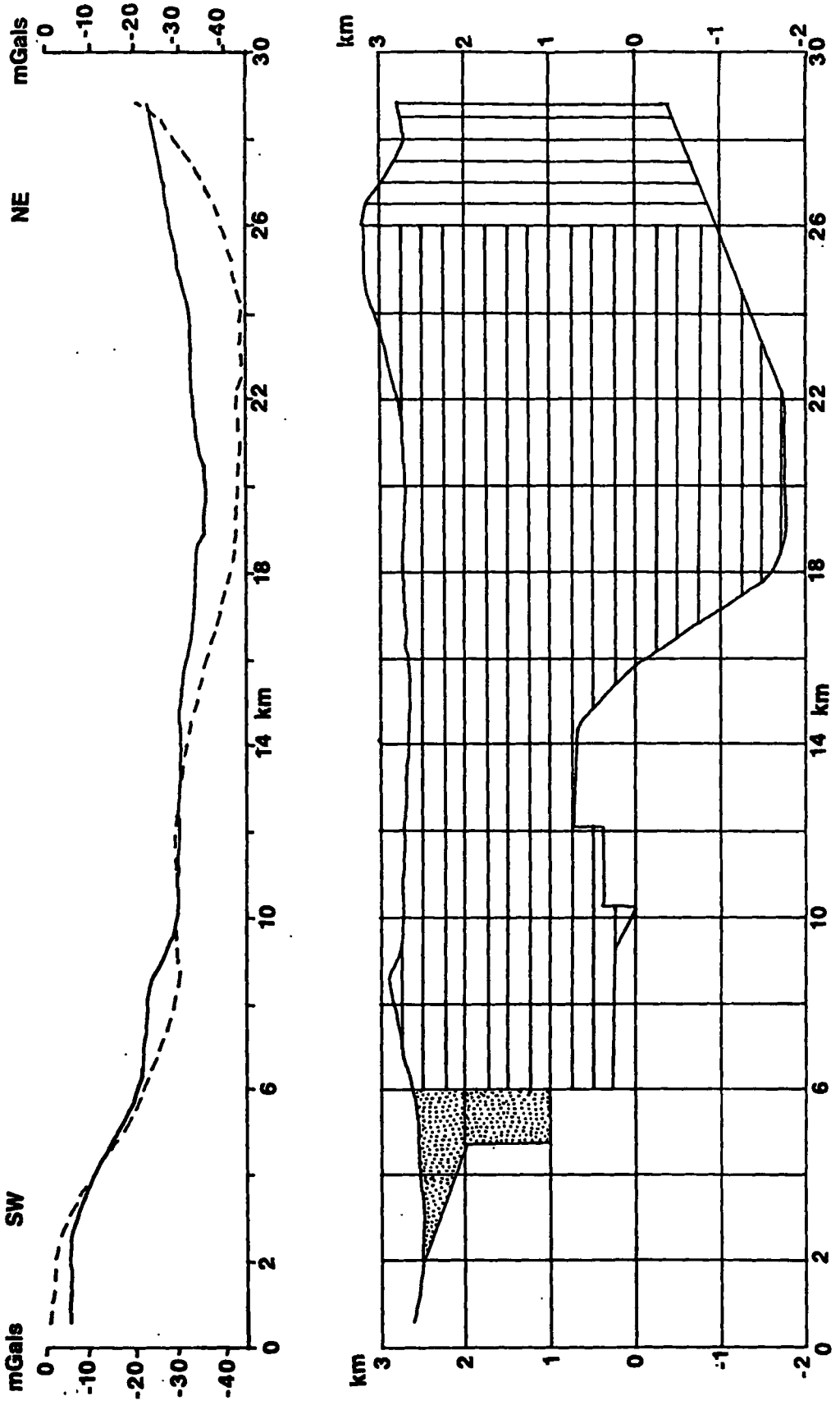

Figure 21b. Profile A-A' SW 555 614 to NE 743 832. Solid line is observed profile, Dashes are calculated profile, based on Segar's (1974) model, horizontal and vertical scales in km. 2·10 g/cm³ density: Dots 2 km half strike; vertical lines 4 km half strike; horizontal lines 6 km half strike; Background density 2·45 g/cm³

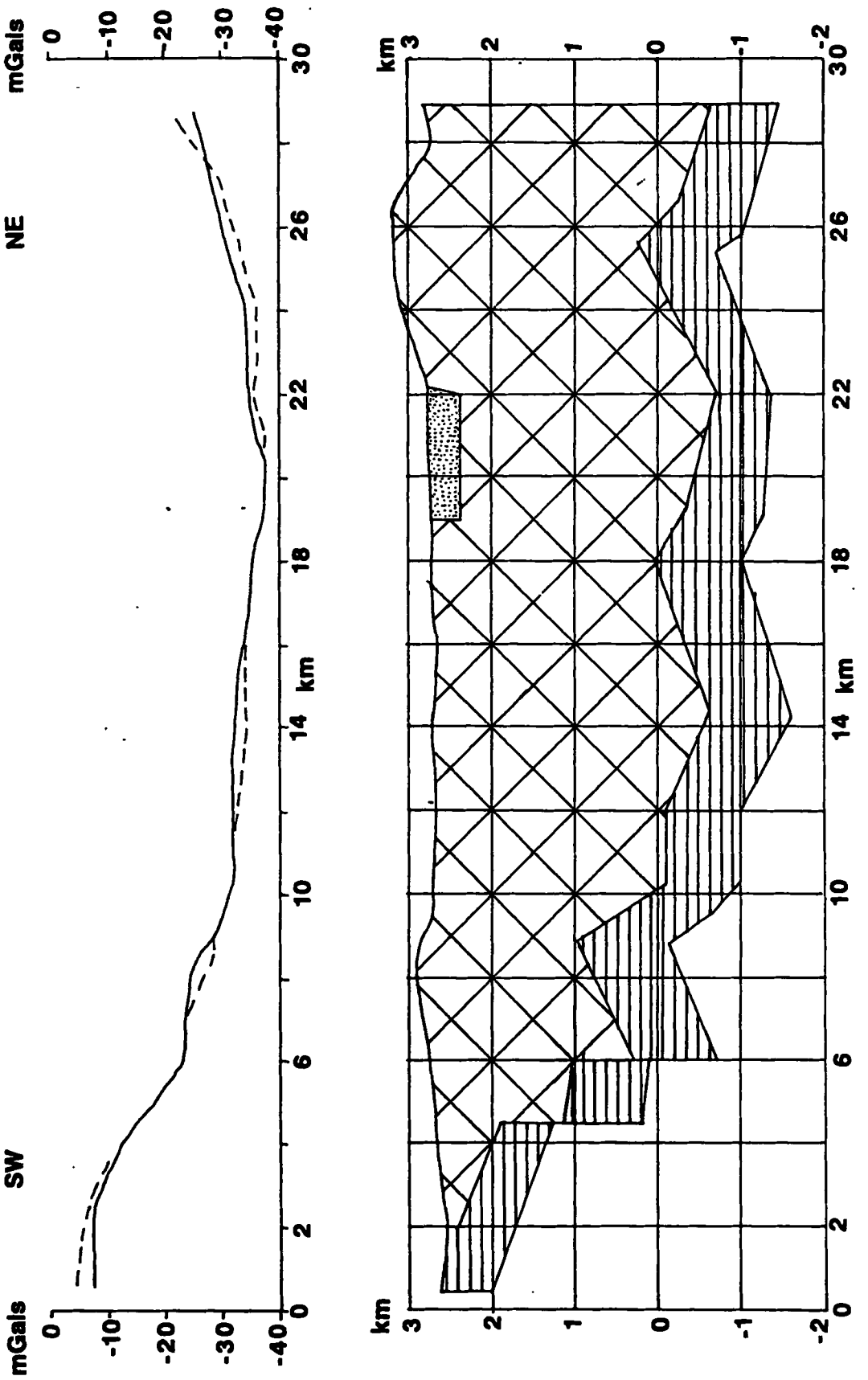

Figure 22. Profile A-A' Alternative SW 555 614 to NE 743 832. Solid line is observed profile, Dashes are calculated profile, horizontal and vertical scales in km. Dots density 2·20 g/cm³ half strike 2 km; Cross-hatching 2·35 g/cm³ half strike 10 km; Horizontal lines 2·55 g/cm³ half strike 10 km; Background density 2·65 g/cm³

further during the formation of the later calderas. The northeastern end of the A-A' profile ends in the Sierra de Toledo and the modelled depth of the caldera at this point would suggest that either the Toledo-Valles caldera complex extends further northeastwards or a regional gravity gradient needs to be removed from the observed values at this end of the profile. The caldera may be slightly shallower towards the middle as the calculated profile is up to 4.5 milligals below the observed values or the densities of the caldera fill may be locally greater than assumed. Using the Bouguer slab formula $g = 2\pi G\rho t$, where g is the value of the anomaly, G is the universal gravitational constant (6.67×10^{-11} Nm^2kg^{-2}), ρ the density of the slab and t the thickness of the slab, a 4.5 milligal anomaly is equivalent to the caldera being 360 m shallower. This is about 10% of the caldera's thickness of 3,150 m at this point. A better fit with the observed gravity values is obtained with a model that has an irregular caldera floor (Figure 22). Such an irregular floor to the caldera would suggest that the process of caldera collapse was in a series of short fragmented blocks rather than a simple hinged trapdoor with a series of faulted horizontal basement blocks. As you would not get such rotation of fault blocks to get this irregular floor, this model is geologically unrealistic.

The second profile B-B' (Figure 23) runs northwest 307 800 on the Jemez Plateau to the southeast 732 666 over the Sierra De los Valles. The model has a simple southeastwards dip of about 11° from the northwestern end with a 800 m fault half way down the slope. The profile reaches a maximum depth of over 3½ km about 1,200 m below sea level, similar to that of Segar's (1974) model (Figure 23b), but does

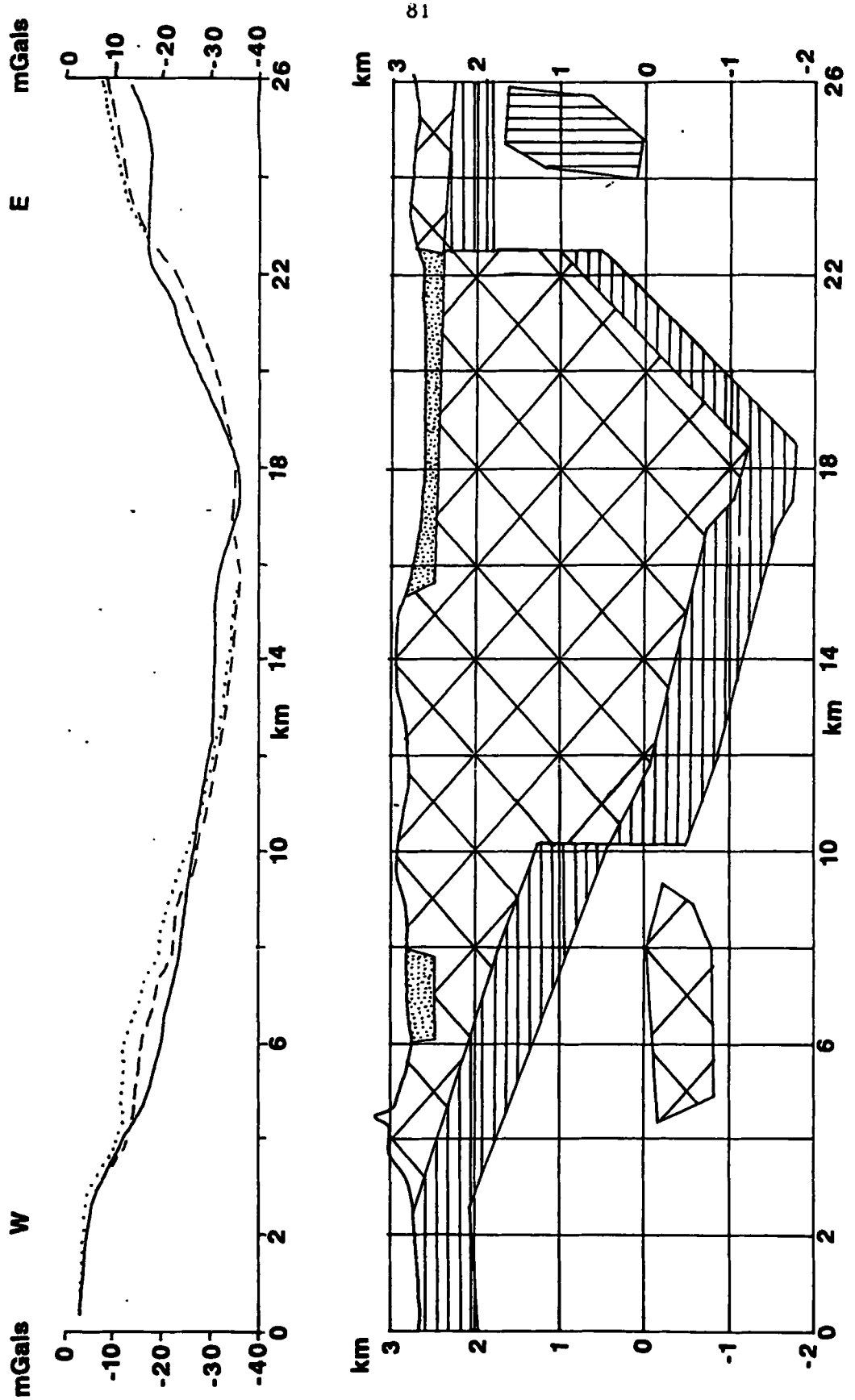

Figure 23. Profile B-B' NW 507 800 to SE 732 666. Solid line is observed profile, Dashes are calculated profile, Dots are calculated profile without deep bodies, horizontal and vertical scales in km. Dots density 2·20 g/cm³ half strike 2 km; Cross-hatching 2·35 g/cm³ half strike 10 km, far right half strike 5 km, deep body half strike 5km; Horizontal lines 2·55 g/cm³ half strike 10 km; Vertical lines 2·50 g/cm³ half strike 1 km; Background density 2·65 g/cm³

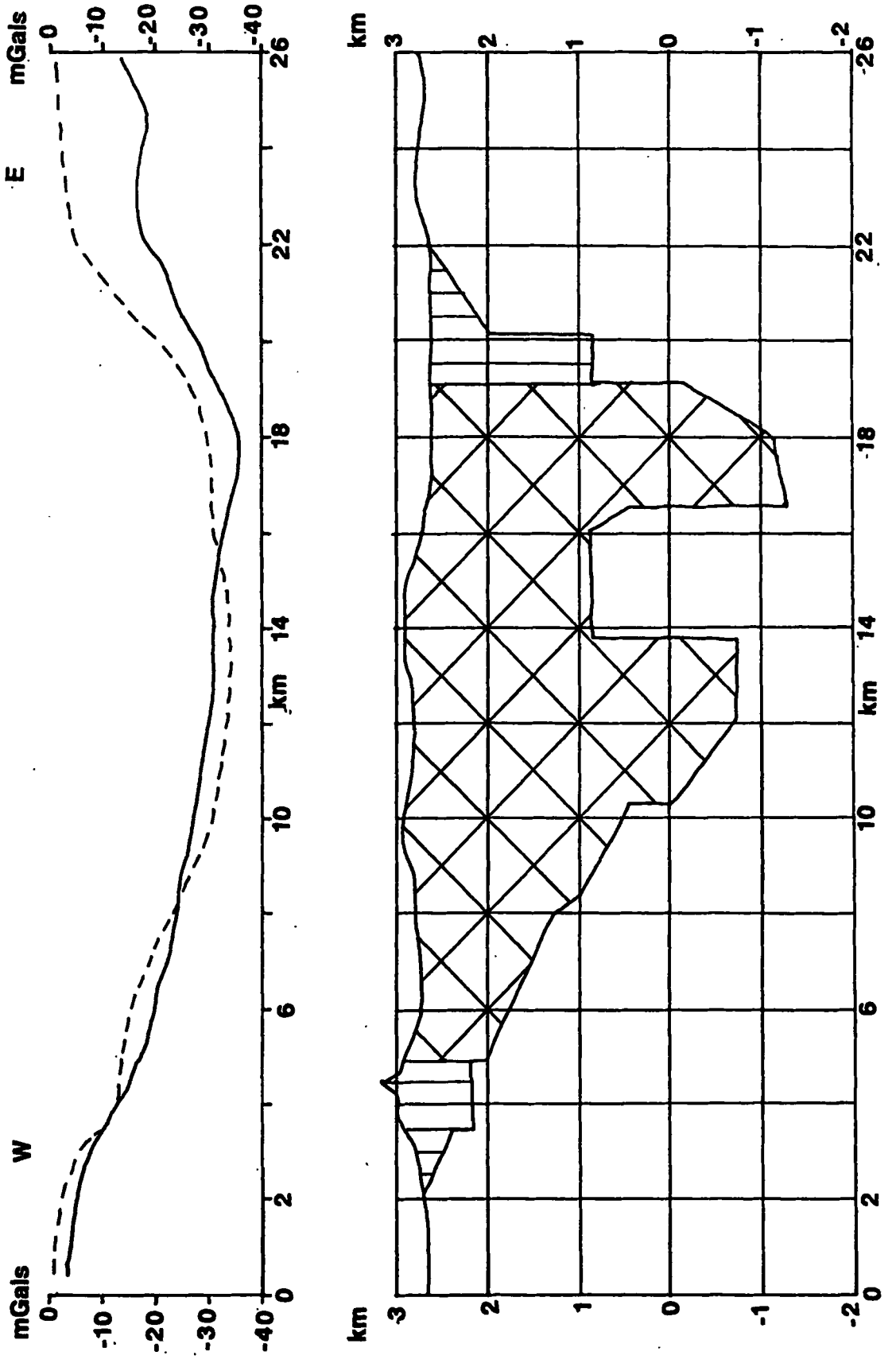

Figure 23b. Profile B-B' NW 507 800 to SE 732 666. Solid line is observed profile, Dashes are calculated profile, based on Segar's (1974) model, horizontal and vertical scales in km. 2·10 g/cm³ density: vertical lines 4 km half strike; cross-hatching 8 km half strike; Background density 2·45 g/cm³

not have a 3 km wide 1,500 m high fault block in the middle of the profile. Towards the southeast the floor of the caldera dips about 29° northwestwards - this may in fact be a series of small faulted blocks - and the margin of the caldera is marked by a 1,400 m high fault. The Palaeozoic sediments below the caldera were modelled as being between 850 m and 500 m thick. Below the northwestern margin of the caldera an intrusion of granite with a density of 2.35 g/cm^3 and a half strike of 5 km was modelled. This may be a small pod of silicic magma with a volume of about 30 km^3 that got trapped beneath the caldera when it cooled and froze before it could reach the surface. A lower density contrast would necessitate a larger body to produce the same anomaly. On the southeastern margin of the profile a small body with a density of 2.50 g/cm^3,half strike of 1 km, and volume of about 4 km^3 was modelled. If this body really exists, it may be related to the Rabbit Mountain rhyolites to the west. The levelling out of observed values to the southeast may be due to a regional anomaly in this direction due to the lower densities of the rocks in the Rio Grande Rift.

The third profile C-C' (Figure 24) was from west at the top of Barley Canyon 485 741 to Cero Rubio in the east 756 794. The western end of the profile is constrained by boreholes. In order to get the observed and calculated anomalies to fit better by about 3.5 milligals an intrusion of granite just below sea level with a density of 2.35 g/cm^3, half strike of 4 km and volume of about 40 km^3 was added. Again this may be a pod of silicic magma that got trapped beneath the caldera when it cooled and froze before it could reach the surface. As this is the only part of the three profiles to be constrained by

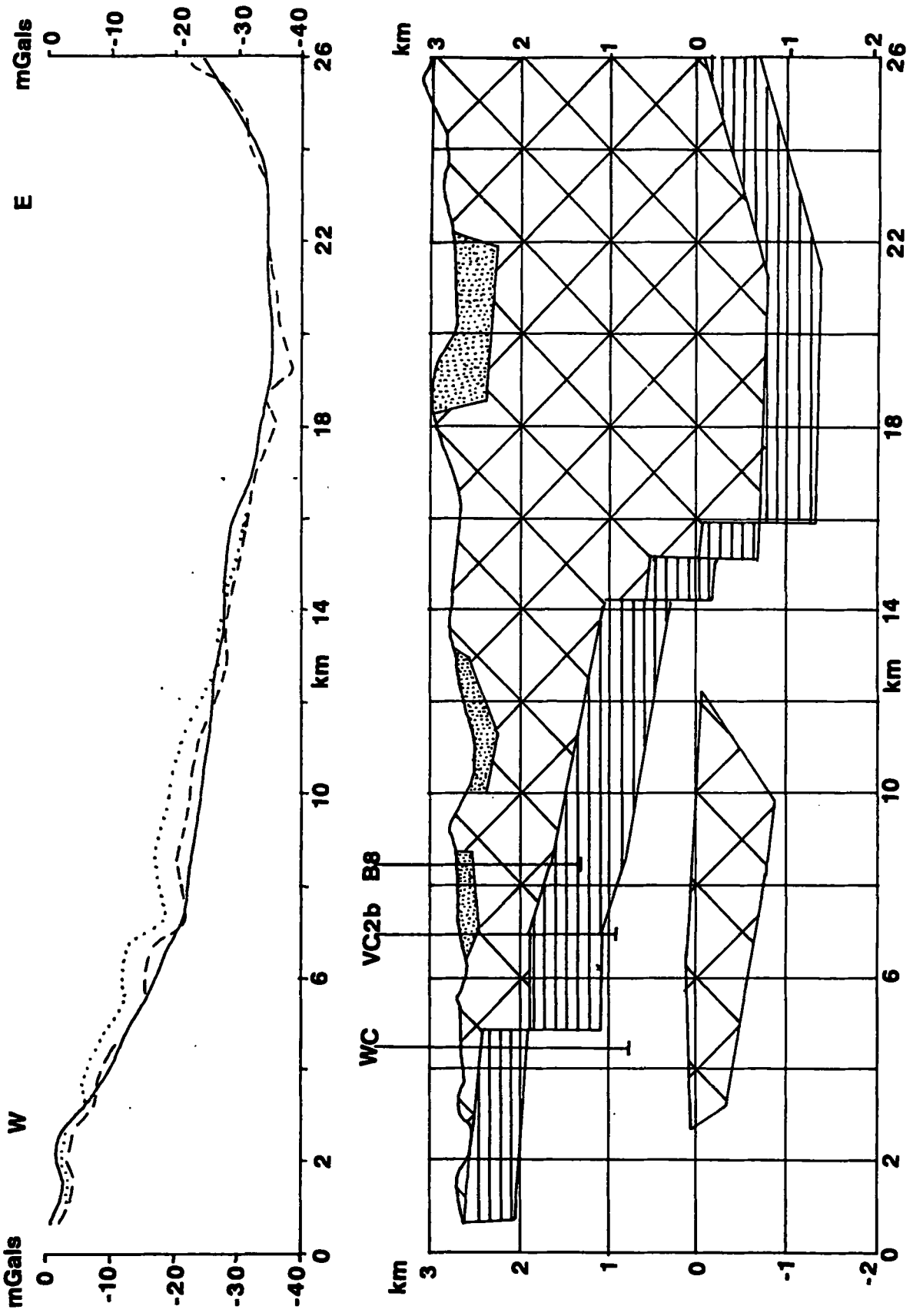

Figure 24. Profile C-C' West 485 741 to East 756 794. Solid line is observed profile, Dashes are calculated profile, Dots are calculated profile without deep body, horizontal and vertical scales in km. Dots density 2·20 g/cm³ half strike 2 km; Cross-hatching 2·35 g/cm³ half strike 10 km, deep body half strike 4 km; Horizontal lines 2·55 g/cm³ half strike 10 km; Background density 2·65 g/cm³

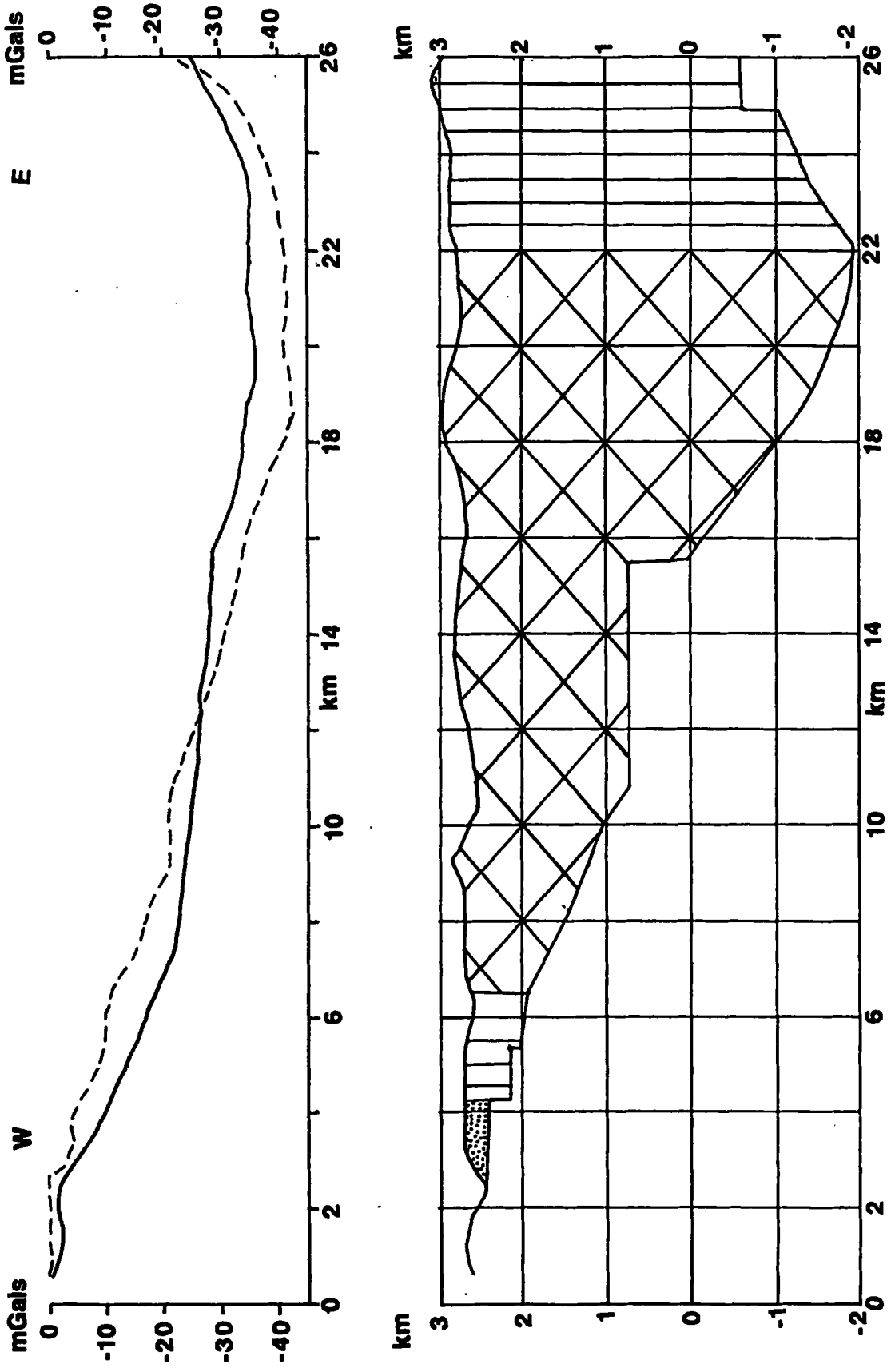

Figure 24b. Profile C-C' West 485 741 to East 756 794. Solid line is observed profile, Dashes are calculated profile, Dots are calculated, based on Segar's (1974) model, horizontal and vertical scales in km. 2·10 g/cm³ density: dots 2 km half strike; vertical lines 4 km half strike; cross-hatching 8 km half strike; Background density 2·45 g/cm³

boreholes, this 3.5 milligal anomaly could be added to the profiles to remove it. Thus instead of removing a 17 milligal regional anomaly as Segar (1974) did, only 13.5 milligals need be removed. If this was done the thickness of caldera fill in the profiles using the Bouguer slab formula would be reduced by an average of 280 m. In the middle of the profile there are a series of faults with downthrows of about 500 m each to the east, this is in the same position as a southwest-northeast fault zone in Segar's (1974) model (Figure 24b). The depth of the caldera tuffs and rhyolites reaches a maximum of 800 m below sea level, a thickness of over 3½ km below the surface, compared with nearly 2,000 m below sea level in Segar's (1974) model. The eastern end of profile C-C' would suggest that either the Toledo-Valles caldera complex extends further east or a regional gravity gradient needs to be added to the observed values at this end of the profile. Such a regional anomaly might due to the lower densities of the rocks in the Rio Grande rift towards the east.

The new 2½D gravity profiles show that the Valles Caldera is filled by up to 3,600 m of tuffs with up to 1,000 m of Palaeozoic rocks below that. These models were used to plot the depth of the Palaeozoic basement (Figure 25), which shows that the caldera is asymmetrical with less than 1,000 m of low density caldera fill in the west and up to 3,600 m under the northern Valle Grande (66,71) (1,000 m below sea level) in the east. The northern and eastern margins of the caldera are fault bounded with in the middle two faults each downthrowing over 500 m to the southeast. The new model profiles tend to fit the observed data better and be smoother than Segar's (1974) profiles, often with lower dips and a short series of faulted

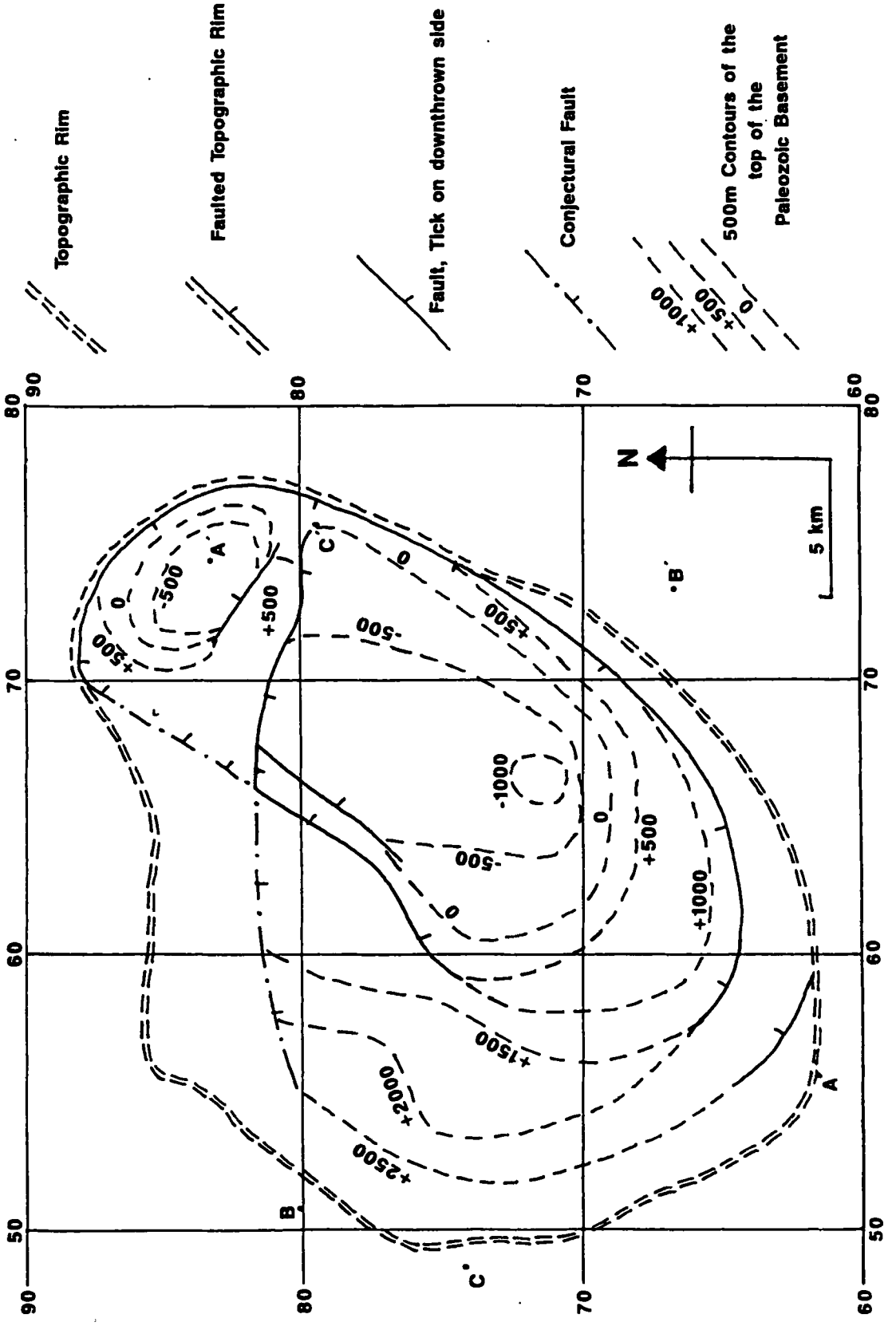

Figure 25. Plot of depth of the Valles basement based on the new 2½D gravity profiles

blocks. The three northeast to southwest trending faults centred on Redondo Peak (59 70) in Segar's (1974) model do not exist in profile B (Figures 23 and 23b) which as a result is a better fit, especially to the east. The maximum depth of the tuffs filling the Valles Caldera is up to 1,000 m less in the new profiles, though in other places along the profiles the tuffs are over 1,000 m thicker than in Segar's model. The new profiles are a better fit with the observed gravity values than Segar's (1974), which on profile A (Figure 21b) is over 10 milligals below the observed line, this also suggests that his maximum thickness of the tuff is too large. The new profiles have numerous faults with downthrows of up to 1,000 m but often less than 500 m which cannot be traced from one profile to another. This would suggest that the floor of the Valles Caldera is a series of jumbled fault blocks. This is consistent with chaotic caldera collapse and eruption of large volumes of magma.

The total volume of the caldera may be calculated by dividing the whole area into a kilometre grid and finding the average height of the topography and basement, to within 100 m, in each square kilometre. From this the difference in height is used to find the volume of caldera fill in each compartment. These are then added together. For Segar's (1974) model, the Toledo Embayment was added by projecting the model into this area, resulting in a total volume of 110 6 km^3. The total volume turned out to be 740 ± 40 km^3, with a maximum depth of 4.6 km for Segar's (1974) model and 740 ± 40 km^3 with a maximum depth of 3.6 km for the new model. The average 800 m of Palaeozoic rocks below the new model is the equivalent of an extra 100 ± 5 km^3 of caldera fill. To this must be added the 74 ± 4 km^3 of small intrusions modelled

below the profiles, which is also part of the anomaly. Thus the equivalent volume of the new model is 914±49 km³. The volume of the new model should be greater because the main density contrast was only 0.3 g/cm³, not the 0.35 g/cm³ of Segar's (1974) model and a lower density mass will take up a larger volume.

Profile A-A' was used as the basis for a geological cross section (Figure 26), as it passes though the Toledo Embayment. On the southwestern side of the caldera is the El Cajete vent which erupted the El Cajete Series of lavas. The older Valles Rhyolites and fan deposits which form a ring of domes around the centre of the caldera,fill the upper most part of the middle of the section as the profile passes to the east of the central dome. Below this are up to 1,400 m of Tshirege Tuff erupted by the collapse of the Valles Caldera (1.1 Ma). On the northeastern side of the section there is the Cerro Toledo Rhyolite erupted between the Toledo and Valles collapses. It is assumed that similar deposits are buried below the southwestern side of the caldera as the later post Valles Caldera domes are found on both sides of the caldera. The bottom of the caldera is filled by up to 1,400 m of Otowi Tuff erupted by the collapse of the Toledo Caldera (1.45 Ma). Below the Toledo Embayment on the northeastern side of the section it is postulated that there are between 1,500 m and 2,500 m thickness of Rubio Volcanics, about 100 km³ in volume. These rocks were erupted between about 4 Ma and the collapse of the Toledo Caldera at 1.45 Ma. The Rubio Volcanics are exposed on the side of the Toledo Embayment 2 km to the southeast of the section. So the Rubio Volcanics may be at a shallower depth than the 1,000 m showen on the section and the Otowi Tuff much thinner or absent at

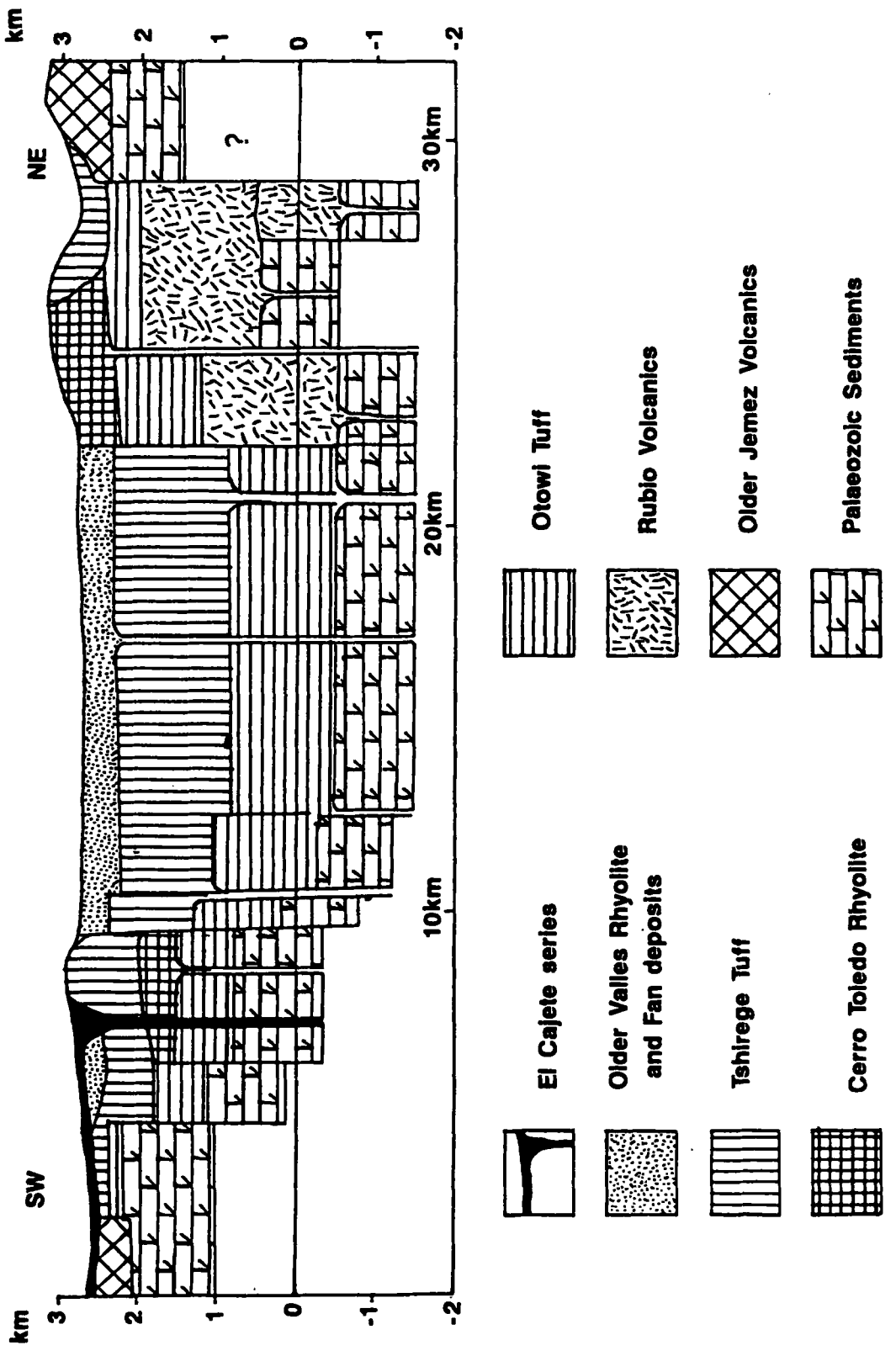

Figure 26. Possible geological cross section across the Valles Caldera and Toledo Embayment based on Profile A-A'.

this point. The Rubio volcano may have had explosive eruptions as it may have deposited the San Diego Ignimbrites 20 km to the southwest, which are of the same age. If this is the case the Rubio Volcanics may form a thin 100 m thick layer of tuffs at the base of the caldera complex. As the Rubio Volcanics were erupted the area beneath them collapsed so that the volcano did not stand up above the surrounding country. Indeed as each formation in the caldera has been erupted there has tended to be an equal amount of collapse, this sequence of events is set out in Figure 27.

The new models presented here, like Segar's (1974) model, show the Valles Caldera to be much deeper on the eastern side than in the west. This asymmetry in fill thickness led Heiken et al. (1986) to call the Valles Caldera a "trap-door" caldera. The present work has shown however that the floor of the Valles caldera is uneven, in that it is broken by a series of fragmented faults with downthrows often less than 500 m and not smooth like a perfect "trap-door". This is similar to though less extreme than the suggested formation mechanism of funnel-shaped calderas which involve a process of chaotic collapse, with greatest collapse towards the centre of the caldera (Scandone, 1990). Boreholes along profile C-C' constrain the thickness of the caldera fill at this point in the model and results in a residual anomaly. This suggests that 70 km^3 of low density silicic material up to 900 m thick is trapped below the western part of the Valles Caldera. A similar residual anomaly in the east beyond the eastern margin of the Valles Caldera can be modelled as silicic material associated with the eruption of the Rabbit Mountain Rhyolites which solidified before it reached the surface. The Toledo Embayment is

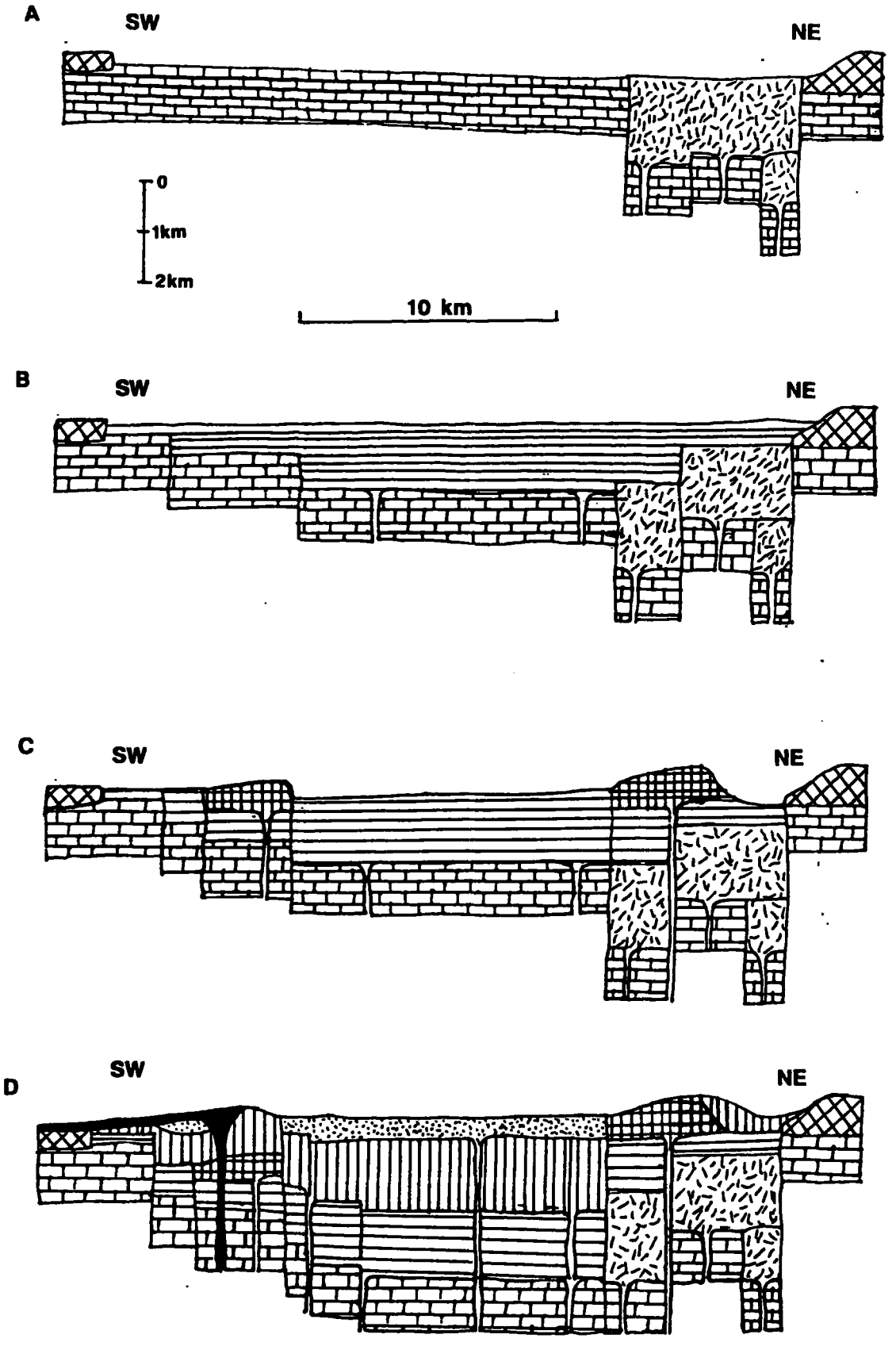

Figure 27. Development of the Valles Caldera: (A) Rubio Volcano (4 Ma to 1·5 Ma); (B) Collapse of the Toledo Caldera (1·45 Ma); (C) Intra-caldera volcanics (1·45 Ma to 1·1 Ma); (D) Collapse of Valles Caldera and post caldera volcanics (1·1 Ma to 0·13 Ma). See Figure 26 for Key.

shown to have been occupied by an earlier Rubio volcano which erupted 100 km^3 of rhyolites and tuffs. Heiken et al. (1986) suggested a smaller caldera erupting silicic tuffs as one of the possible origins of the Toledo Embayment. It is clear that the Toledo Caldera and the later Valles Caldera have similar centres because the Otowi Tuff deposited by the collapse of the Toledo Caldera and the Tshirege Tuff deposited by the later collapse of the Valles Caldera have the same distributions and volumes. This suggests that the earlier Toledo Caldera occupied a similar area as the later Valles Caldera with the centre of the calderas moving slightly to the southwest leaving the Toledo Embayment outside the later Valles Caldera ring fracture. Because the material in the Toledo Embayment is of the same density as the later Valles Caldera fill it can not be separated on gravity profiles.

The profiles suggest that the Toledo Caldera and the later Valles Caldera are a pair of nearly coincident "trap-door" calderas with an uneven floor due to chaotic collapse. The only part of the Toledo caldera not occupied by the later Valles Caldera is the Toledo Embayment on the northeastern side of the caldera, which was the site of an earlier Rubio volcano.

3.10 New ideas about the Jemez Mountains

The following new ideas about the Jemez Mountains are developed by the author. The back-arc basin associated with the northern part of Baja California developed into the Rio Grande Rift. The Jemez Mountains volcanic field developed where the Rio Grande Rift is

dextrally offset by about 50 km along the northeastward trending Jemez Lineament which deflected in the rift normal to the rift axis as a result of rifting. It is suggested that the Rio Grande Rift has in part acted as a dextral pull-apart basin in the Jemez Mountains-Espanola Basin area. The stratigraphy of the Jemez volcanic field has been revised in line with new radiometric dates. The Toledo Embayment was the site of the Rubio volcano (4 Ma to 1.5 Ma) which developed at the intersection of the Jemez Lineament and faults on the western flank of the Rio Grande Rift, before the eventual collapse of the Toledo Caldera. The Rubio volcano may have had explosive eruptions, including the San Diego Ignimbrites 20 km to the southwest, which are of the same age. The volume of the Valles Caldera was found to be 740 km^3 with a further 74 km^3 of acidic material trapped beneath the caldera. This compares with 740 km^3 estimated from the Segar (1974) model which used a higher density contrast. The amount of collapse during the history of the caldera has roughly equalled the amount of material erupted.

4. The tectonic setting of the Icelandic region.

4.1 Introduction

Beneath the North Atlantic Ocean are mantle plumes of various sizes, which result in hot elevated areas, one of which underlies Iceland. These mantle plumes are largely responsible for the variation in basalt geochemistry, physiographic and geophysical parameters of the North Atlantic ocean crust (Walker 1991). It is still strongly debated as to what constitutes a mantle plume, the origin of the material in it and which part of the mantle it has come from (Walker 1991). As distinct from the globally extensive source region of the mid-ocean ridge system, the source of any plume is geochemically unique (Walker 1991). The opening of the Atlantic and the development of the Icelandic and other plumes underlying the Mid-Atlantic ridge and flanks may be related (Bott, 1988; Silver et al. 1988; White and McKenzie 1989a,b; White 1990). However, this does not mean that to form new oceans plumes are necessary for continental rifting. The Icelandic plume was initiated approximately 62 Ma ago and by about 57 Ma rifting between Greenland and the Rockall Plateau became well established (White, 1988; White and McKenzie 1989a). Relative to a 'fixed' 'hot-spot' reference frame the axial rift zone (plate boundary) may gradually migrate.

Before discussing the morphology and structure of Iceland it is worth outlining that of the Mid-Atlantic Ridge in general. To the south the Atlantic Ocean is deeper, older and spreading faster, as shown by the following half spreading rates: 15 mm/yr at the Kane

Fracture Zone (25°N), 11-12 mm/yr at the Azores (38°N) and 10 mm/yr at the Reykjanes Ridge (60°N) and on Iceland (65°N)(Walker 1991). Typical features of the North Atlantic ridge are: (i) a median valley at the ridge crest on average 30 km in width; (ii) an axial neovolcanic zone less than 10 km wide; and (iii) discontinuities in the ridge axis such as transform faults. The Mid-Atlantic ridge is segmented by large transform faults and by smaller non-transform discontinuities, on average every 55 km (Macdonald 1986). Between such offsets the floor of the median valley is elevated towards the centre of that segment (Lin et al 1990; Sempere et al 1990).

In the vicinity of a 'hot-spot' the characteristic geomorphological features of the mid ocean ridge are disturbed (Walker 1991). On the Reykjanes Ridge adjacent to the Iceland hot-spot the depth of the ridge shallows (Talwani et al. 1971), and the median valley and segmentation becomes less pronounced. Over the ocean floor away from the axis a 'hot-spot' often leaves an aseismic ridge or chain of islands. The trace of the Iceland hot-spot is recorded by the aseismic ridge between the Faeroes and Greenland. The increase in thickness of the crust towards Iceland along the Reykjanes Ridge represents an increased rate of magma production caused by locally elevated mantle temperature (White and McKenzie 1989b).

4.2 The development of the Icelandic plate boundary

The Iceland plateau developed around 36 Ma ago (Oskarsson et al. 1985) when the amount of magma generated by the plume increased relative to the spreading rate and thus the thickness of the plate

(Vogt and Avery 1974). Since this time the neovolcanic zone has never reached stability as the plume has moved relative to the Mid-Atlantic plate boundary in a series of ridge jumps, when the main ridge has jumped from one axis to another and ridge propagation episodes, when a new ridge has developed along an axis (Oskarsson et al. 1985). The plate boundary has moved westwards relative to the stationary Icelandic plume. As a result there have been ridge jumps across the plume from east to west, but these have been temporally, small oscillations in the overall west to east ridge jump pattern, so that the ridge stays in the same position as the plume (Walker 1991). The following description of the development of the Icelandic plate boundary, the origin of the currently active and recently extinct zones is based on Walker (1991).

The plume was located to the west of the Mid Atlantic plate boundary 36 Ma ago. The Kolbeinsey Ridge apparently propagated northwards from the area of the plume resulting in the extinction of a more easterly ridge segment (Figure 28) (Vink 1984). By 27 Ma ago, the Reykjanes Ridge bent into the Snaefellsnes peninsula and was connected to the Kolbeinsey Ridge to the north by the Skagi Volcanic Zone (Figure 28). For about 17 Ma, this pattern remained stable as the plate boundary moved westwards relative to the Icelandic plume. By 9 Ma ago this configuration was unstable and the Snaefellsnes Ridge jumped eastwards to form the Western Volcanic Zone between Langjokull and the Reykjanes Peninsula (Figure 28). The Northern Volcanic Zone and the Tjornes Fracture Zone may have developed prior to this time (Oskarsson et al. 1985), or not until 7 Ma ago at which time the Skagi Volcanic Zone became extinct (Jancin et al. 1985) (Figure 28). The

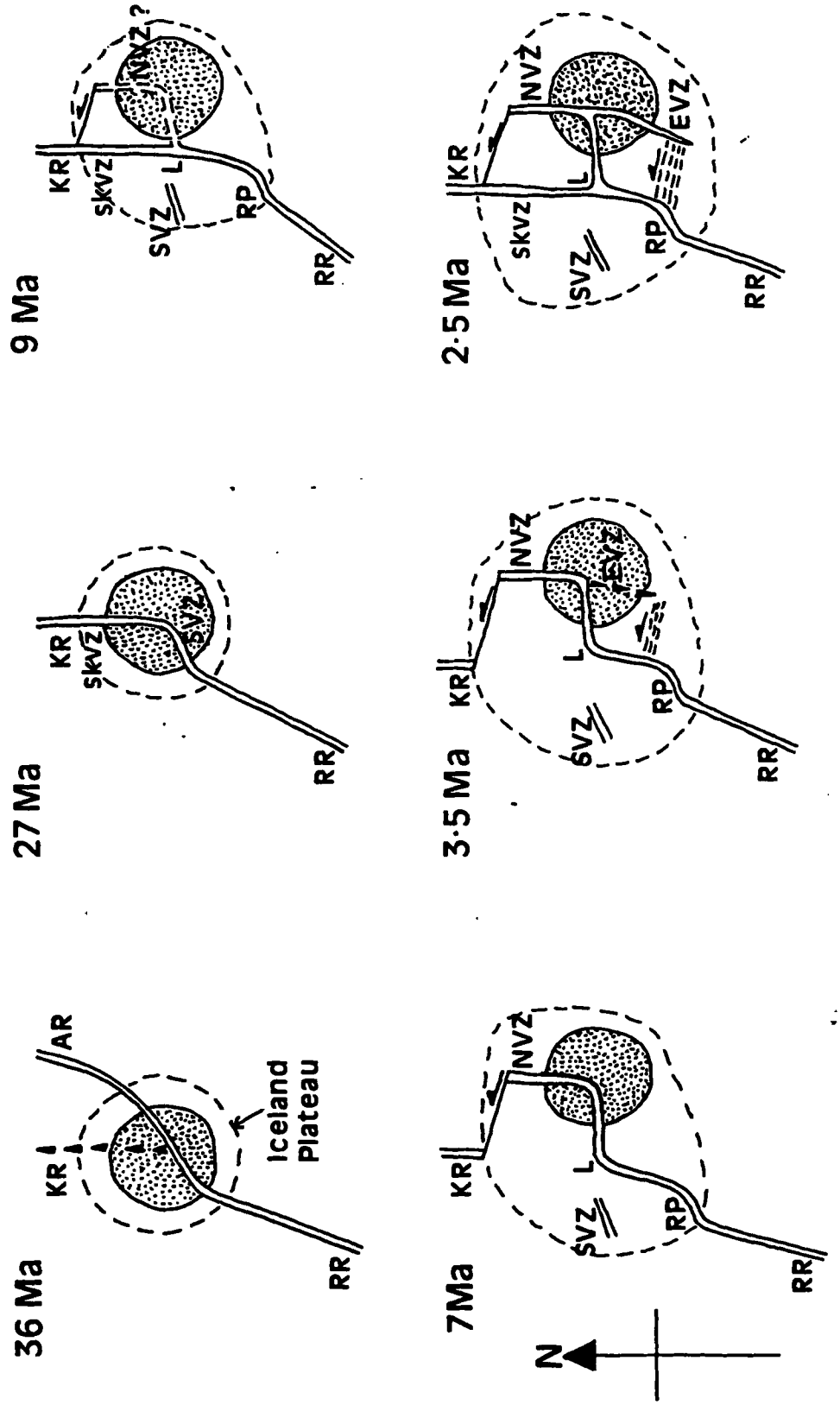

Figure 28. Evolution of the plate boundary through time (36 Ma ago to 2·5 Ma ago) (information extracted from Saemundsson, 1974; Oskarsson et al., 1985; Jancin et al., 1985: based on Figure 13·7, Walker 1991): KR = Kolbeinsey Ridge; RR = Reykjanes Ridge; AR = Aegir Ridge; SKVZ = Skaggi Volcanic Zone; SVZ = Snaefellsnes Volcanic Zone; NVZ = Northern Volcanic Zone; EVZ = Eastern Volcanic Zone; RP = Reykjanes Peninsula; L = Langjokull; Patterned area indicates the location of the centre of the head of the Icelandic plume; Arrows propagating ridge. The Western Volcanic Zone is from the Skaggi Volcanic Zone to the Reykjanes Peninsula.

Northern Volcanic Zone began to propagate southwards at about 3.5 Ma ago (Jakobsson 1979b; Einarsson and Eriksson 1982) at a rate of between 3.5 cm/yr and 5 cm/yr. This resulted in the development of the Eastern Volcanic Zone and the South Iceland Seismic Zone. At 2.5 Ma ago the Skagi Volcanic Zone was reactivated for about 1.8 Ma (Everts et al. (1972)(Figure 28). The present day configuration developed about 0.7 Ma ago and since then the neovolcanic zones have changed little, remaining in their current positions with minor oscillations of up to 10 km, away from the axis of the neovolcanic zone.

4.3 The present plate boundary on Iceland

Iceland is dominated by a central topographic high in the area of Vatnajokull, 2,000 m above sea level (Figure 29). Between 64°N and 66°N the Mid-Atlantic plate boundary is exposed on land as a complex arrangement of active volcanic and seismic zones and presents an excellent opportunity to study Oceanic crust. Detailed accounts of the geology of Iceland are given by Ward (1971), Palmason and Saemundsson (1974), Saemundsson (1974, 1978, 1979) and Einarsson (1991). The volcanic zones have often had different names, but this account will use the most widely used names by Walker (1991) (Figure 28). The main spreading volcanic zones in Iceland are divided into the Western, Eastern and Northern neovolcanic zones (Figure 28). On land, the Reykjanes Ridge is continued in the Western Volcanic Zone. As it extends inland it progressively widens and trends dominantly northeast over half of Iceland. At Langjokull it bends east to join

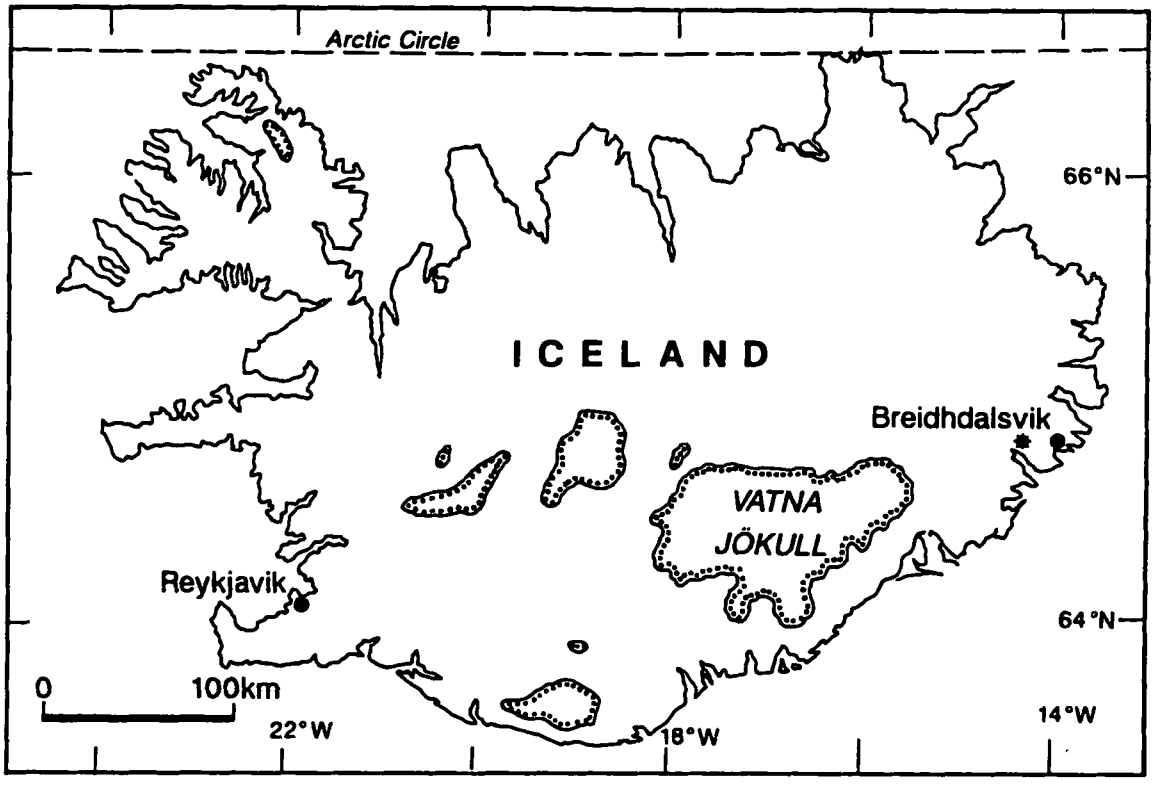

Figure 29. The location of the Breiddalur central volcano in Iceland, shown by an asterisk, ice caps marked by dotted and solid line.

the Eastern and Northern Volcanic Zones under Vatnajokull. The Northern Volcanic Zone has a northerly trend between the Vatnajokull ice cap and the northern coast of Iceland. The Eastern Volcanic Zone is the widest of the three at 72 km and trends southwest from Vatnajokull to the southern coast of Iceland and the island of Surtsey. At the southeastern corner of Vatnajokull there is the small Oraefajokull Volcanic Zone (Steinthorsson et al. 1985). The Snaefellsnes Peninsula in western Iceland is a possible fifth volcanic zone, with an east-west trend and a seaward extension as the Jokulbanki Ridge which swings southward to run parallel to the Reykjanes Ridge for over 150 km. The Northern Volcanic Zone is offset sinistrally by a 75 km wide 100 km long belt of high seismicity which represents a transform zone between the Northern Volcanic Zone and the Kolbeinsey (Iceland-Jan Mayen) Ridge (Figure 28). This is the Tjornes Fracture Zone which consists of at least three parallel north-west to south-east seismic belts about 30 km to 40 km apart (Saemundsson 1974; Einarsson 1991). The South Iceland Seismic Zone is another 10 km to 15 km wide, 100 km long east-west zone between the Western and Eastern Volcanic Zones but it does not laterally offset either (Einarsson et al. 1982).

The topography of the axis of the ridge crest or neovolcanic zone in Iceland is a slightly elevated region relative to the distal parts of Iceland. The neovolcanic zone is made up of a number of individual units or volcanic systems (Walker 1963, 1974; Saemundsson 1978). Each volcanic system is composed of parallel eruptive ridges or fissures which vary from 17 km to 105 km in length and 5 km to 30 km in width and have a life span of between 300 ka and 500 ka. A

fissure swarm or volcanic system may develop a central volcano (Saemundsson 1978) such as Breiddalur (located on Figure 29). At one site a central volcano may develop on the main volcanic axis and it is topographically elevated relative to the rest of the volcanic system, due to a relative increase in the rate of magma eruption. Shield volcanoes or lava shields of various sizes may also develop 5 km to 10 km away from the axis on axis fissure volcanic systems. In Iceland there is a correlation between the composition of the lavas and the shape of the volcano which erupted them (Jakobsson et al. 1978, 1979a,b). Some of this variation is due to differences in the stage of development and the thickness of the crust in that region.

Compared with the normal thickness of oceanic crust in the range of 3 km to 8 km thick (6 km average given by White 1989), Iceland has crust between 8 km and 16 km thick (Palmason 1971). The crust is thinner below central volcanoes in the neovolcanic zones and extinct central volcanoes. There is a noticeable increase in thickness in northern and north-western Iceland as well as under the proposed propagating Eastern Volcanic Zone (Palmason 1971; Flovenz 1980). In the neovolcanic zone faulting is dominated by normal extension faulting with a horizontal minimum compressive stress direction to the northwest. This stress direction varies between different volcanic zones and transform regions (Einarsson 1991). The Tertiary volcanic systems in eastern Iceland have been interpreted in terms of volcanic systems similar to the presently active Western and Northern neovolcanic zones (Walker 1963; Helgason 1984, 1989). The lava piles of Iceland dip towards the present neovolcanic zones (Walker 1991).

5. The Breiddalur central volcano

5.1 The Geology of the Breiddalur central volcano

In eastern Iceland there are several central volcanoes, Reydarfjördur, Lodmundarfjördur, Bardsnes, Thingmuli, Álftafjördur, Lon, Heinabergsjökull and Breiddalur. The Breiddalur central volcano (14½°W 65°N)(located on Figure 29) was investigated and geologically mapped by Walker (1963). The area of the Breiddalur volcano is mountainous with summits rising up to 1,200 m and is deeply dissected by erosion; the main valleys are Breiddalur, Nordurdalur and Berufjordur (Figure 30). The volcano is well exposed but the valleys are floored by spreads of alluvium and screes, and glacial debris conceals some of the upper slopes.

The following summary is derived largely from Walker (1963) (Figure 31). The Breiddalur central volcano has a volume of about 400 km^3 and consists of basic, intermediate and silicic (acid) lavas and smaller amounts of pyroclastic rock with a maximum thickness of between 1,500 m and 1,800 m. The basic lavas within the volcanic sequence are unusually thin and were therefore probably erupted on the sloping flanks of the volcano. The localised central volcanoes of eastern Iceland contrast with the normal extensive Icelandic flood basalt fissure-eruptions with dyke emplacement in the surrounding area. When the volcano was active it probably stood up as a cone above surrounding flood-basalt plains over which further flood-basalts were being erupted at the same time. This resulted in the interdigitation of the flood-basalts with the products of eruptions

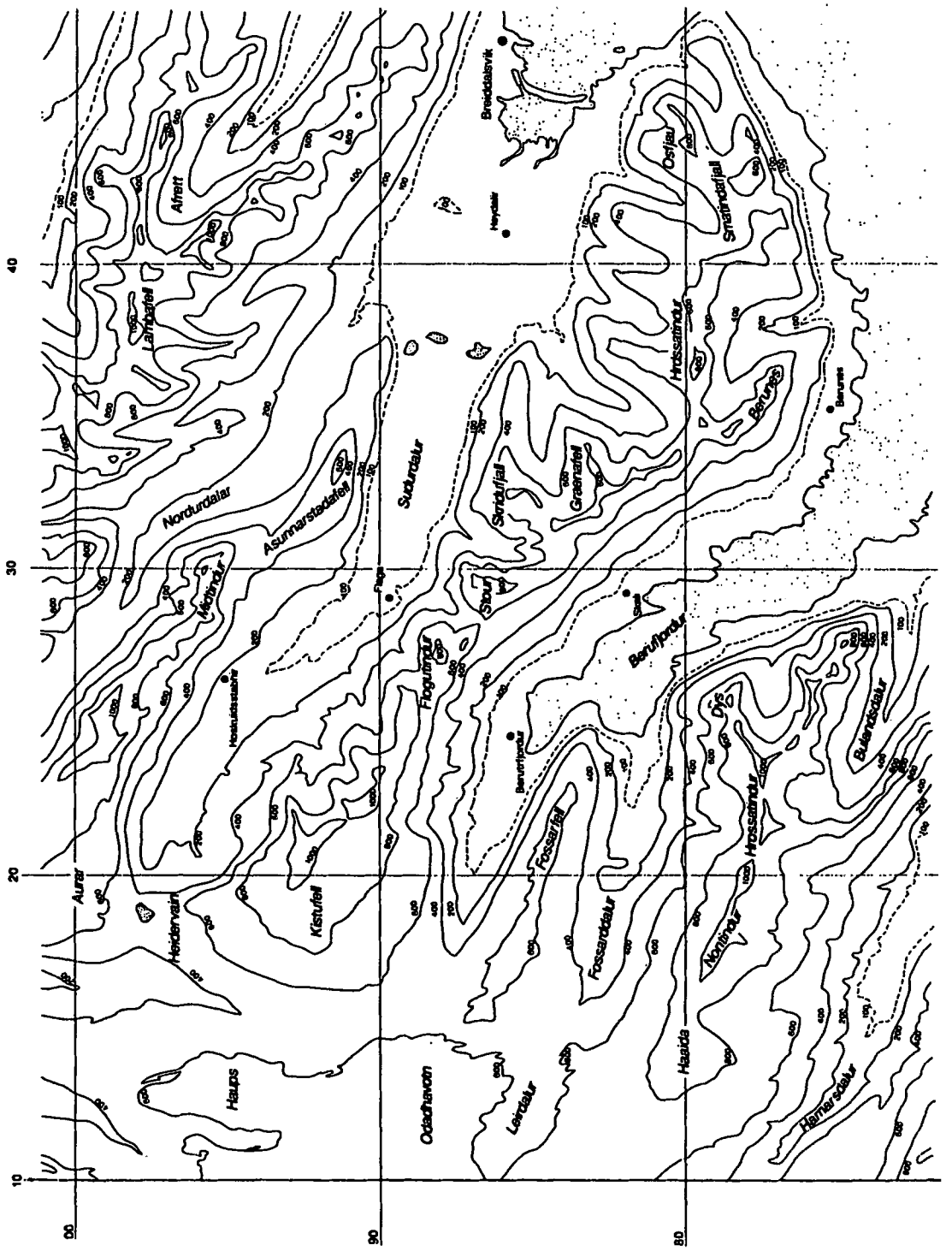

Figure 30. Topographic map of the Breiddalur area, contour in meters, 10km grid spacing.

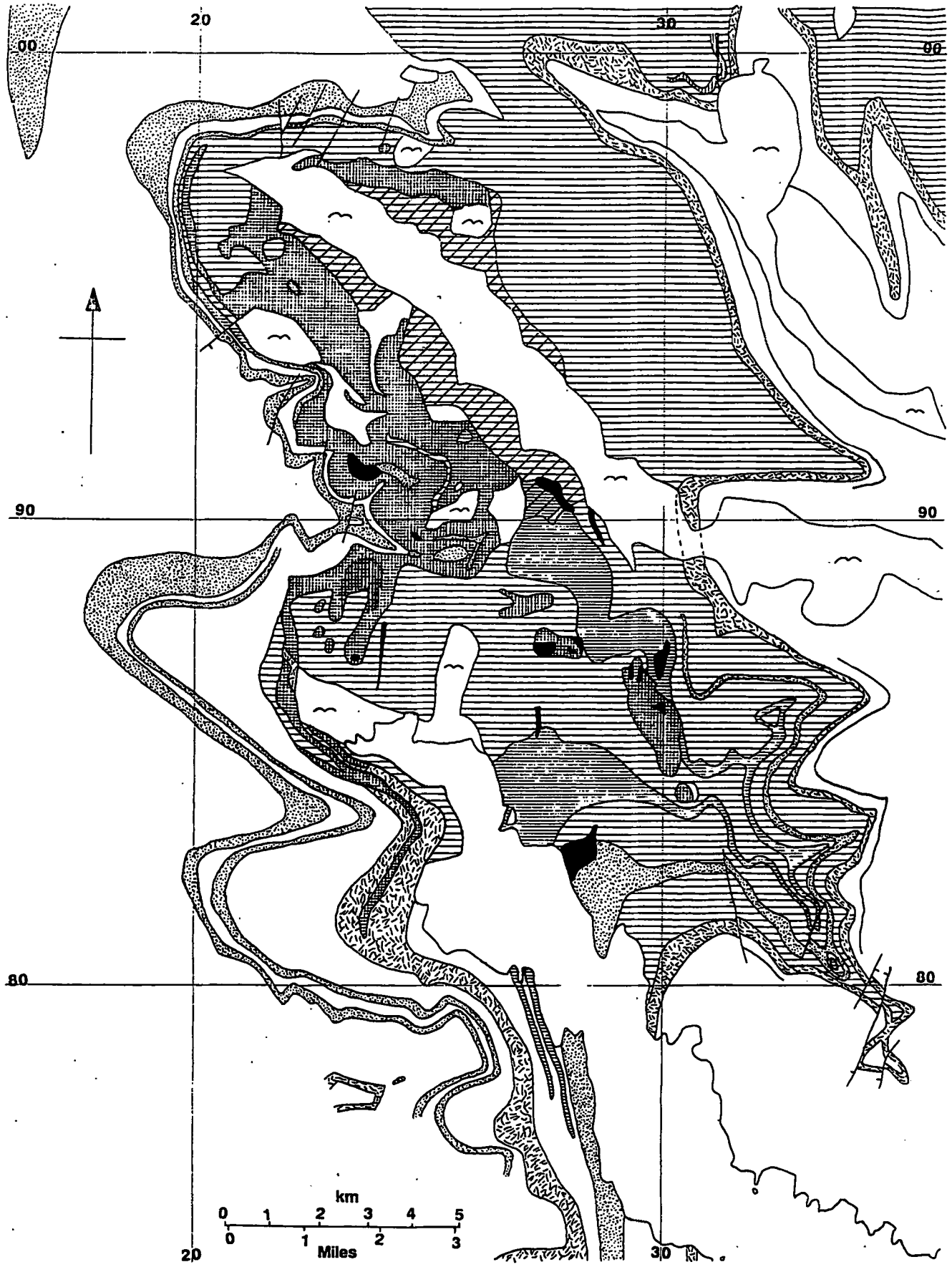

Figure 31a. Geological map of the Breiddalur volcano, based on Walker 1963.

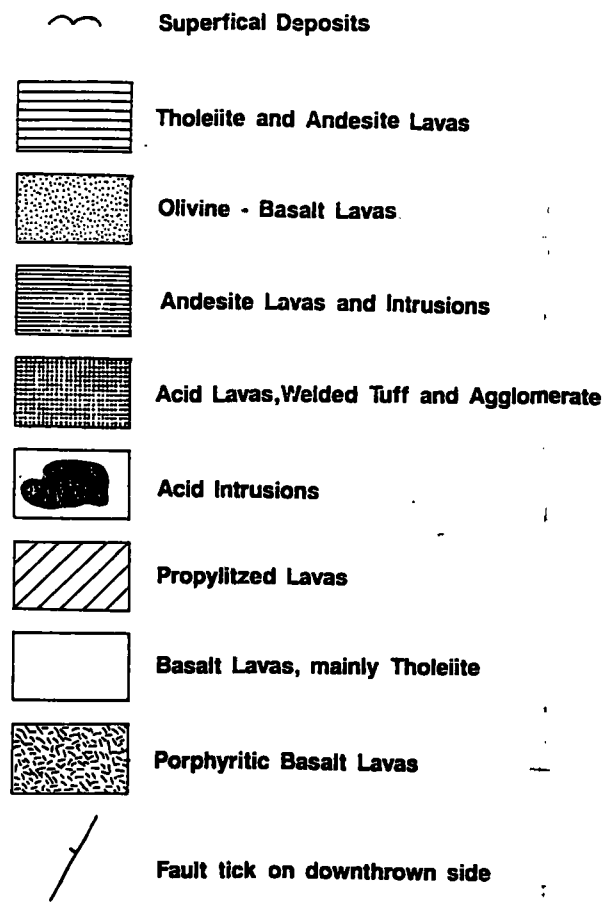

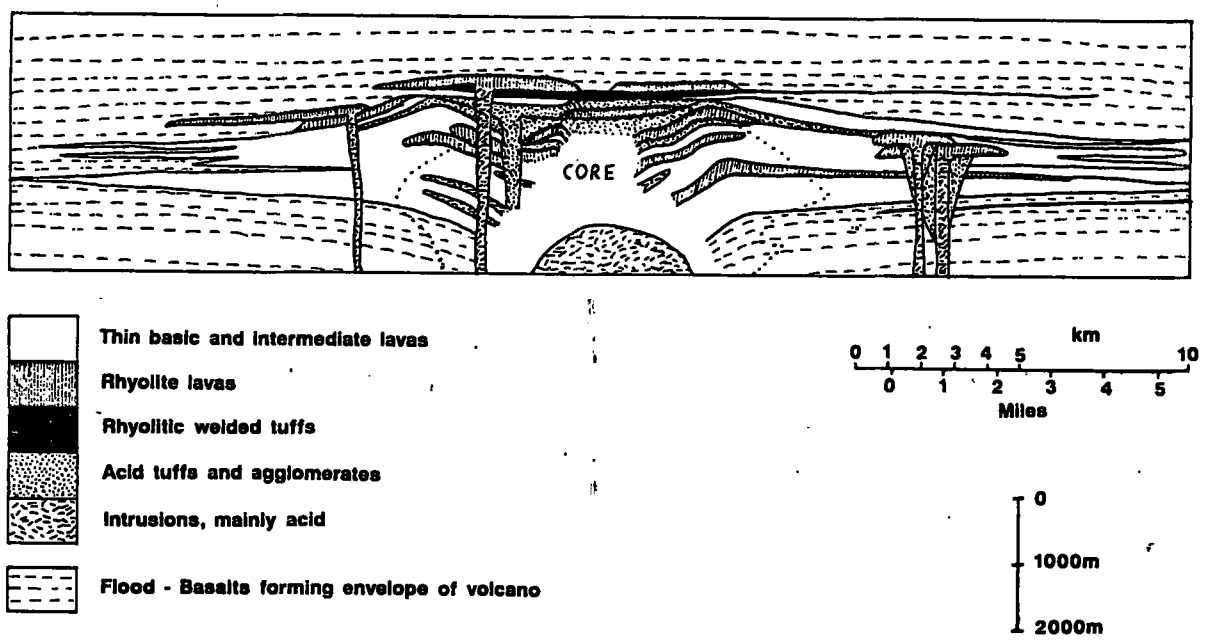

Figure 31b. Schematic composite section across the Breiddalur volcano and its envelope (based on Walker 1963, Figure 10).

from Breiddalur which was later completely buried by flood-basalts. The term cedar-tree volcano was coined to illustrate this phenomenon (Walker 1963) (Figure 31b). The core of the volcano is characterised by lavas, pyroclastic rocks and minor intrusions of silicic composition. These rocks are strongly hydrothermally altered and show variable and sometimes abnormally high dips which suggest cauldron-subsidence. Within the core a swarm of basic regional dykes constitutes between four and ten per cent and locally up to twenty per cent of the total volume and the dykes have a north-south trend, the same direction as the central Icelandic spreading axis, Park (1988, page 81). Some of the rocks exposed above the central core probably occupy a crater or caldera and include: agglomerate containing blocks of granophyre, granite and gabbro from inferred syngenetic intrusions below the volcano; a palagonite-tuff and breccias including basalt pillows which suggest eruption into a crater lake; two welded silicic tuffs; and a thick rhyolite flow clearly joined to its plug feeder. The silicic rocks are mostly concentrated in or near the core, except for a spectacular group of parasitic rhyolites in the Rondolfur area (Grid reference, 29 86)(Figure 31), where the plug-feeders can be seen in various stages of uncovering due to erosion down to 200 m below the extruded rocks. There is evidence of simultaneous eruption of basic and silicic magma as one outcrop consists of an emulsion of the two magmas and another of a composite lava with basic and silicic components, erupted from a composite dyke.

The basalt envelope around the volcano has been divided into three rock types: Tholeiite, Olivine-basalt and Porphyritic basalt. Near to the base of the volcano is the Graenavatn porphyritic group

(Walker 1959, p. 382) an easily mapped basalt group very rich in feldspar phenocrysts. No silicic or intermediate rocks are known below this horizon apart from the Skessa welded tuff towards the base of the volcano, but there is evidence that the volcano started to form earlier as typical products of the volcano are found up to 100 m below this level. Below the Graenavatn group, which had been mapped along 80 km of strike, 2,750 m in thickness of flood-basalts are seen, which contain some tuffs that are believed to be the products of other volcanoes. The rocks of the Breiddalur volcano are distinguished from the flood-basalts of its envelope by the difference in dip and individual thickness of the lavas and the presence of silicic and intermediate rocks within the volcano. On the southern slopes of Ofaerudalsnafir (23 89) the volcano lavas dip southwesterly 10° to 15° in contrast to 6° to 7° for the adjacent flood-basalts. The regional dip of the flood-basalts is due to tilting after eruption and the volcano must have been tilted by a similar amount and so this tilt can be removed from the dips of rocks within the volcano. The residual dips are approximate to the original slope of the volcano and are between 9° and 3°. The tholeiite lava-flows of Breiddalur volcano are only 5 m thick in contrast to the average 14 m thickness of the surrounding flood-basalts. This is due to the sloping volcano flanks, which reduced the thickness of the lavas as the angle of the slope increased. The top of the volcanic sequence is marked by the Heidarvatn group, up to 100 m of zeolite-rich olivine-basalts that form a prominent cliff at the head of the Breiddalur valley but thin out along 30 km of strike to the north and south.

The andesite lavas in the flanks of the volcano are probably in a

ratio of 1:3 or 1:4 relative to the tholeiites and, above Flaga (27 89) the andesite flows have an average thickness of 15 m. At this point there is a total thickness of 335 m of andesite lavas which thin markedly away from the core. It is reduced to two flows about 30 m thick below Stong (30 83) and 5½ km away a single 18 m thick flow which persists to Kerlingatindur (34/5 79), 12 km from Flaga. On Eyvindarnes (26/7 80), the andesites total about 120 m thick and thin southwards to about 12 m in 3 km. The thinning of these andesites from the core is due to a reduction in the number of flows, not the thickness of individual units. The rhyolite flows on the flanks of the volcano have a maximum thickness of about 275 m at Thorgrimsstadhir (23 97). They are prominent in the upper parts of the flanks of the volcano but only one flow, 30 m thick, has been encountered in the lower part. This may be because silicic eruptions occurred only towards the end of the volcano's history. Alternatively, the lack of exposure of early silicic lavas may be due to an accident of erosion. Also, the lower parts of the volcano, close to the core, where silicic lavas are more likely to be located are unexposed. Consistent with this view is the presence of silicic tuffs low down on the flanks of the volcano.

Above the core, the summit group comprises up to 460 m of basaltic lavas and pyroclastic rocks which are best seen on Berufjardartindur (25 89) and Matarhnjukur (23/4 90/1) overlaying the core. These rocks are sometimes unconformable with the core, and are not involved in the propylitization of the core. The summit group includes the highest-exposed parts of the volcano and Walker (1963) supposed that in part it occupies a crater or caldera. The summit

group formations are overlain by typical regional flood-basalts and have approximately the same dip and strike as the rocks above them. The summit group is surmounted by a thick silicic lava-flow, the summit rhyolite, which is seen to be joined to its plug-feeder or feeders on the northern face of Matarhnjukur (23 90) and Ytri-Ljosa (25 90). The summit rhyolite covers 6 km^2 and must have had an original extent of about 13 km^2, it has a maximum exposed thickness of 180 m and an average of 120 m, which would give an original volume of about 1.6 km^3

The core of the volcano occupies an area of about 39 km^2 in the upper Breiddalur valley and its southern flanks (Figure 31); the limits of the core are defined by the extent of propylitized rocks. It is clear that this area includes the true core of the volcano, for the following reasons. The basalt and andesite lavas to the north and south of the core dip outwards, as does the residual dip of the rocks to the east; the vicinity of the core has the greatest thickness of volcanic rocks (1,500 m to 1,800 m). Pyroclastic rocks are best developed in the core between 600 m to 900 m thick and some blocks in the agglomerate are 3 m in diameter, and so cannot be far from their source. One agglomerate vent and rhyolite plugs feeding the silicic flows pass though the core, indicating that some eruptions must have occurred in this area. Propylitization could only have been caused by the passage of large amounts of hot fluids though the rocks, which implies the existence of a major heat source, such as a volcanic core. Silicic rocks probably make up over half the total volume; silicic and intermediate members of the dyke-swarm associated with the volcano are confined to the vicinity of the core. Dips of the rocks in the core

are often abnormally high and are very variable in direction and amount due to the collapse of the central volcano in a form of cauldron-subsidence or downsag. In the Blagil area (23 94), the rocks have been downwarped between 450 m and 600 m.

For the following reasons, the interpretation of the core's structure is incomplete: the rocks have been drastically altered so that basalts and andesites are sometimes difficult to distinguish from rhyolite and silicic tuffs; the core is not well exposed, a third of the outcrop is covered by the alluvial floor and associated gravel fans of the Breiddalur valley and the hillsides are drift-mantled; there is a lack of distinctive strati-graphical horizons in the core; it is often difficult to decide whether some bodies are lava-flows or intrusions. A gravity survey was undertaken and $2\frac{1}{2}$D modelling was carried out in an attempt to resolve the structure of the Breiddalur volcano. This technique requires an assumed density contrast between the various units. A form of cauldron-subsidence into an inferred magma-chamber is probably involved, in the late history of the volcano before the eruption of the summit group. However it is significant that no signs of ring-dykes or ring-fractures have been found. This suggests ductile sagging of thickened oceanic crust rather than brittle fracture as in the upper continental crust, as suggested for the volcanic complexes of western Scotland (Richey et al 1961). The altered core of the volcano can be divided into an inner epidote rich zone and an outer zone without epidote and with less laumontite than in the inner zone. These zones are interpreted as a broad hydrothermal aureole around a concealed intrusion of granophyre or gabbro below the core. Above the core up to 450 m of summit group

lavas and pyroclastic rocks are found which probably occupy the subsided core. The rocks give the distinct impression of having been deposited in a topographic basin either due to erosion or more likely due to a major explosive eruption. In turn these rocks are overlain by typical Icelandic flood-basalts with a conformable regional dip and strike.

5.2 Gravity survey of the Breiddalur area in eastern Iceland

A gravity and levelling survey of the Breiddalur area in eastern Iceland was undertaken by G.C. Brown, H. Rymer and a team of Earthwatch Volunteers in August 1989. Maps used during the survey were prepared under the direction of the chief of Engineers by the Corps of Engineers, U. S. Army Map Service (AM) Washington D.C. in 1948 at a scale of 1:50,000. Grid references for Iceland refer to the kilometre grid printed on these maps. The heights of the gravity stations were levelled in the Sudhurdalur valley relative to the level of a lake 1½ km east of Inari-kleif near Ytri-Keif, location N001, (372 892) and Brakkuborgarvain lake, location S02, (374 867). To the north of Berufjordhur, heights of the gravity stations were levelled relative to sea level at location Skali07, (259 852). The heights of other gravity stations away from these areas were obtained by barometric levelling; this method was also used to tie together the levelling lines for the whole survey (Appendix 6). The raw gravity and relative elevation data were provided for this work. The corrections applied to the raw data and the models and interpretations derived constitute the new work presented here.

The barometric levelling survey of the gravity stations was corrected for the following factors: wet and dry bulb temperature difference; humidity; and gravity effects both due to height and latitude (Erwes and Wild 1975). Errors quoted by Erwes and Wild (1975) were a mean square error for 15 points of ± 0.81 m and for a test survey showing errors in the region of ± 0.50 m and ± 1.15 m. The largest difference between levelling altitudes at Breiddalur was ± 1.50

m between Oda2 (139 906) and Oda3 (145 898), but normally the difference was less than $\pm$1.0 m and often much less. An error of 1.5 m would result in an error in the final Bouguer gravity anomaly of about 0.3 milligals.

Levelling between stations was carried out by trilateration using an EDM theodolite set up in-between pairs of stations as shown on Figure 32. The distance along the line of sight, as well as the horizontal and vertical components of the line of sight distance and the angle of the horizontal part of the line of sight relative to north were noted. From a pair of such readings, back to the last location and forward to the next location, the height difference, distance and direction relative to north between two locations could be found.

The gravity survey was carried out with three different LaCoste and Romberg gravity meters G16, G105 and G513. Surveys by each of the gravity meters were interlinked by measuring gravity at some stations with more than one gravity meter and using a common gravity base station at Breiddalsvik (469 858) (also at sea level), 100 m south of Hotel Blafell on the northern abutment of the bridge over a small creek. Errors due to tares were also reduced by revisiting gravity stations during the survey as well as measuring gravity at the start and end of each day at the Breiddalsvik base station. Readings were converted to relative gravity values in milligals using the manufacturer's calibration charts for each gravity meter (Appendix 5). The following corrections were applied to the data gathered for each gravity station: Earth tides (ET), calculated by computer for the eastern Iceland area, which vary periodically with an amplitude of up

to 0.120 milligals; the latitude correction (LC), due to the difference in gravity between stations as a result of the differing effect of the Earth's rotation on the shape of the Earth at different latitudes; free air correction (FA), due to the decreasing value of gravity away from the centre of the Earth; Bouguer correction (BC), due to the attraction of an infinite horizontal slab of rock with a density of 2.6 g/cm^3 (the standard background density used on the regional gravity survey of Iceland (Porbergesson et al. 1990)) between sea-level and the height of the station; and Terrain correction (TC)(at the same density, 2.6 g/cm^3), for the effects due to hills above and valley below the station resulting in a reduction in gravity at that location. The corrections applied to gravity values at each gravity station can be summarized as, Anomaly = reading $\pm$ ET $\pm$ LC + FA - BC + TC.

The Terrain correction up to a radius of 170.1 m from the station was calculated from the slope of the ground (Sandberg 1958) estimated at the time of survey in four directions at 90° to each other. Between a radius of 170.1 m and 21,944 m the terrain correction was calculated for a series of vertical cylinders divided into compartments (Hammer 1939). Where the Hammer compartment covered sea, the corrections were applied to the sea-bed not sea-level. The effect of the water above the sea bed can be corrected for and modelled as part of the interpretation of the data. A series of clear overlays on U.S. army maps were used to find the average height of each Hammer zone compartment, so that the terrain correction could be calculated and added together to give the total terrain correction, for each gravity station. The standard Hammer zones were

used, with inner and outer radii and number of compartments as follows: E 170.1 m to 390.1 m (8); F 390.1 m to 894.9 m (8); G 894.9 m to 1,530 m (12); H 1,530 m to 2,615 m (12); I 2,615 m to 4,469 m (12); J 4,469 m to 6,653 m (16); K 6,653 m to 9,903 m (16); L 9,903 m to 14,742 m (16); and M 14,742 m to 21,944 m (16). The terrain effect at a radius of further than 21,944 m was considered to be negligible, as it changes relatively little with a station spacing of between a few 100 m and 5 kilometres, i.e. it is a very long wavelength effect. Hallinan (1991) found that for terrain zones greater than M (21,944 m) stations could be clustered into areas of up to 5 km in diameter and even 20 km for more distant terrain zones. The terrain correction for the outermost zone M was never greater than 0.4 milligals (about 6% of the total correction) and was often less than 0.1 milligals (Appendix 6). It is worth noting that at this distance (21,944 m) the surface of the Earth is about 38 m below the horizontal of the gravity station, thus the curvature of the Earth begins to be a significant effect. For a zone between 21,944 m and 40,000 m with an average height below the horizontal of about 82 m, this is significant relative to the average height above or below the station, and would make calculating the true terrain correction at large distances difficult. Hallinan (1991) found that the underestimate of total terrain correction at 22 km by ignoring further out terrain corrections is height dependent, less than one milligal for a station at 500 m elevation above the topography to 11 milligals for a station at 2,000 m up. However, in this case, the stations are all below 640 m (most below 200 m) and as the terrain correction is small at large distances it can be neglected.

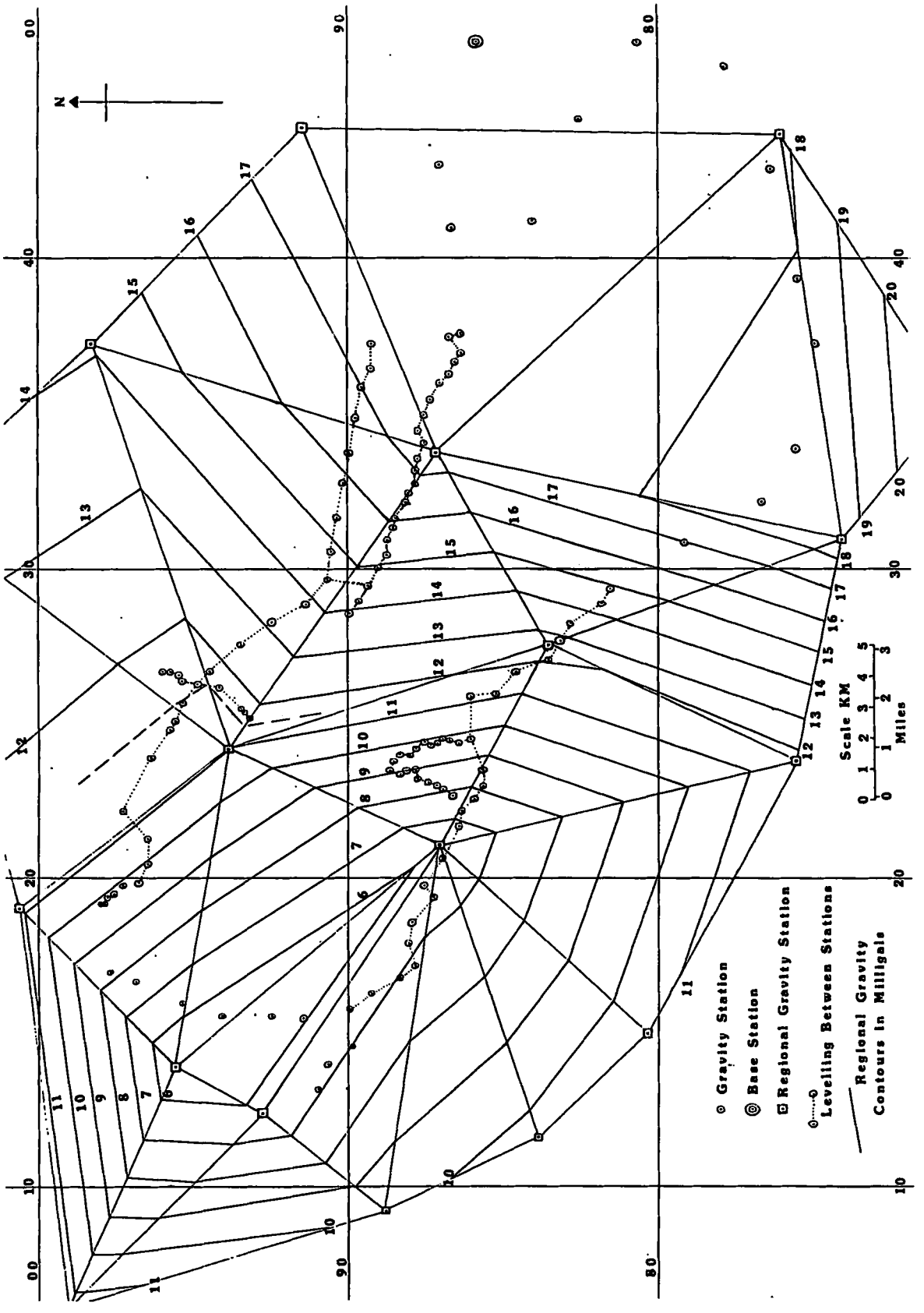

Figure 32. The location of gravity stations in the Breiddalur area and regional Icelandic gravity stations and field.

Once the data had been corrected for terrain and Bouguer effects a further correction for the Icelandic regional gravity field was applied (Figure 32), based on the data of Porbergesson et al. (1990) (Appendix 4). This was calculated by plotting Porbergesson's gravity stations for the area and interpolating the regional gravity field between regional gravity stations. The regional gravity field (Figure 32) reaches a low of under 6 milligals in the northwest of the area and increases to the east to 17 milligals and 20 milligals in the southeast of the area. The regional gravity effect for each local gravity station was estimated and removed, before the local gravity anomaly was deduced (Figures 30 and 31) and cross sections drawn up for 2½ D modelling.

5.3 2½D gravity profiles across the Breiddalur area.

Four 2½D gravity profiles were modelled using GRAVMAG across the Breiddalur central volcano, Iceland using gravity data reduced as described in the last section. The profiles were chosen to intersect as many real data points as possible so as to minimize the need for extrapolation. The residual local gravity field (Figures 33 and 34) varies from -19 milligals in the northwest to a high of -4 milligals in the north, which decreases down to -14 milligals in the east and -16 milligals in the south, where there are local highs of -10 milligals and -11 milligals to the west and east of this low respectively. Rock samples from the Breiddalur area were used to obtain the densities for modelling (Appendix 3). The values chosen for the various bodies in the profiles were as follows: 2.2 g/cm^3 with

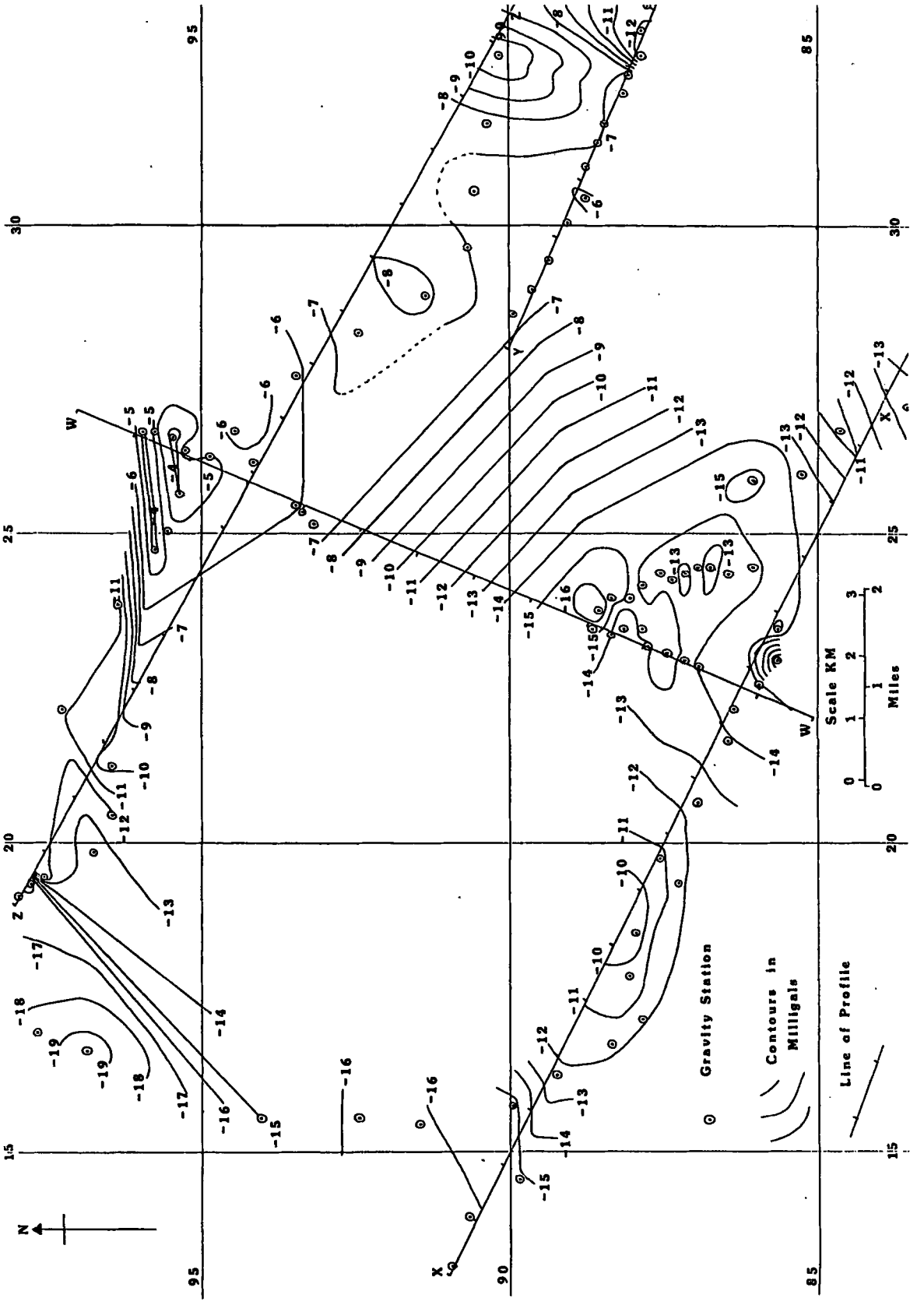

Figure 33. Local residual gravity anomalies in the northwestern half of the Breiddalur area.

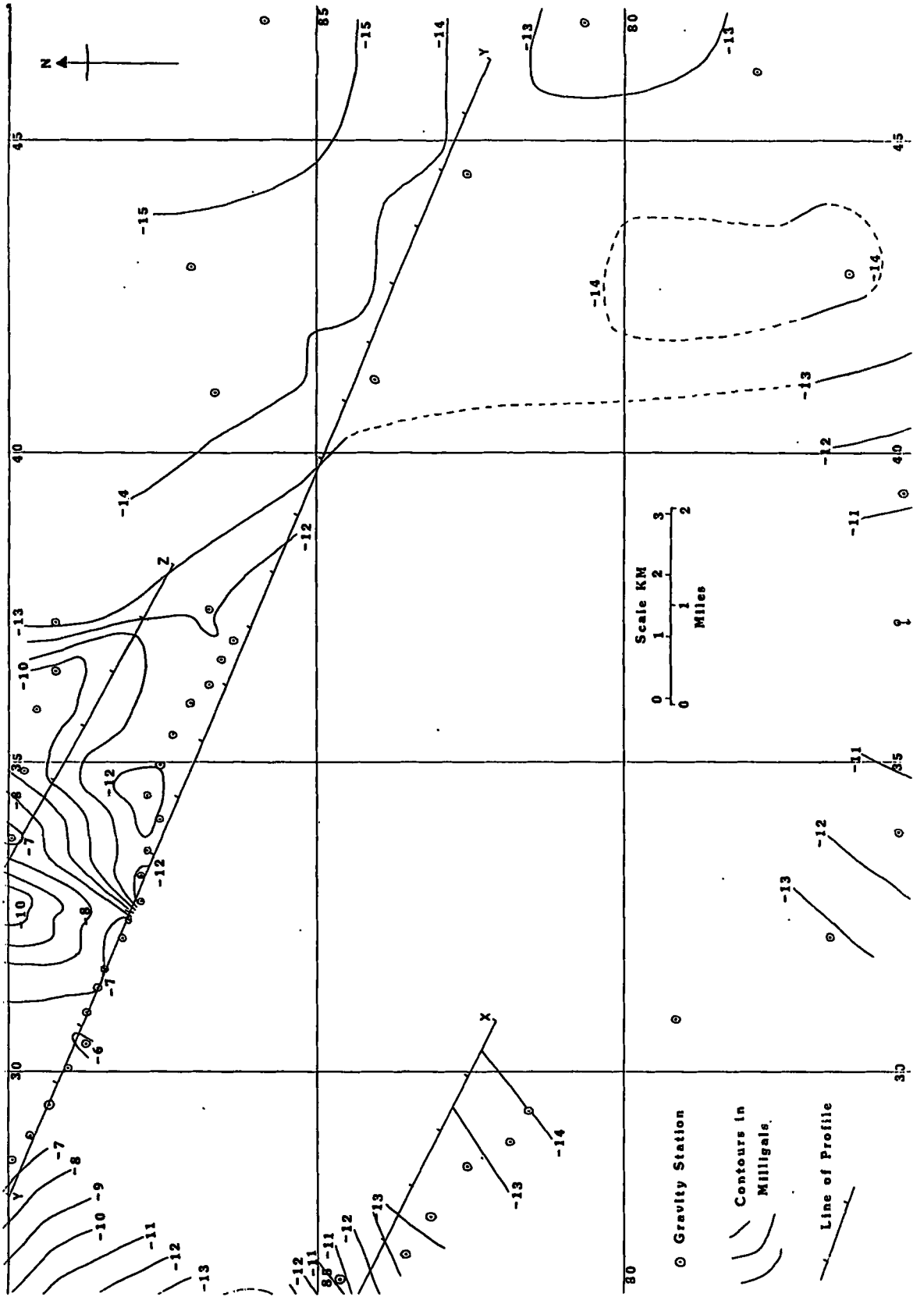

Figure 34. Local residual gravity anomalies in the southeastern half of the Breiddalur area.

a half strike of 2 km or 1km for alluvium deposits; 2.33 g/cm^3 with a half strike of 4 km or 2 km for silicic rocks; 2.50 g/cm^3 with a half strike of 4 km for Andesites; 2.8 g/cm^3 with a half strike of 2 km for Olivine - Basalts; and a background density of 2.6 g/cm^3 for the basalts around the volcano. The densities for the bodies in the profiles were based on those measured on rocks from the Breiddalur area and the half strikes were adapted from the outcrop widths and strike lengths for different rock types. The three profiles that interconnect (W-W', X-X' and Z-Z') were modelled so that they were in agreement to within 100 m at intersections between them. Profile W was taken over the centre of the volcano (Figure 33) so that the core of the exposed volcano could be modelled. This profile was linked to profile Z along the Sudhurdalur valley to the north and Profile X along the head of Berufjordur to the south, these are the two main valleys through the Breiddalur area. A fourth profile Y, about 3 km south of the eastern and of profile Z, was run to model the gravity for stations along the eastern end of the Sudhurdalur valley.

The first profile W-W' (Figure 35) runs north (270 970) to south (220 850) across the centre of the Breiddalur volcano. The most obvious feature of this profile is the decrease in gravity from north to south. Low gravity in this area would most likely indicate the presence of silicic material. To reduce the apparent thickness of silicic rocks beneath the southern end of the profile at the edge of the volcano, a gradient of 0.77 milligals per kilometre increasing southwards, was applied. This regional gravity gradient away from the centre of Iceland, is due to the sea having lower values of gravity than the mainland. The station spacing for the regional field

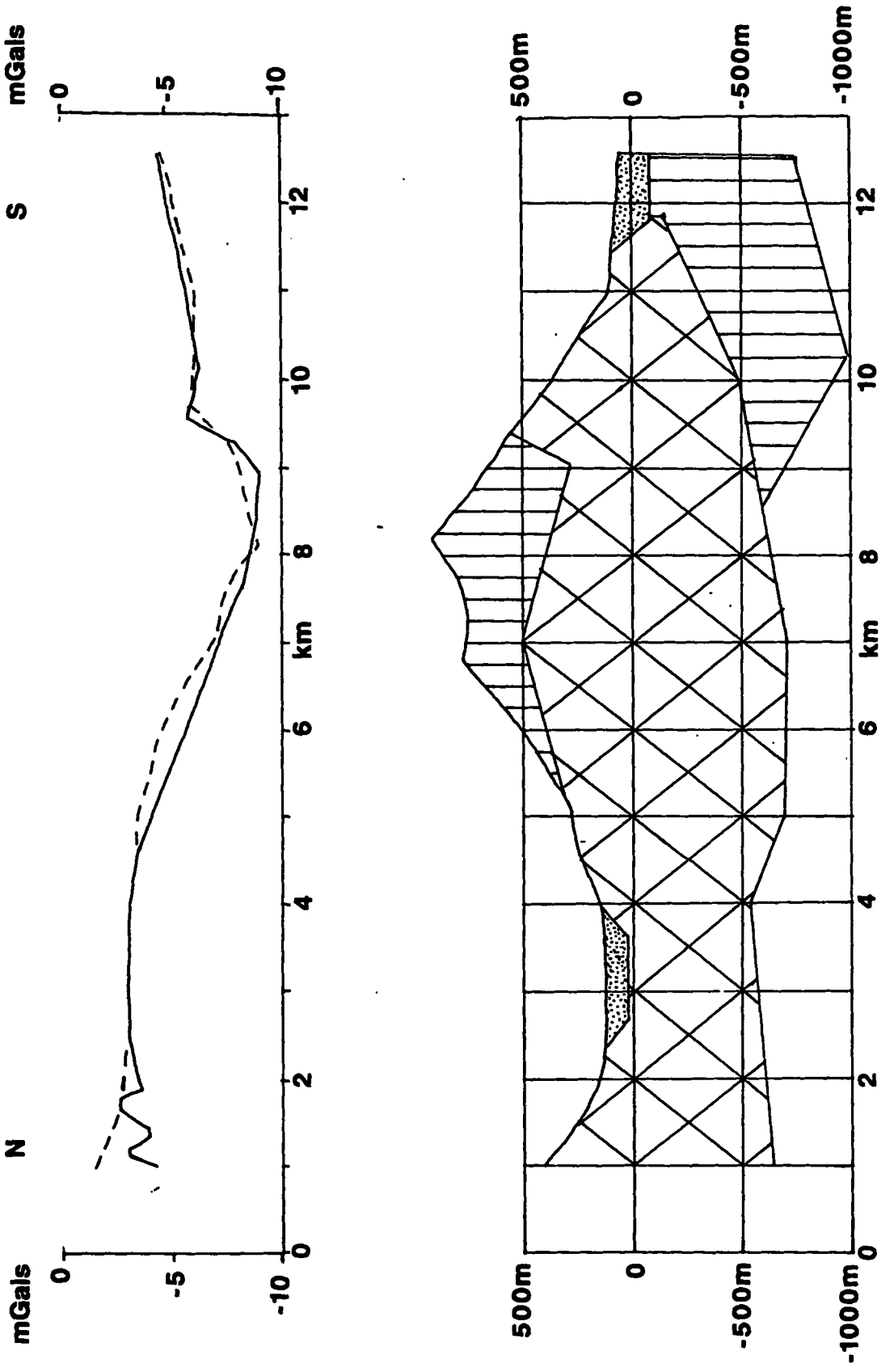

Figure 35. Profile W-W' N 270 970 to S 220 850. Solid line is observed profile, Dashes are calculated profile, horizontal scale km, vertical scale in meters. Dots density 2·20 g/cm³ half strike 2 km (on left) 1km (on right); Cross-hatching 2·50 g/cm³ half strike 4 km; Vertical lines 2·33 g/cm³ half strike 4 km; Background density 2·60 g/cm³. Zero milligals at the northern end up to 10 milligals added to profile at southern end (13 km).

(Porbergesson et al. 1990) was too large to detect the 10 milligal anomaly identified at the southern end of profile W-W'. The original 10 milligal anomaly was far too large to model as a silicic intrusion below the Berufjardara area (22 86) as it would have had to have been many kilometres thick. No additional east-west gradient was assumed and so the corresponding values of 2.3 milligals to profile Z-Z', 4.6 milligals to profile Y-Y' and 9.0 milligals to profile X-X' were added on the basis of the gradient along profile W-W'. From the geological map (Figure 31) alluvium deposits about 100 m thick were modelled in the bottom of the two valleys along the section and the solid rocks were taken to be andesites and acid rocks. The model for profile W-W' shows that the top of the exposed volcano is capped by up to 500 m of silicic rocks (vertical lines on Figure 35) with a volume of 8 km^3, below this are up to 1200 m of andesites (cross hatching) 72 km^3 in volume with a further wedge of up to 700 m thick of silicic rocks, 15 km^3 in volume (24 km^3 when extended in the geological cross section beyond the southern end of the profile) at the southern end of the profile, a total thickness of about 2,000 m. This wedge of silicic rocks in the Berufjardara area (22 86) cannot be modelled as valley alluvium as it is too large and so suggests that the volcano had an earlier southern centre in this area, which was covered by later eruptions.

The second profile Z-Z' (Figure 36) runs along the Sudhurdalur valley on the northern side of the volcano from West (190 980) and east (380 874). At the far western end of the profile there is a 5 milligal drop which may be due to the profile leaving the valley and errors with gravity stations not linked by EDM levelling. A sharp 5

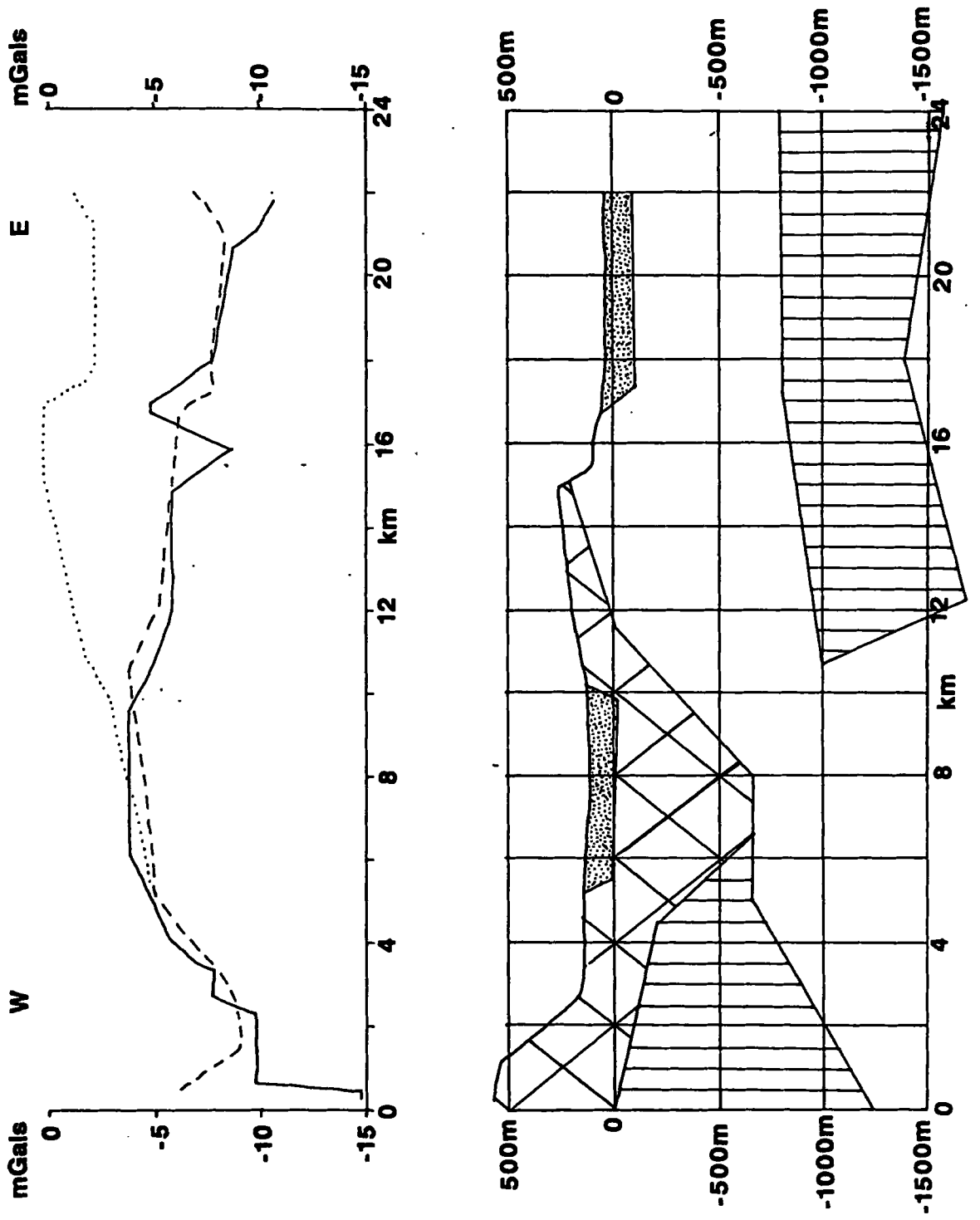

Figure 36. Profile Z-Z' W 190 980 to E 380 874. Solid line is observed profile, Dashes are calculated profile, Dots are calculated profile with no deep body below eastern half, horizontal scale km, vertical scale in meters. Dots density 2·20 g/cm³ half strike 1 km; Cross-hatching 2·50 g/cm³ half strike 4 km; Vertical lines 2·33 g/cm³ half strike 4 km; Background density 2·60 g/cm³. 2·3 milligals added to profile.

milligal drop is unexpected, since to the west there are the denser basalts of the surrounding country rocks. Alluvium deposits (dots on Figure 36) about 100 m thick were modelled filling the bottom of the Sudhurdalur valley and the solid rocks were assumed from the geological map (Figure 31) to be andesites in the west (cross hatching) and flood basalts (background) to the east. In order to model the drop in the anomaly at the western end of the profile a silicic body up to 1,200 m thick and 35 km^3 in volume is postulated, this could be a buried extension of the silicic centre of the volcano to the southeast. To the east there is apparently a silicic body up to 750 m thick, 70 km^3 in volume and over 12 km long. Either this is a real, earlier volcanic centre linked to that of profile Y-Y' or there is an unaccounted for regional anomaly to the east of the Breiddalur central volcano, which is less likely.

The third profile Y-Y' (Figure 37) runs along the southern side of the eastern Sudhurdalur valley about 2 km south of profile Z-Z' between west 280 900 and east 463 822. On the basis of evidence from the geological map (Figure 31) a wedge of andesites dipping 7° westward at the western end of the profile, with the rest of the surface outcrop as flood basalts was modelled. To fit with profile W-W' 4.6 milligals were added to gravity values along the profile. At the western end of the profile the Andesites of the volcano are modelled dipping at about 7° westwards. Once again to the east a silicic body up to 1200 m thick, 140 km^3 in volume and over 18 km long is apparent. This is thought to be an earlier volcanic centre linked to that shown in profile Z-Z'. The anomaly is far too large to be modelled as alluvium filling the valley floor,

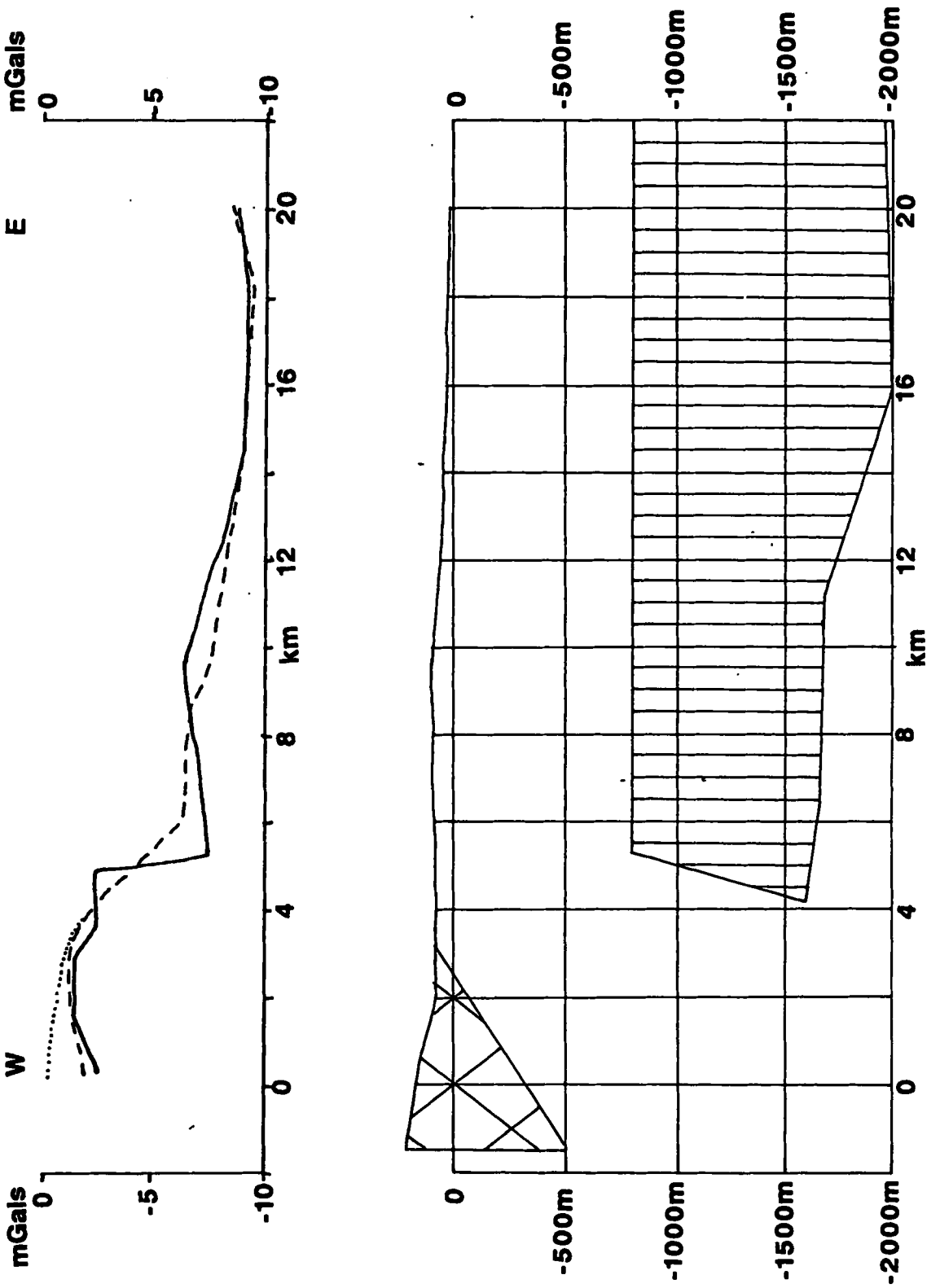

Figure 37. Profile Y-Y' W 280 900 to E 463 822. Solid line is observed profile, Dashes are calculated profile, Dots are calculated profile without Cross-hatched body, horizontal scale km, vertical scale in meters. Cross-hatching 2·50 g/cm³ half strike 4 km; Vertical lines 2·33 g/cm³ half strike 4 km; Background density 2·60 g/cm³. 4·6 milligals added to profile.

though the thickness and volume for such a body would be less than those for a silicic body.

The fourth profile X-X' (Figure 38) runs along the southern side of the Breiddalur central volcano along the top of the Berufjordhur from the west (130 910) to the east (310 820). The drop in value of the anomaly at the western end of the profile could possibly be due to a large hidden volume of low density silicic rocks in the Odadhavotn area. To give a better fit, a small wedge of denser Olivine - basalt 0.8 km^3 in volume, along its outcrop across the profile was modelled. To fit profile W-W' up to 600 m thickness and 14 km^3 volume of silicic rocks were modelled: as a result the calculated profile does not fit the centre of the low in the middle of the profile by about two milligals. At the eastern end of the profile a silicic body up to 500 m thick and 8 km^3 in volume was added: this may be linked with the silicic centre at Rondolfur and Slottur a few kilometres to the north of this profile. In addition, andesites 52 km^3 in volume consistent with their outcrops along the profile were added to the model.

5.4 Discussion

The perceived need to add between 0 and 10 milligals at the southern end of profile W-W' has a significant effect on the other profiles, especially profile X-X'. The regional field was originally removed so that any remaining local anomalies in the Breiddalur area could be modelled. Further adjustment had to be made because part of the remaining anomaly was far too large to be modelled as a low

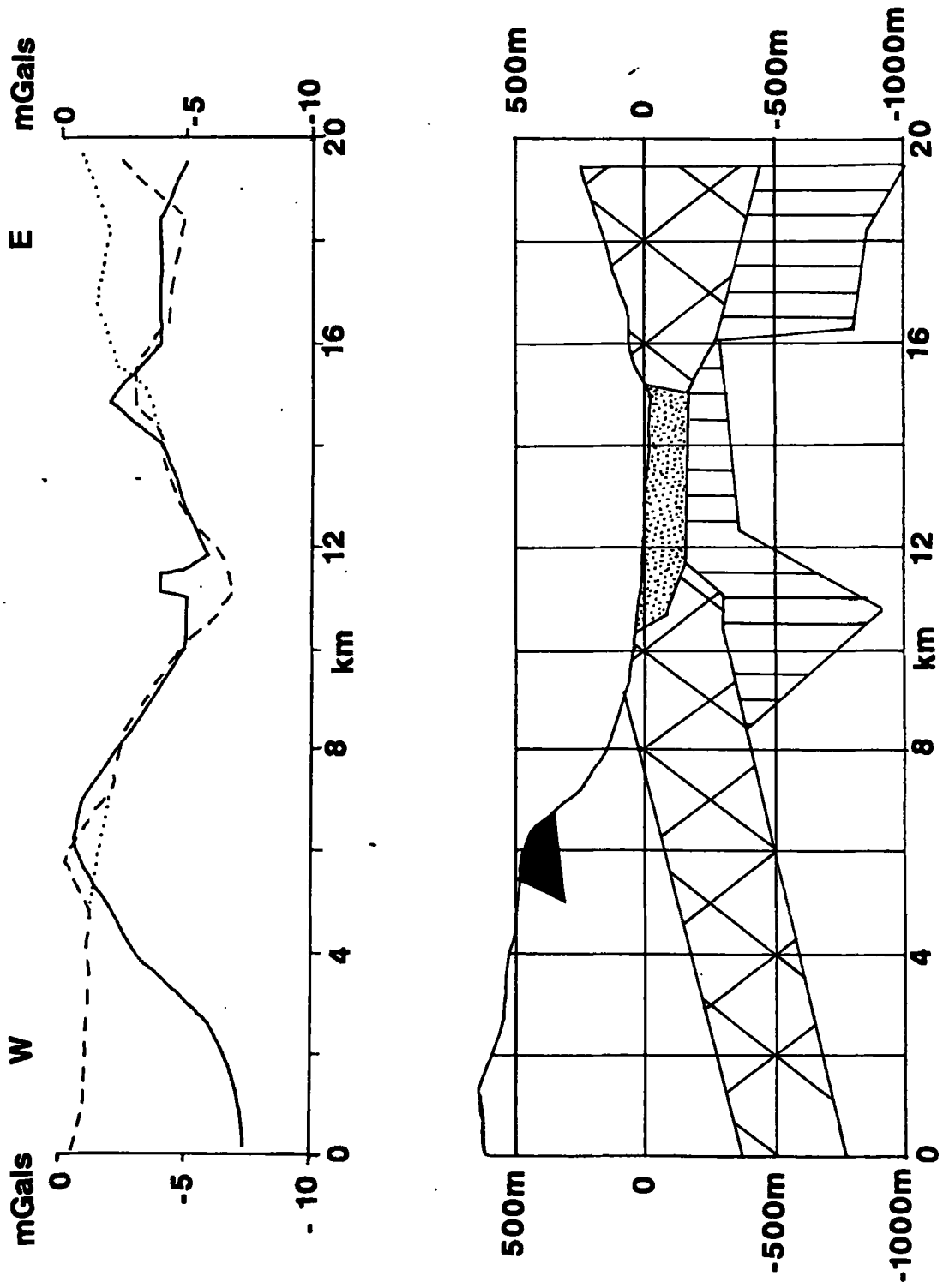

Figure 38. Profile X-X' W 130 910 to E 310 820. Solid line is observed profile, Dashes are calculated profile, Dots are calculated profile without black body and eastern vertically lined body, horizontal scale km, vertical scale in meters. Dots density 2·20 g/cm³ half strike 1 km; Cross-hatching 2·50 g/cm³ half strike 4 km; Vertical lines 2·33 g/cm³ half strike 4 km (on left) 2 km (on right); Black 2·80 g/cm³ half strike 2 km; Background density 2·60 g/cm³. 9·0 milligals added to profile.

density silicic intrusion. The southern end of the profile could have been moved slightly to the east to intercept a gravity station 4 milligals higher in value, but as only one station has this value it could be a possible error and it would still leave 6 milligals to be removed from the profile. The regional field may also be complicated by the proximity of the sea to the south and east of the Breiddalur area, and thus the decrease in the residual local gravity field along profile W-W' may be due to this. Once the regional field has been removed the remaining lows may each be representative of a hidden silicic centre between 500 m and 1,200 m thick. The possibility of these lows being due to low density basalt scoria is unlikely as no large volumes of scoria are reported in the area and enormous volumes would be needed. If this is not the case then the residual local gravity field would have to be the result of deeper density contrasts: as these features have short wavelengths below 10 km, this seems unlikely. If the silicic centres have associated magnetic anomalies then this would greatly strengthen the case that they exist. Unfortunately the only way to prove that these buried silicic volcanic centres exist would be to drill boreholes down to them which is unrealistically expensive.

A geological cross section (Figure 39) based on profile W-W' is presented. Silicic rocks outcrop at the southern end of the profile at the northwestern end of Berufjordur (Berufjordara)(22,86) and have been modelled as a silicic intrusion 700 m thick and 15 km^3 in volume. These rocks are considered to represent part of an earlier centre of the Breiddalur volcano, which because it extends to the south of the profile W-W' has a total volume of 24 km^3. The base of the volcanic

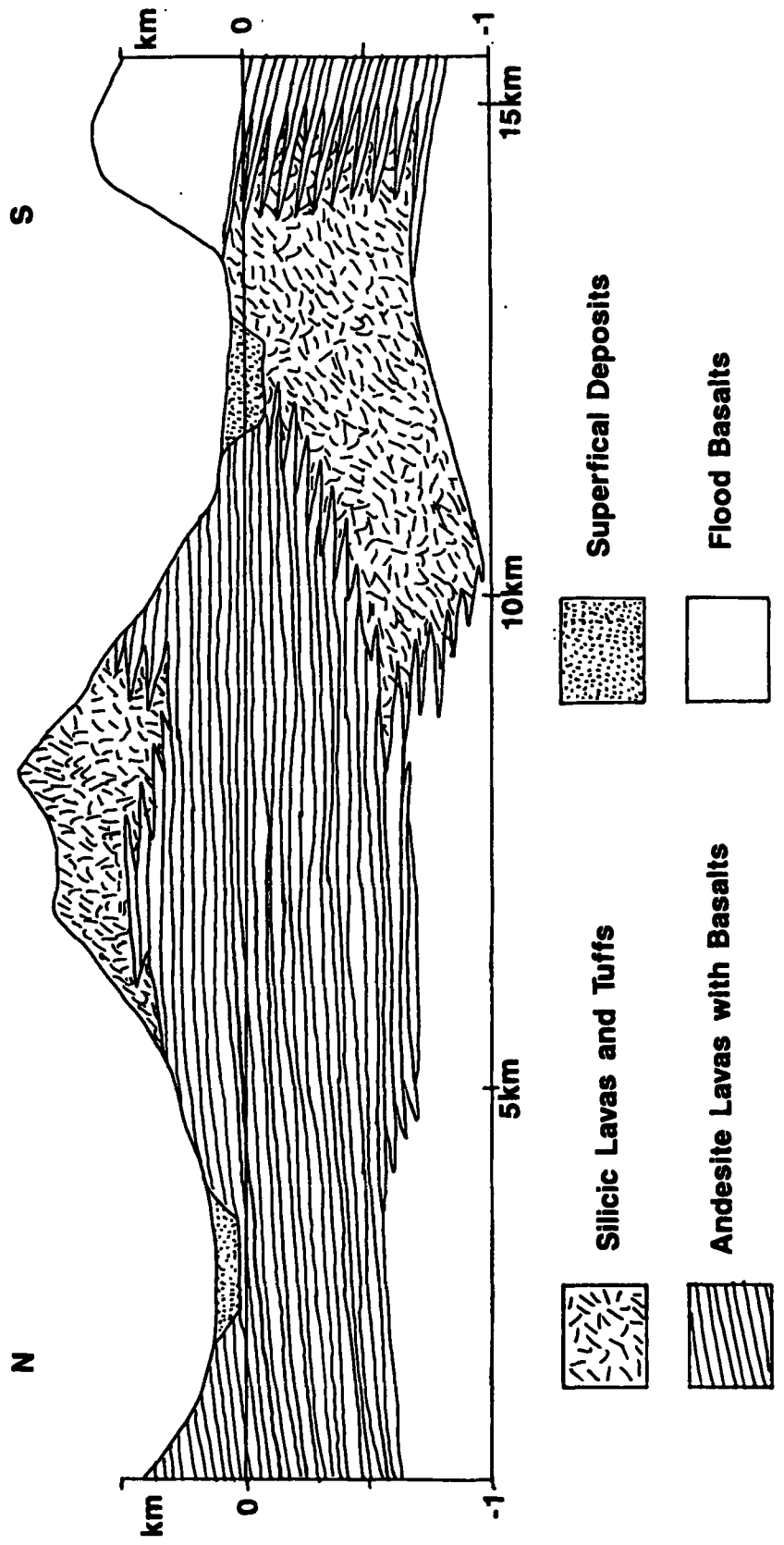

Figure 39. Geological cross section of Breiddalur Volcano based on modelling along Profile W-W'.

centre is assumed to rest on the surrounding flood basalts, unlike the later exposed centre of the volcano. The edges of the silicic lavas and tuffs interdigitate with the surrounding andesite lavas and occasional basalts as silicic lava flows thin out at the edge of the volcanic centre. The andesitic rocks form a series of thin lava flows which probably extend for up to 10 km away from the silicic centres. Before erosion the upper silicic volcanic centre may have had a volume of about 12 km^3 (based on its modelled thickness and diameter), much greater than the 1.6 km^3 suggested by Walker (1963) for the summit rhyolite. The Breiddalur volcano had a total thickness of about 2,000 m, based on profile W-W' (Figure 35).

These profiles suggest that the Breiddalur central volcano not only has a silicic centre in the Matarhnjukur area (24 91) but also buried centres at the western end of the Sudhurdalur valley (19 97), at the northwestern end of Berufjordur (Berufjardara) (22 86). With possibly other buried volcanic centres along the eastern end of the Sudhurdalur valley (36 87), the Odadhavotn area (13 91) and as a southeastward extension of the Berufjordur centre (30 82). These hidden silicic centres are between 500 m and 1,200 m thick, 8 km^3 and 140 km^3 in volume and from 5 km to 18 km long. They may represent volcanic centres similar to the exposed Breiddalur central volcano which were buried by flood basalts before the formation of the Breiddalur volcano. They have a total volume of about 250 km^3 including the largest 140 km^3 body over an area of at least 500 km^2. This suggest that silicic rocks form 10% of the upper 5 km of crust in this area. This fits in with the 10% of acid differentiate that may be derived from a basic parental liquid (Cox et al. 1979, p. 310) and

the up to 8% for the granitic rocks modelled in the Skye Tertiary central intrusive complex in northwestern Scotland (Bott and Tuson, 1973). This may represent a series of silicic central volcanoes associated with parallel eruptive ridges or fissure swarm volcanic systems. These silicic centres could represent pods of material generated by partial melting of the thickened oceanic crust that did not reach the surface to erupt.

6.1 The Generation and Emplacement of Silicic Magma.

The key problem in the study of silicic volcanic systems such as the Valles Caldera and Breiddalur central volcano is the generation and emplacement of this type of magma. A solution to this problem has been proposed by Huppert and Sparks (1988a) involving the intrusion of basalt sills into the continental crust resulting in its partial melting and the generation of granitic magmas. A mathematical model by Huppert and Sparks (1988b) for this is partly based on experiments with wax or ice substituted for the continental crust and a hotter salt solution representing the intruding basalt. They model sills as they allow for the transfer of substantial amounts of heat vertically into the country rocks. In dykes, the basalt is moving upwards too rapidly and too locally to transfer much heat to the walls of the dyke, and when the basalt solidifies most of the heat will be lost vertically within the dyke. Dykes tend to be only up to a few meters wide and so do not have a significant volume with which to melt the surrounding country rock, also melting due to horizontal heat flow from the wall of a dyke is both difficult to model and of limited significance, Bruce and Huppert (1990).

Published models of sill emplacement suggest that basalt emplaced into continental crust will generate significant volumes of silicic magma by melting silicic continental crust over geologically short periods of time. Furthermore, such rapid generation of magma does away with the need for large, long-lived, high-level magma chambers below silicic volcanic complexes. The question of how hydrothermal and geothermal systems within the volcanic complex are maintained, may

thus be answered by the raised geothermal gradient due to the intrusion of basic magma in to the roots of the complex. A common sequence of events in large silicic caldera complexes has been identified by Lipman (1984). They are initiated with basic to intermediate lava shields, that evolve to more silicic explosive eruptions, which in their final stage often develop a small number of very large volume silicic ignimbrite eruptions and the formation of calderas.

Continental crust at an initial temperature of 500°C, about 25 km depth for an average continental geotherm (Brown and Mussett 1981), will melt at the roof of a basaltic sill to form a stable low density melt layer that does not mix with the underlying hot basalt at a temperature of 1200°C (Huppert and Sparks 1988a). Near surface crustal melting occurs at about 850°C by conduction from the melt layer and by the time the basalt solidifies, the melt generated will reach temperatures of between 900°C and 950°C, depending on the ratio of volumes involved, and the degree of mixing between the melt and the crust. This suggests that the silicic melt could also generate further melting of the crust, but there is not much evidence of strong superheating in acid magmas and 800°C is a typical maximum temperature (G.C. Brown pers. comm.). This would suggest that the model temperature for melt generated by crustal melting is 100°C to 150°C too high, and once melting occurs at 850°C the melt cools to below 800°C but remains liquid. The effect of a series of basalt sills raising the background temperature of the crust will mean that even larger volumes of silicic melt will be generated by the cooling of a basaltic sill of a given thickness. The raised geothermal gradient

is often likely in active volcanic regions and rift zones to be the result of the intrusion of such basic sills. The depth at which melting can occur will be much less than 25 km in such regions: below the Valles Caldera at present, the 500°C isotherm may be at about 10 km below the surface (based on the temperature gradient in the lower part of the Fenton Hill borehole (Sass and Morgan 1988)). Melting may also occur at the floor of a sill. Experimental studies are presented by Huppert and Sparks (1988c), but a theoretical model has yet to be developed due to the complications of the generation of light melt on the composition and temperature of the system.

The Huppert and Sparks (1988a) model predicts the temperature of the interface between the basic sill and the rhyolite melt layer, the temperatures of these layers and the thickness of the rhyolitic melt layer as functions of time. The times at which convection begins and ceases in the silicic magma generated and when it ceases in the emplaced basaltic layer are also predicted. The model does not allow however for the drawing off of melt to higher levels in the crust while the newly emplaced sill is heating the crust and what effect this would have on the further melting of the residual material above the sill. The temperature at which crustal rocks reach the critical melt fraction, when the connectedness of the crystalline framework is destroyed and the rock becomes a liquid or magma, will vary according to the rock's composition and the availability of volatiles, mainly water. It has been found that the critical melt fraction must be at least 40% for a lava to be sufficiently fluid to be erupted (Marsh 1981). Hydrous minerals such as mica and hornblende vary from trace amounts to about 2% depending on rock type in upper crustal rocks

(Huppert and Sparks 1988a). This intrinsic water content may cause substantial melting over a narrow temperature interval as these mineral break down (Wyllie 1984). Most crustal rocks have a low intrinsic water content (less than 1%), but the first melt fraction may have a higher water content as it depends on the water pressure temperature relationship. Water and other volatiles however can be added to the melting rock by the degassing of basaltic magma into the melt, assuming the pressure at a given depth is not too great, and circulating hydrous metamorphic fluids could also increase the water content of a rock during melting (Wickham 1987).

When melting has occurred it is estimated by Huppert and Sparks (1988a) that the silicic layer will take at least 10,000 years to cool back down to the ambient temperature of 500°C. For a basalt sill at 1,200°C the following range of thicknesses will generate melt of a given thickness, maximum temperature and time to become 50% crystalline: 10 m basalt sill will generate 5 m of melt at 943°C and take 3 years to cool; 150 m basalt sill will generate 84 m of melt at 935°C and take 58 years to cool; 1,500 m basalt sill will generate 878 m of melt at 933°C and take 650 years to cool. A series of sills emplaced over a shorter period of time than 10,000 years will generate a thicker layer of silicic magma as the crust is already hot and partially molten. This is a long period of time compared with the 272 years after emplacement for even a 1500 m thick basic sill to become 60% crystalline and cease to convect (Huppert and Sparks 1988a). This short 'model' time will actually be longer than predicted as any natural system is not ideal, because of such factors as: the high viscosity of silicic magma; non-newtonian properties of crystal-rich

areas of the melting region; the anisotropic structure of the country rock; and the formation of a chilled crust at the top of the sill. If a sill is too thin, the model is not appropriate as the silicic layer does not start to convect, or the buoyant crustal melt moves upwards away from the sill at too fast a rate for a convecting layer of silicic melt to form above the sill. This minimum for a sill is about 3 m or 4 m in thickness and so Huppert and Sparks (1988a) did not present calculations for sills thinner than 10 m. In their models a basaltic sill at 1,200°C intruded into continental crust at about 500°C will result in the generation of a silicic melt layer just over half the thickness of the sill. Melting will not occur if the country rock is cooler than 500°C, since the contact with the sill will not reach melting point, and the heat will be conducted away into the cool crust. However repeated basic intrusions over a few thousand years would raise the temperature of the country rock to the point that melt will be generated by the intrusion of a sill.

The Huppert and Sparks (1988a) model is different from previous ideas, such as Smith (1979): there is no need for a shallow long-lived magma chamber, although there is no reason that magma chambers cannot form as a consequence of melt generation; crustal melting and crystallization occur on geologically very short time-scales, a few tens to hundreds of years, compared with the millions of years lifetime of a large silicic magmatic system. Every time a batch of basalt arrives in the root zone at the base of a silicic system a melting event is triggered and magma may rise to the surface or be emplaced at a shallow level either to differentiate, to generate more evolved magma, or to freeze as plutons. Crystallization in the

generated magma can occur at source and does not have to occur after the magma has ascended to a shallow level to cool. Many crystals formed from such melts are of genuinely igneous origin but geochemically represent refractory components of the crust.

Smith (1979) developed a chemical model of silicic magma evolution, the key features of which are set out below. Smith (1979) suggested that there is a positive correlation between caldera area and ejecta volume. This places constraints on magma draw down during eruption and further suggests a link between caldera area and ejecta volume with the volume of the magma chamber beneath. Smith (1979) observed that calderas range from 1 km^2 to 10,000 km^2 in area with ejecta volumes in the range of 1 km^3 to 10,000 km^3 and suggested magma chamber volumes of 10 km^3 to 100,000 km^3. A tentative correlation between ejecta volume and time of magma generation reveals a production rate of about 10^{-3} km^3/yr or 1,000,000 m^3/yr. Variations revealed in the pyroclastic deposits from an eruption to the maximum eruptible level give insight into differentiation processes and the physical and chemical gradients within the pre-eruption magma chamber. Compositional contrasts are commonly greater in small volume systems, but all systems tend to become more mafic with depth. Successive caldera-forming eruptions from a system become more mafic with time unless a very strong resurgence of primitive magma reactivates the system to start a new phase of magmatic activity. A system may become more mafic with time due to two possible effects, decreasing thermal input and progressive depletion of "residual" elements. In high SiO_2 rhyolite magmas such as the Bandelier Tuff, minor elements show striking alternations in enrichment and depletions

in successive eruptions from the most-fractionated boundary layer at the top of the magma chamber. Smith (1979) felt that it was unrealistic to define precisely the term "high-level magma chamber", but suggested, on the basis of estimates for the maximum known pluton sizes, that such chambers are less than 10 km thick.

Smith (1979) suggested that the Bandelier Tuff reflects a major thermal event or series of events caused by basalt injection into the lower part of the magma chamber. This concept is very similar to the generation of silicic magma by the intrusion of basic sills into the crust in the Huppert and Sparks (1988a) model. The primitive magma of Smith (1979), is thought to be a mantle-derived mafic magma in most places, analogous to the basalt of Huppert and Sparks (1988a). The derivative (silicic) magma is defined as any magma that derives its existence and mobility from the thermal source provided by the primitive magma. Derivative magma may be a primitive magma changed by crystallization differentiation, assimilation or mixing; a magma derived from primitive magma by any process of fractionation; or a melt or melt fraction of the crust formed as a result of the thermal contact with primitive magma from the mantle. The latter is basically the Huppert and Sparks (1988a) model for silicic magma generation. The distinction between crust and mantle source is made because the processes discussed by Smith (1979) are dependent on the interaction of mantle-derived mafic magma with crustal rocks, mostly in high-level magma chambers. It is probably best to think of a magma chamber as a large volume of crystal mush which has fluid movements over geological periods of time (100,000 years) and not as a liquid body. Only just before an eruption does the magma chamber

become fluid, due to a thermal input: this results in caldera collapse into the magma chamber as upper liquid fraction of the Smith (1979) magma chamber is erupted.

Huppert and Sparks (1988a) take as a rival view of silicic magmatism the partial melting of crustal source rocks and ascent of these melts to higher crustal levels where long-lived magma chambers are formed - as envisaged in the conceptual models of Smith (1979) and Hildreth (1981), involving crystallization and differentiation in a pluton-sized shallow magma chamber (km to 10's km in diameter) with compositional zoning as a common consequence. It is argued that a zoned silicic cap develops in these magma chambers, beneath a dominant mafic volume. The involvement of mafic magma in the development of such systems is seen as essential (Hildreth 1981). Huppert and Sparks (1988a) view the diversity of ideas on how silicic magmas are generated and differentiated as appearing to be in conflict with one another. They suggest that none of these concepts (including their own) have a monopoly on the truth. This conflict seems mainly to be the product of the differences in biases between physical and chemical models of silicic magma evolution.

6.2 The implications of the Huppert and Sparks model for the Jemez Mountains volcanic field.

The eruption of the Bandelier Tuff by the collapse of the Toledo and Valles calderas to form respectively the Otowi and Tshirege tuffs in the Jemez Mountains volcanic field would need the generation of over 300 km^3 of silicic magma on each occasion and similarly for other

big western U.S. calderas. The volume of each tuff deposit is about 300 km^3 to which must be added material that has been removed by erosion, or was lost to the atmosphere during the eruption and material that did not reach the surface. A maximum volume of about 500 km^3 would seem to be a reasonable upper estimate of the material involved in each case. Based on Huppert and Sparks (1988a) model, if melting occurred at the top of the supposed zone of basaltic underplating below the Rio Grand Rift over a radius of 50 km, about 64 m thickness of melt would be needed over the area, this would need the intrusion of a basaltic sill or sills about 100 m thick. Melting at the base of the 27 km wide magma collection zone, as inferred from the cylindrical low seismic velocity body about 1½ km to 10 km below sea level (Ankeny et al. 1986), below the Jemez Mountains would need about 875 m thickness of melt or a basalt sill 1,500 m thick using the model of Huppert and Sparks (1988a). This assumes that the country rock was already at a temperature of at least 500°C and that little of the melt formed either 'froze' on the way to the surface or melted significant amounts of material higher up in the magma collection zone. The raised geotherms due to the rift means that melting is more than likely at 15 km to 20 km below the surface of the Rio Grande Rift as the crust is hotter than normal. As higher temperatures are possible because the crust has thinned below the Rio Grande rift, this would mean that a thinner basaltic sill could melt the same amount of crust.

Due to the magma chamber or collection zone becoming compositionally and density zoned, it becomes impermeable to primitive high-density magma during the later magmatic phase of its life (Smith

1979). The history of the Jemez mountains volcanic field begins with the direct eruption of basalts. This is followed by the eruption of intermediate magmas formed as the basalts mix with the crust melted by the injection of hot basaltic magma. Further heating of the crust by basic magmas results in the ponding of silicic material in a magma chamber or collection zone. A further thermal pulse results in the melting of this material and the inevitable collapse of the area above the zone. This results in the formation of a caldera and the eruption of large volumes of silicic magma in the latter stages of the development of a volcanic field and can be seen as the result of progressive injection of basic magma into the crust.

Both physical solutions (the 100 km and 27 km wide melting diameters) are possible under the Jemez Mountains and can fit in with the geochemical models of Smith (1979) and Hildreth (1981). The evolution of the Jemez Mountains volcanic field has been one of mixed basalt to rhyolite systems which can be explained by the underplating and emplacement of basaltic magmas below the Rio Grande Rift (Figure 14). A 50 km dextral offset in the Rio Grande Rift developed after the inception of rifting about 31 Ma ago due to the Jemez Lineament intercepting the rift. This has resulted in the Rio Grande Rift at this location acting in part as a pull-apart basin and has, in turn, allowed the preferential collection of magma below the weakened crust of the Jemez Mountains. Silicic magma generated by such basaltic sills rises in the crust to melt additional rock which together forms the diverse range of volcanic rocks seen at the surface in the Jemez Mountains. The intrusion of sills under the Jemez Mountains slowly lead to the heating of the crust. As melting due to the heat from

cooling of basic sills results in silicic melt, and so mixing of this melt with further material from the crust must occur in order to generate intermediate magmas. Larger amounts of melt were generated and differentiated in the crust to give rise to intermediate magma types, seen in the pre-caldera volcanic rocks of the Jemez Mountains. Finally a series of basaltic sills emplaced into the magma collection zone below the area led to the rapid generation of massive amounts of buoyant silicic magma which explosively erupted the Otowi and Tshirege tuffs and formed first the Toledo and then the Valles calderas. The magma collection zone may be acting as the long-lived magma chamber in both the Smith (1979) and Hildreth (1981) conceptual models. In contrast to these models, the long-lived magma chamber is below its melting point for long periods of time, when it behaves as the heated country rock of the Huppert and Sparks (1988a) physical model.

6.3 The implications of the Huppert and Sparks model for the Breiddalur central volcano

The eruption of the Breiddalur central volcano would have needed the generation of over 100 km^3 of silicic magma (up to 250 km^3 for the whole area). This is much less than 500 km^3 for both the Toledo and Valles calderas, but the source of the magma is thickened oceanic crust and not silica rich continental crust. The intrusion of a sill beneath Breiddalur would generate far less silicic magma, though if the process were repeated often enough silicic magma would begin to pond in the crust and start rising to the surface. Thus a much greater volume of oceanic crust would be needed to generate a given

amount of silicic magma than with continental crust. As with the Jemez Mountains volcanic field the history of the Breiddalur central volcano begins with the direct eruption of basalts. This is followed by the eruption of andesites formed as the basalts mix with the silicic material melted by the injection of hot basaltic magma. Further heating of the crust by basic magmas results in the ponding and then eruption of buoyant silicic material, in the latter stages of the volcano's development.

If the generation of this silicic magma was not possible by the intrusion of sills into the crust, it could have been generated by magmatic differentiation of basic magmas. Magmatic differentiation is the processes that cause a magma to separate into two or more parts which have different compositions, this topic is discussed by Wilson (1993). Cox et al. (1979, p. 310) state that 10% silicic differentiate can be derived from a basic parental liquid, thus the up to 250 km^3 of acid material in the Breiddalur area of over 500 km^2 could be generated from basic oceanic crust only 8 km thick. The intrusion of basic sills and the partial melting of the crust may thus be the final stage of the differentiation process in generating silicic magmas in this case.

7. Summary and Conclusions

a) Valles Caldera, New Mexico

Dextral movement between the Pacific and North American plates replaced subduction beneath North America in the Cenozoic. This led to tectonic collapse and the development of the Basin and Range province. The Colorado Plateau has rotated clockwise as collapse within the neighbouring Basin and Range moved northwards in response to subduction ceasing northwards to the west. The back-arc basin associated with northern Baja California developed in to the Rio Grande Rift between the Colorado Plateau and the Great Plains to the east.

The Jemez Mountains are located at the intersection of the northeastward trending Jemez Lineament and the western margin of the north-south Rio Grande Rift, which is displaced eastwards at this point. The Jemez Mountains volcanic field has developed over the last 17 million years and is progressively downfaulted to the east. Prior to caldera formation the volcanic rocks are divided into two, the older Keres group and the younger Polvadera group: they range from basalts to rhyolites in composition. The Tewa group represents the formation, collapse and resurgence of first the Toledo Caldera and then the Valles Caldera over the last 1½ million years. The Rubio volcano (4 Ma to 1.5 Ma) in the area of the Toledo Embayment formed the centre of a depression which migrated southwestwards as it grew until stopped by a major rift fault to the west and then collapsed to form the Toledo Caldera. The Tewa group is almost all rhyolite and is dominated by the Otowi Tuff (300 km^3) deposited by the collapse of

the Toledo Caldera (1.45 Ma) and the Tshirege Tuff (300 km^3) deposited by the collapse of the Valles Caldera (1.12 Ma), collectively known as the Bandelier Tuff. The earlier Toledo Caldera has roughly the same size, shape and location as the later Valles Caldera. After the formation of the Valles Caldera there was resurgent volcanic activity in the caldera represented by the Valles Rhyolite up to about 130,000 years ago. The present Valles Caldera has a high-temperature geothermal system probably with a shallow magmatic heat source. This may be an approximately cylindrical low-velocity body below the southern part of the Valles Caldera from about 1½km down to 10km below sea level.

Gravity data from the Valles Caldera were modelled iteratively in 3D with a single density contrast (Segar 1974). The results suggest that the caldera is asymmetrical with only 760 m of caldera fill in the west and over 4,570 m in the east. The original corrected data from this gravity survey were used to model three 2½D gravity profiles across the Valles Caldera. In places these profiles indicate that the caldera floor is up to 1 km shallower than shown by the earlier iterative 3D model with a 3,600 m maximum depth but have a similar shape. In places faults that exist in one model are not found in the other. Small bodies with different density contrasts were identified along the 2½D profiles in this work which could not be modelled previously. The proposed model is that the caldera collapsed in a series of short fragmented blocks. In agreement with previous models, Valles appears to be a trapdoor caldera hinged to the west with some faulted basement blocks. The earlier Toledo Caldera had approximately the same area and extent as the Valles Caldera. The 2½D profiles

were extended to the Toledo Embayment and show that this is an area of low density rocks and it is suggested that this was the site of the earlier Rubio Volcano. The top of a fault block in this area on one of the profiles may mark the base of the earlier Rubio Volcano which failed to sink further during the formation of the later calderas.

b) Breiddalur, Iceland

Iceland lies astride the Mid-Atlantic ridge in an area of a mantle plume which results in hot elevated areas, to the south of Iceland the Atlantic Ocean is deeper and spreading faster. The Iceland plateau developed about 36 million years ago when the amount of magma generated by the plume increased relative to normal mid ocean rifting. The active volcanic zone has been unstable as the location of the plume has changed relative to the Mid-Atlantic plate boundary. At present, the Mid Atlantic boundary is exposed on Iceland with a crust twice as thick as normal Oceanic crust and is divided into three main neovolcanic zones. These are made up of volcanic systems composed of parallel eruptive ridges or fissures which may develop a central volcano like Breiddalur due to an increase in magma extrusion at one point.

The Breiddalur central volcano has a volume of about 400 km^3 and consists of basic to silicic lavas with a maximum thickness of 2,000 m. The active volcano stood above the surrounding flood-basalt plains which interdigitated with the products of the volcano before later burying it. Silicic rocks are concentrated in or near the core which probably occupied a small crater or caldera. A gravity survey of the Breiddalur area was carried out by G.C. Brown and H. Rymer and

processed by the author. Regional gravity effects were removed before 2½D modelling of the volcano. The profiles show that the silicic core of the volcano is 500 m thick in the Matarhnjukur area (24 91) (where it is exposed at the surface) and that at least two other buried silicic centres developed at the western end of the Sudhurdalur valley (19 97) and at the northwestern end of Berufjordur (Berufjardara) (22 86) during the active history of the volcano.

c) Basalt intrusion

The intrusion of basalt into the continental crust results in partial melting and the generation of granitic magmas (Huppert and Sparks 1988a,b). Published models suggest that significant volumes of silicic magma can be generated over geologically short periods of time, which fits in with the histories of both volcanic complexes. The Valles Caldera has far greater volumes of silicic magma than the Breiddalur central volcano - the latter is situated above thickened oceanic crust. There is far less silicic material available in oceanic crust than continental crust, and so when basalt is intruded into oceanic crust a far smaller volume of granitic magma results. It is suggested that magmatic differentiation of silicic magma from a basic parental liquid could be the main source of granitic magmas in Iceland, though partial melting of the crust due to the emplacement of basic sills, may still be the final stage in this differentiation process.

d) Future work

Following on from this work on these two silicic volcanoes there

are several possibilities for future work.

In the case of the Jemez Mountains, New Mexico, more work should be done on the development of North America and its effects on the history of the Rio Grande Rift. This could be compared with other inter-continental rifts, in different tectonic environments and stages of development, to see what were the similarities and differences between them.

Satellite images and aerial photographs of the Rio Grande Rift in the vicinity of the Jemez Mountains may help to define large scale structures. Often these cannot be traced on the ground and the few key exposures on the ground either go unnoticed or are not interpreted in the larger context. Such studies should be combined with structural field work on outcrops in the area.

Further seismic studies are needed to refine the near surface seismic structure, so that models of the deeper seismic structure below the Jemez Mountains can be enhanced. Seismic reflection profiles across the margins and middle of the Valles Caldera could yield significant new information especially if combined with another method such as gravity.

At least one borehole to a depth of over a kilometre is needed in the east of the Valles Caldera to constrain the hydrothermal and hydrological models for ground water circulation within the caldera. It would also yield further valuable information on the structure of this part of the caldera, which has not been drilled before. A borehole in the Toledo Embayment might help resolve this area's structural relationship to the rest of the Central caldera complex.

Radiometric age determinations using the Ar-Ar method instead of

the K-Ar method might resolve some problem age determinations, since a better understanding of the timing of events in the Jemez Mountains volcanic field and especially the inter-caldera and post-caldera periods would result. A sample from Ignimbrite A on the northwestern side of the Canon de San Diego, with only 4% ^{40}Ar, has an error range nearly as large as its K-Ar age. The two oldest formations in the Valles Rhyolite have not been dated due to extensive hydrothermal alteration: Ar-Ar dating and the careful selection of the less altered rocks in these formations might yield sensible dates. Many undated volcanic formations remain through out the Jemez Mountains.

The gravity survey of the Valles Caldera could be expanded to the whole of the Jemez Mountains to develop a model for the whole volcanic field and a better understanding of the central caldera in particular. Nettleton profiles might be needed to establish the density of formations with poor outcrop and borehole control.

In the case of the Breiddalur central volcano, Iceland, seismic studies similar to those carried out in the Jemez Mountains would help model the structure of the crust below the volcano. A study based on simultaneous three-dimensional (3D) travel-time inversion of earthquake and refraction survey data would reveal the velocity structure below the area. A seismic refraction survey along the valleys in the area would help to refine the 2½D gravity models by giving a depth to the base of the low density material filling the valleys.

Boreholes would help define the structure of the volcano, but are unlikely due to cost.

Radiometric age determinations would help define the development

of the Breiddalur central volcano which occurred either in the late Miocene or early Pliocene. They would also give a time frame for stages in the development of the volcano.

The original gravity survey could be expanded over the mountains between the valleys in the area, and further away from the volcanic centre. However, levelling in mountainous terrain could be difficult and time-consuming, unless G.P.S. equipment was used to locate stations.

8. References

Aldrich, Jr.M.J. 1986. Tectonics of the Jemez Lineament in the Jemez Mountains and Rio Grande Rift. Journal of Geophysical Research, Vol.91.B 1,753-62

Aldrich, Jr.M.J. and Laughlin, A.W. 1984. A Model for the Tectonic Development of the Southeastern Colorado Plateau Boundary. Journal of Geophysical Research, Vol.89.B 10,207-18

Aldrich, Jr.M.J., Chapin, C.E. and Laughlin, A.W. 1986. Stress History and Tectonic Development of the Rio Grande Rift, New Mexico. Journal of Geophysical Research, Vol.91.B 6,199-211

Ankeny, L.A., Braile, L.W. and Olsen, K.H. 1986. Upper crustal structure beneath the Jemez Mountains volcanic field, New Mexico, determined by three-dimensional simultaneous inversion of seismic refraction and earthquake data: Journal of Geophysical Research, Vol.91.B 6,188-98

Bachman, G.O., and Mehnert, H.H. 1978. New K-Ar dates and the late Pliocene to Holocene geomorphic history of the central Rio Grande region, New Mexico. Geological Society of America, Bulletin 89, 283-292.

Bailey, R.A., Smith, R.L. and Ross,C.S. 1969. Stratigraphic nomenclature of volcanic rocks in the Jemez Mountains New Mexico. U.S. Geological Survey Bulletin, 1,274-P. 19pp

Baldridge, W.S., Damon, P.E., Shatiqullah, M. and Bridwell, R.J. 1980. Evolution of the central Rio Grande rift, New Mexico: New Potassium-Argon ages. Earth and Planetary Science Letters Vol. 51: 309-21

Bott, M.H.P. and Tuson, J. 1973. Deep Structure beneath the Tertiary Volcanic Regions of Skye, Mull and Ardnamurchan, North-west Scotland. Nature Vol. 242, 114-6

Bott, M.H.P. 1988. A new look at the causes and consequences of the Iceland hot-spot. In: Morton,A.C. and Parson,L.M.(eds.) Early Tertiary Volcanism and the Opening of the North East Atlantic. Geol. Soc. London, Spec. Publ. 39, 15-23.

Brookins, D. and Laughlin, A.W. 1983. Rb-Sr geochronologic investigation of Precambrian samples from deep geothermal drill holes, Fenton Hill, New Mexico. Journal of Volcanology and Geothermal Research, Vol.15: 43-58

Brown, G.C. and Mussett, A.E. 1981. The Inaccessible Earth. George Allen & Unwin. 235pp.

Bruce, P.M. and Huppert, H.E. 1990. Thermal control of basaltic fissure eruptions. Nature Vol. 342: 665-7

Chapin, C.E. 1989. Volcanism along the Socorro accommodation zone, Rio Grande, New Mexico, in Field Excursions to Volcanic Terranes in the Western United States Vol I, Southern Rocky Mountain Region, edited by C.E. Chapin and J Zidek. New Mexico Bureau of Mines & Mineral Resources. Memoir 46: 46-57

Cordell, L. 1976. Aeromagnetic and gravity studies of the Rio Grande graben in New Mexico between Belen and Pilar. Special Publication New Mexico Geological Society 6: 62-70

Cordell, L., Keller, G.R. and Hildebrand, T.G. 1982. Bouguer gravity map of the Rio Grande Rift, 1:1,000,000 U.S. Geological Survey Geophysical Investgation Map, GP-949

Cordell, L. and Keller, G.R. 1984. Regional structural trends inferred from gravity and aeromagnetic data in the New Mexico-Colorado border region. Field Conference Guidebook New Mexico Geological Society 35: 21-3

Cox, K.G., Bell, J.D. and Pankhurst, R.J. 1979. The Interpretation of Igneous Rocks. George Allen and Unwin. London

Dey, T.N. and Kranz, R.L. 1988. State of Stress and Relationship of Mechanical Properties to Hydrothermal Alteration at Valles Caldera core hole #1, New Mexico. Journal of Geophysical Research, Vol. 93.B. 6,108-12

Doell, R.R.,Dalrymple, G.B., Smith, R.L. and Bailey, R.A. 1968. Paleomagnetism, Potassium-Argon Ages, and Geology of Rhyolites and Associated Rocks of the Valles Caldera, New Mexico. Geological Society of America, Memoir 116: 211-48

Dondanville, R.F. 1978. Geologic characteristics of the Valles caldera geothermal system: Geothermal Resources Council, Transactions, 2: 157-60

Dransfield, B.J. and Gardner, J.N. 1985. Subsurface geology of the Pajarito Plateau, Española Basin, New Mexico. Los Alamos Scientific Laboratory Report LA, 10455-MS.

Druitt, T.H. and Sparks, R.S.J. 1984. On the formation of calderas during ignimbrite eruptions, Nature, Vol. 310: 679-681

Dungan, M.A., Muehlberger, W.R., Leininger, L., Peterson, C., McMillan, N.J., Gunn, G., Lindstrom, M. and Haskin, L. 1984. Volcanic and sedimentary stratigraphy of the Rio Grande gorge and the late Cenozoic geologic evolution of the southern San Luis valley. Field Conference Guidebook New Mexico Geological Society, 35. 157-78

Dzurisin, D., Savage, J.C. and Fournier, R.O. 1990. Recent crustal subsidence at Yellowstone Caldera, Wyoming. Bulletin of Volcanology Vol. 52: 247-70

Einarsson, P. 1991. Earthquakes and present tectonics in Iceland. Tectonophysics 189, 261-280

Einarsson, P. and Eriksson, J. 1982. Earthquake fractures in the districts land and the Rangarvellir in the South Iceland Seimic Zone. Jokull Vol. 32, 113-119.

Erwes, H., and Wild, C. 1975. Experiences and accuracy of Barometric levelling. 1st Venezuelan Congress of Geodesy.

Everts, P., Koerfer, L.E. and Schwartsbach, T. 1972. Neue K/Ar-Datierungen islandischer Basalte: Vorlaefige Mitteiglung. Neues Jahrbuch fur Geologie und Palaontologie. Monatshefte 5, 280-284.

Flovenz, O.G. 1980. Seismic structure of the Icelandic crust above layer three and the relation between body wave velocity and the alteration of the basaltic crust. Journal of Geophysics, Vol 47, 211-220.

Gardner, J.N. 1985. Tectonic and petrologic evolution of the Keres Group: Implications for the development of the Jemez volcanic field, New Mexico. Unpublished Ph.D. thesis, University of California Davis, 295pp

Gardner, J.N., Goff, F., Garcia, S. and Hagan, R.C. 1986. Stratigraphic Relations and Lithologic Variations in the Jemez Volcanic Field, New Mexico. Journal of Geophysical Research, Vol.91.B 1,763-78

Goff, F. 1983. Subsurface structure of Valles caldera: A resurgent cauldron in northern New Mexico. Geological Society of America, Abstracts Programs 15. 381

Goff, F. and Grigsby, C.O. 1982. Valles caldera geothermal systems, New Mexico, USA. Journal of Hydrology, Vol. 56: 119-36

Goff, F., Heiken, G., Tamanyu, S., Gardner, J., Self, S., Drake, R. and Shafiqullah, M. 1984. Location of Toledo caldera and formation of the Toledo embayment, Jemez Mountains, New Mexico. American Geophysical Union, Transactions, Vol. 65: 1,145

Goff, F., Gardner, J.N., Baldridge, W.S., Hulen, J.B., Nielson, D.L., Vaniman, D., Heiken, G., Dungan, M.A. and Broxton, D. 1989. Volcanic and hydrothermal evolution of Valles caldera and Jemez volcanic field. New Mexico Bureau of Mines & Mineral Resources. Memoir 46. 381-434

Goff, F. and Shevenell, L. 1987. Travertine deposits of Soda Dam, New Mexico, and Their implications for the age and evolution of the Valles caldera hydrothermal system: Geological Society of America, Bulletin, 99: 292-302

Griggs, R.L. 1964. Geology and groundwater resources of the Los Alamos area, New Mexico. U.S. Geological Survey, Water Supply Paper 1753: 107pp

Hallinan, S.E. 1991. Gravity studies of the Guayabo Caldera and the Miravalles Geothermal Field, Costa Rica. Unpublished PhD thesis, The Open University, Milton Keynes 381pp.

Hammer, S. 1939. Terrain corrections for Gravimeter Stations. Geophysics, Vol. 4, 184-94

Harland, W.B., Cox, A.V., Llewellyn, P.G., Pickton, C.A.G., Smith, A.G. and Walters, R. 1982, A geological time scale, Cambridge University Press, 131 pp.

Harrison, T.M., Morgan, P.M. and Blackwell, D.D. 1986. Constraints on the age of heating at the Fenton Hill site, Valles caldera, New Mexico. Journal of Geophysical Research, Vol.91, 1899-1908.

Heiken, G., Goff, F., Stix, J., Tamanyu, S., Shafiqullah, M., Garcia, S. and Hagan, R. 1986. Intracaldera Volcanic Activity, Toledo Caldera and Embayment, Jemez Mountains, New Mexico. Journal of Geophysical Research, Vol.90.B 1,799-815

Helgason, J. 1984. Frequent shifts of the volcanic zone in Iceland. Geology, Vol. 12, 212-216.

Helgason, J. 1989. The Fjallgardar volcanic ridge in NE Iceland: an aborted early stage plate boundary or a volcanically dormant zone. In: Saunders, A.D. and Norry, M.J. (eds.) Magmatism in the Ocean Basins. Geological Society, London, Special Publication 42, 201-213.

Hildreth, W., 1981. Gradients in silicic magma chambers: implications for lithospheric magmatism. Journal of Geophysical Research, Vol.86, 10,153-92

Huppert, H.E., and Sparks, R.S.J., 1988a. The generation of Granitic Magmas by the Intrusion of Basalt into the Continental Crust. Journal of Petrology, Vol. 29, part 3, 599-624

Huppert, H.E., and Sparks, R.S.J., 1988b. Melting the roof of a chamber containing a hot, turbulently convecting fluid. Journal Fluid Mechanics, Vol. 188, 107-131

Huppert, H.E., and Sparks, R.S.J., 1988c. The fluid dynamics of crustal melting by injection of basaltic sills. Philosophical Transactions Royal Society Edinburgh: Earth Sci. Vol. ___, ____-__

Izett, G., Obradovich, J., Maeser, C. and Cebula, G. 1980. K-Ar and fission track zircon ages of Cerro Toledo Rhyolite tephra units in the Jemez Mountains, New Mexico. U.S. Geological Survey Professional Paper, 1,199: 37-41

Izett, G.A., Obradovich, J.D., Naeser, C.W. and Cebula, G.T. 1981. Potassium-argon and fission-track zircon ages of Cerro Toledo rhyolite tephra in the Jemeż Mountains, New Mexico: U.S. Geological Survey Professional Paper, 1,199-D: 37-43

Jakobsson, S.P., Jonsson, J. and Shido, F. 1978. Petrology of the Reyjanes Peninsula, Iceland, Journal of Petrology, Vol. 19, 669-705.

Jakobsson, S.P. 1979a. Outline of the petrology of Iceland. Jokull Vol. 29, 57-73.

Jakobsson, S.P. 1979b. Petrology of Recent basalts of the Eastern Volcanic Zone, Iceland. Acta. Natur. Islandica 26, 103.

Jancin, M., Young, K.D., Voight, B., Aronson, J.L. and Saemundsson, K. 1985. Stratigraphy and K/Ar ages across the west flank of the northeast Iceland axial rift zone, in relation to the 7 Ma volcanotectonic reorganization of Iceland. Journal of Geophysical Research, Vol. 90. 9,961-9,985.

Karig, D.E., Cardwell, R.K., Moore, G.F. and Moore, D.G. 1978. Late Cenozoic subduction and continental margin truncation along the northern Middle America Trench. Geological Society of America Bulletin, 89, 265-76

Kite, W.M. 1985. Caldera-forming eruption sequences and facies variations in the Bandelier Tuff, central New Mexico. Unpublished M.S. thesis Arizona State University, Tempe. 377pp

Kolstad, C.D. and McGetchin, T.R. 1978. Thermal evolution models for the Valles caldera with reference to a hot-dry-rock geothermal experiment. Journal of Volcanology and Geothermal Research, Vol.3: 197-218

Lachenbruch, A.H., Sorey, M.L., Lewis, M.L. and Sass, J.H. 1976a. The near-surface hydrothermal regime of Long Valley caldera. Journal of Geophysical Research, Vol.81.B 763-8

Lachenbruch, A.H., Sass, J.H., Munroe, R.J. and Moses, T.H. 1976b. Geothermal setting and simple heat conduction models of the Long Valley caldera. Journal of Geophysical Research, Vol.81.B 1,769-84

Lin, J., Purdy, G.M., Schouten, H., Sempere, J.C. and Zervas, C. 1990. Evidence from gravity data for focused magmatic acceretion along the Mid-Atlantic, Ridge. Nature, Vol. 344, 627-632.

Lipman, P.W., 1984. The roots of ash-flow calderas in Western North America: windows into the tops of granitic batholiths. Journal of Geophysical Research, Vol. 89, 8801-41

Loeffler, B.M. 1984. Major and trace-element and strontium and oxygen-isotope geochemistry of the Polvadera Group, Jemez volcanic field, New Mexico. Unpublished Ph.D. thesis, University of Colorado, Boulder. 259pp

Loeffler, B.M., Vaniman, D.T, Baldridge, W.S. and Shafiqullah, M. 1988. Neogene rhyolites of the northern Jemez volcanic field, New Mexico. Journal of Geophysical Research, Vol.93.B 6,157-68

Macdonald, K.C. 1986. The crest of the Mid-Atlantic Ridge: models of crustal generation processes' and tectonics. In: Vogt,P.R. and Tucholke, B.E. (eds.) The Geology of North America, volume M: The Western North Atlantic, Geological Society of America, Boulder, Colorado, 51-68.

Marsh, B.D., 1981. On the crystallinity, probability of occurrence and rheology of lava and magma. Contributions to Mineralogy and Petrology Vol. 78, 85-98.

Marvin, R.F. and Dobson, S.W. 1979. Radiometric ages: Compilation B, U.S. Geological Survey, Isochron West, 16. 3-32

May, S.J., 1980. Neocene geology of the Ojo Caliente - Rio Chama area, Espanola basin, New Mexico. Ph.D. thesis, University of New Mexico, Albuquerque, N.M., 205 pp.

Mayo, E.G. 1958. Lineament tectonics and some ore districts of the southwest. Mining Engineering, Vol. 10. 1,169-75

McPherson, J.G., Waresback, D.B. and Flanney, J.R. 1984. Volcanogenic fan building, Puye Formation Jemez mountains, New Mexico. Eos: Transactions, American Geophysical Union, Vol. 65. 1,134

Morgan, P., Blackwell, D.D., Spafford, R.E. and Smith, R.B. 1977. Heat flow measurements in Yellowstone Lake and the thermal structure of the Yellowstone caldera. Journal of Geophysical Research, Vol.82.B 3,719-32

Morgan, P., Harder, V. and Giordano, T.H. 1986. Heat and fluid flow in the Rio Grande rift: A possible modern thermal analogue of a Mississippi Valley type ore-forming system, in Geology in the Real World-The Kingsley Dunham Volume, edited by Nesbitt,R.W. & Nichol,I. 295-305pp, Institution of Mining and Metallurgy, London

Muehlberger, W.R. 1979. The Embudo fault between Pilar and Arroyo Hondo, New Mexico: An active intercontinental transform fault. Field Conference Guidebook New Mexico Geological Society, 30. 77-82

Munroe, R.J. and Sass, J.H. 1987. Thermal Conductivity of samples from borehole VC-1 Valles Caldera, New Mexico. U.S. Geological Survey Open-file Report 87-184 Menio Park, California

Musgrave, J.A., Goff, F., Shevenell, L., Trujillo, Jr., P.E., Counce,D., Luedemann,G., Garcia,S., Dennis, B., Hulen, J.B., Janik, C. and Tomei, F.A. 1989. Selected Data from Continental Scientific Drilling Core Holes VC-1 and VC-2a, Valles Caldera, New Mexico. Los Alamos Scientific Laboratory Informal Report LA-11496 - OBES

Nettleton, L. 1939. Determination of density for the reduction of gravimeter observations. Geophysics, Vol. 4. 176-83

New Mexico Geological Society 1982. New Mexico Highway Geological Map 1:1,000,000.

Nielson, D.L. and Hulen, J.B. 1984. Internal geology and evolution of the Redondo dome, Valles caldera, New Mexico. Journal of Geophysical Research, Vol.89.B 8,695-711

Olsen, K.H., Braile, L.W., Stewart, J.N., Daudt, C.R., Keller, G.R., Ankeny, L.A. and Wolff, J.J. 1986. Jemez Mountains volcanic field, New Mexico: Time term interpretation of the CARDEX seismic experiment and comparison with Bouguer gravity: Journal of Geophysical Research, Vol.91.B 6,175-87

Oskarsson, N., Steinthorsson, S. and Sigvaldason, H. 1985. Iceland geochemical anomaly: origin, volcanotectonics, chemical fractionation and isotope evolution of the crust. Journal of Geophysical Research, Vol. 90, 10,011-10,025.

Palmason, G. 1971. Crustal structure of Iecland from explosion seismology. Soc. Sci. Islandica Rit, Vol. 40, 187-198.

Palmason, G. and Saemundsson, K. 1974. Iceland in relation to the Mid-Atlantic Ridge. Annual review of Earth and Planetary Sciences Vol. 2: 25-50.

Pedley, R. 1990. GRAVMAG - User Manual. Integrated Geophysical Services B.G.S., Keyworth, England

Porbergesson, G., Pór Maghússon, I. and G. Pálmason 1990. Pyngdarmæligögn og pyngdarkort af Islandi. Orkustofnun.

Park, R.G. 1988. Geological Structures and Moving Plates. Blackie & Son Ltd. 337pp

Potter, D.B. 1983. Flow directions and possible sources of the Otowi ash flows, Jemez Mountains, New Mexico. Geological Society of America Abstracts Programs, 15(5) 389

Reilinger, R.E. and York, J.E. 1979. Relative crustal subsidence from leveling data in a seismically active part of the Rio Grande rift, New Mexico. Geology, Vol. 7: 139-43

Richey, J.E., MacGregor, A.G. and Anderson, F.W. 1961. British Regional Geology - Scotland: The Tertiary Volcanic Districts (third edition) H.M.S.O. 120pp.

Saemundsson, K. 1974. Evolution of the axial rifting zone in northern Iceland and the Tjomes Fracture Zone. Geological Society of America, Bulletin, 85: 495-504.

Saemundsson, K. 1978. Fissure swarms and central volcanoes of the neovolcanic zones in Iceland. Geological Journal Special Issue 10, 415-432.

Saemundsson, K. 1979. Outline of the geology of Iceland. Jokull Vol. 29: 7-28.

Sandberg, C.H. 1958. Terrain corrections for an inclined plane in gravity computations. Geophysics, Vol. 23: 701-711.

Sasada, M. 1988. Microthermometry of fluid inclusions from the VC-1 core hole in Valles caldera, New Mexico. Journal of Geophysical Research, Vol.93.B 6,091-6

Sass, J.H. and Morgan, P. 1988. Conductive heat flux in VC-1 and the thermal regime of Valles caldera, Jemez Mountains. New Mexico. Journal of Geophysical Research, Vol.93.B 6,027-40

Scandone, R. 1990. Chaotic collapse of calders. Journal of Volcanology and Geothermal Research, Vol. 42, 285-302

Segar, R.L. 1974. Quantitative gravity interpretation. Valles caldera area. Sandoval and Rio Arriba counties, New Mexico. University of Utah Research Institute, Earth Science Laboratory, Open-File Report NM/BACA-27: 12pp

Self, S., Goff, F., Gardner, J.N., Wright, J.V. and Kite, W.M. 1986. Explosive Rhyolitic Volcanism in the Jemez Mountains: Vent Locations, Caldera Development and Relation to Regional Structure. Journal of Geophysical Research, Vol.91.B. 1,779-98

Self, s., Wolff, J.A. and Kircher, D.E. 1987. Volcanological investigation of the Banco Bonito eruption and subsurface geology of the ring fracture zone, Valles Caldera, New Mexico. D.O.E. Tech. Rep. DE-FG05-85ER13413-2, 80pp., Dep. of Energy, Washington, D.C.

Self, S., Kircher, D.E. and Wolff, J.A. 1988. The El Cajete Series, Valles Caldera, New Mexico. Journal of Geophysical Research, Vol.93.B 6,113-28

Sempere, J.C., Purdy, G.M. and Schouten, H. 1990. Segmentation of the M.A.R. between 24°N and 30°41'N. Nature, Vol. 344: 427-31

Silver, P.G., Carlson, R.W., and Olson, P. 1988. Deep slab, geochemical heterogeneity and the large-scale structure of mantle convection: investigation of an enduring paradox. Annual review of Earth and Planetary Sciences Vol. 16, 477-541.

Smith, R.L. 1979. Ash-flow magnetism. Geological Society of America special paper 180, 5-27.

Smith, R.L., Bailey, R.A. and Ross, C.S. 1961. Structural evolution of the Valles Caldera, New Mexico and its bearing on the emplacement of ring dikes: U.S. Geological Survey Professional Paper 424-D: (340) 145-149

Smith, R.L. and Bailey, R.A. 1968. Resurgent cauldrons. Geological Society of America, Memoir 116, 613-62

Smith, R.L., Bailey, R.A. and Ross, C.S. 1970. Geologic map of the Jemez Mountains, New Mexico (1:125,000) U.S. Geological Survey Miscellaneous Geological Investigations Map, I-571.

Stein, H.L. 1983. Geology of the Cochiti mining district, Jemez mountains, New Mexico. Unpublished M.S. thesis, University of New Mexico, Albuquerque 122pp

Steinthorsson, S., Oskarsson, N. and Sigvaldason, G.F. 1985. Origin of alkali basalts in Iceland: a plate tectonic model. Journal of Geophysical Research, Vol. 90, 10,027-10,042.

Stix, J. Goff, F. Gorton, M.P. Heiken, G. and Garcia, S.R. 1988. Restoration of Compositional Zonation in the Bandelier Silicic Magma Chamber Between Two Caldera-Forming Eruptions: Geochemistry and Origin of the Cerro Toledo rhyolite, Jemez Mountains, New Mexico. Journal of Geophysical Research, Vol.93.B 6,129-47

Talwani, M., Windish, C.C. and Lahgseth, M. 1971. Reykjanes Ridge crest: a detailed geophysical study. Journal of Geophysical Research, Vol. 76, 473-517

Thompson, G. and Melson, W.G. 1972. The petrology of oceanic crust across fracture zones in the Atlantic Ocean: evidence of a new kind of sea-floor spreading. Journal of Geology, Vol. 80: 526-38

Turbeville, B.N. 1986. Mineralogy, facies analysis, and interpretation of felsic pyroclastic deposits of the Puye Formation, Jemez Mountains, New Mexico: Unpublished M.S. thesis, University of Texas, Arlington 427pp

Turbeville, B.N. and Self, S. 1988. San Diego canyon ignimbrites: Pre-Bandelier tuff explosive rhyolitic volcanism in the Jemez Mountains, New Mexico: Journal of Geophysical Research, Vol.93.B 6,148-56

United States Geological Survey 1:5,000,000 Tectonic Map of North America.

Vink, G.E. 1984. A hotspot model for Iecland and Voring Plateau. Journal of Geophysical Research, Vol. 89, 9,949-9,959.

Vogt, P.R. and Avery, O.E. 1974. Detailed magnetic surveys in the north east Atlantic and Labrador Sea. Journal of Geophysical Research, Vol. 79, 363-389.

Vuataz, F.D. and Goff, F. 1986. Isotope geochemistry of thermal and nonthermal waters in the Valles caldera, Jemez Mountains, northern New Mexico: Journal of Geophysical Research, Vol.91.B 1835-53

Walker, C. 1991 North Atlantic ocean crust and Iceland, In: Oceanic Basalts, P.A.Floyd (Ed.) Blackie 456p.

Walker, G.P.L. 1959. Geology of the Reydarfjördur area, eastern Iceland. Journal of the Geological Society, London, Vol. 114, 367-93

Walker, G.P.L. 1963. The Breiddalur central volcano, eastern Iceland. Journal of the Geological Society, London, Vol. 119, 29-63.

Walker, G.P.L. 1974. Eruptive mechanisms in Iceland. In: Kristjansson, I. (ed) Geodynamics of Iceland and the North Atlantic regions, D.Reidel, Amsterdam, 189-202.

Walker, G.P.L. 1980. The Taupo pumice: Product of the most powerful known (ultraplinian) eruption ?, Journal Volcanology and Geothermal Research 8: 69-94

Walker, G.P.L. 1981. Plinian eruptions and their products. Bulletin of Volcanology 44: 223-40

Walker, G.P.L. 1985. Origin of coarse lithic breccias near ignimbrite source vents. Journal Volcanology and Geothermal Research 25: 157-72

Ward, P.L. 1971. New interpretations of the geology of Iceland. Geological Society of America, Bulletin 82, 2,991-3,012

White, R.S. 1988. A hotspot model for the early Tertiary volcanism in the N. Atlantic. In: Morton, A.C. and Parson, L.M. (eds.) Early Tertiary Volcanism and the opening of the North East Atlantic, Geological Society, London. Special Publication, 39, 3-13.

White, R.S. 1989. Asthenospheric control on magmatism in the ocean basins. In: Saunders, A.D. and Norry, M.J. (eds.) Magmatism in the Ocean Basins. Geological Society, London Special Publication 42 17-27.

White, R.S. 1990. Initiation of the Iceland plume and opening of the North Atlantic. In: Tankard, A.J. and Balkwill, H.R. (eds.) Extensional Tectonics and Stratigraphy of the North Altanic Margins, Memoir American Association of Petroleum Geologists 46, 149-154.

White, R.S. and McKenzie, D. 1989a. Volcanism at rifts. Sci. Am. 260, 62-71.

White, R.S. and McKenzie, D. 1989b. Magmatism at rift zones: the generation of volcanic continental margins and flood basalts. Journal of Geophysical Research, Vol. 94, 7,685-7,729.

Wickham, S.M. 1987. The segregation and emplacement of granitic magmas. Journal of the Geological Society, London, Vol. 144, 281-98

Williams, L.M. 1979. Gravity Study of the Los Alamos Area, New Mexico. Los Alamos Scientific Laboratory Informal Report LA-8154-MS

Williston, McNeal and Associates, 1979. A time domain survey of the Los Alamos region, New Mexico: Los Alamos Scientific Laboratory, Report LA-7657-MS: 32pp

Wilson, M. 1993. Magmatic differentiation. Journal of the Geological Society, London, Vol. 150, 611-24

Wilt, M. and Vonder Haar, S. 1986. A geological and geophysical appraisal of the Baca geothermal field, Valles Caldera, New Mexico. Journal of Volcanology and Geothermal Research, Vol. 27, 349-70

Woldegabriel, G. 1990. Hydrothermal alteration in the Valles caldera ring fracture zone and core hole VC-1: evidence for multiple hydrothermal systems. Journal of Volcanology and Geothermal Research, Vol.40 105-22

Wright, J.V. and Walker, G.P.L. 1977. The ignimbrite soure problem: Significance of a co-ignimbrite lag-fall deposit, Geology Vol. 5: 729-32

Wyllie, P.J., 1984. Constraints imposed by experimental petrology on possible and impossible magma sources and products. Philosophical Transactions Royal Society London, Vol. A 310, 439-56

Zoback, M.L., Anderson, R.E. and Thompson, G.A. 1981. Cainozoic evolution of the state of stress and style of tectonism of the Basin and Range provice of the western United States. Philosophical Transactions Royal Society London, Vol. A 300, 407-34

Appendix 1: K-Ar dates for the Jemez Mountains

Rock = Rock type, stratigraphic unit or well

M.F. = Mineral or size fraction sample derived from (W.R.= whole rock)

K_2O = Percentage Potassium oxide

mol Ar = Radiogenic Argon 10^{-12}mol/g

^{40}Ar = Percentage Radiogenic Argon

Age = Published Age in millons of years

Ref = Reference

Rock	Geographic Coordinates		M.F.	K_2O	mol Ar	^{40}Ar	Age	Ref
Andesite	35°59'40"	106°30'04"	W.R.	3.862	39.35	45	7.07±0.11	W
Basalt	35°49'	106°35'	W.R.	1.775	20.62	56	8.05±0.13	W
Dacite	35°58'19"	106°30'04"	<2 μm	5.636	66.68	5	8.20±0.29	W
Andesite	35°58'19"	106°29'57"	<2 μm	4.208	42.22	23	6.96±0.38	W
VC-1	35°50'27"	106°37'15"						
Arg Sst.	" 479.0m	"	<0.25 μm	8.601	16.59	10	1.34±0.05	W
Arg Sst.	" 479.0m	"	0.25-2 μm	8.946	15.60	12	1.21±0.08	W
Sst.	" 817.4m	"	<0.25 μm	8.236	204.09	46	17.14±0.40	W
Sst.	" 843.6m	"	<0.25 μm	8.71	204.88	59	16.27±0.30	W
Shale	" 854.4m	"	0.25-2 μm	8.943	197.93	54	15.31±0.30	W
Shale	" 854.4m	"	<0.25 μm	8.577	137.16	38	1.08±0.23	W
Shale	35°48'	106°41'	<0.25 μm	4.115	1215.15	81	194.32±3.53	W
Rhyolite	36°05.03'	106°25.35'	feldspar	3.911	13.66	67.6	2.01±0.06	LVB
Rhyolite	36°01.07'	106°28.53'	"+ glass	1.499	15.1	41.8	5.80±0.20	LVB
Rhyolite	36°02.17'	106°28.97'	Biotite	6.921	90.7	61.1	7.54±0.28	LVB

Rock	Geographic Coordinates	M.F.	K_2O	mol Ar	^{40}Ar	Age	Ref
Pumice Rhyolite							
	36°05.68' 106°24.35'	Biotite	6.543	59.2	81.5	5.21±0.25	LVB
Ignimbrite B	F84-10	Sanidine	4.8	21.6	67.8	2.84±0.07	S
Ignimbrite A	V81-56B	Sanidine	4.6	29.06	4	3.64±1.64	S
Puye Ignimbrite	BNT25-P	Plagioclase	1.85	8.136	76.9	2.53±0.1	T
Tshirege	PED51-60	Sanidine	5.98	10.89	70.4	1.1± 0.1	B
Otowi		Sanidine				1.45±0.06	I
Pumice	Tsankawi	Sanidine	Mean of 3 samples			1.12±0.03	i
Pumice	Fall unit D?	Sanidine	7.25	5.11	56.8	1.23±0.02	i
Pumice	Fall unit C	"+ glass	3.928	5.59	13.3	1.52±0.04	s
Obsidian	Pinnacle Peak	glass	3.74	7.797	46.3	1.20±0.02	t
Rhyolite	Turkey Ridge	Sanidine	5.881	1.26	40.9	1.24±0.03	Dr
Obsidian	unnamed dome	glass	3.71	8.582	20.0	1.33±0.02	t
Obsidian	Rabbit Mountain	"+ glass	3.682	9.135	45.6	1.43±0.04	s
Obsidian	Rabbit Mountain	glass	3.733	9.838	65.0	1.52±0.06	Dr
Rhyolite	Cerro Toledo	"+ glass	3.870	0.924	30.2	1.38±0.05	s
Obsidian	Cerro Toledo	glass	3.69	10.378	50.5	1.62±0.02	t
Rhyolite	Warm Springs	Sanidine	5.85	12.65	53.9	1.25±0.04	Do
Obsidian	Cerro Trasq	glass	3.75	8.235	51.0	1.27±0.03	t
Rhyolite	East Los Posos dome	"+ glass	2.537	0.646	41.0	1.47±0.05	s
Rhyolite	West Los Posos dome	Sanidine	5.595	1.46	45.0	1.50±0.05	Dr
Pumice	Guaje	Sanidine	Mean of 3 samples			1.40±0.04	i
Dacite	Dome north of Cerro Rubio						
		Plagioclase	0.428	0.162	44.1	2.18±0.09	s
Dacite	Cerro Rubio dome	Plagioclase	0.353	0.220	26.4	3.59±0.36	Dr

Rock	Geographic Coordinates		M.F.	K_2O	mol Ar	^{40}Ar	Age	Ref
Pumice	Ignimbrite B		Sanidine	4.379	21.6	67.8	2.84±0.07	s
Pumice	Ighimbrite A		Sanidine	4.6	29.06	4	3.64±1.64	K
Rhyolite	35°59.2'	106°26.5'	Sanidine	5.881	12.6	40.9	1.24±0.03	HGS
Rhyolite	35°59.6'	106°26.2'	"+ glass	3.87	9.236	30.2	1.38±0.05	HGS
Rhyolite	35°55.8'	106°25.2'	" & plag	2.537	6.46	41	1.47±0.05	HGS
Rhyolite	35°56.8'	106°25.8'	Sanidine	5.595	14.6	45	1.50±0.05	HGS
Dacite	35°56.8'	106°24.0'	Plagioclase	0.353	2.2	26.4	3.59±0.36	HGS
Dacite	35°57.0'	106°24.2'	Plagioclase	0.428	1.618	44.1	2.18±0.09	HGS

W = Woldegabriel 1990

LVB = Loeffler et al. 1988

S = Self et al 1986 in Turbeville & Self 1988

T = Turbeville 1986 in Turbeville & Self 1988

B = Baldridge et al. 1980 in Turbeville & Self 1988

I = Izett et al. 1981 in Turbeville & Self 1988

i = Izett et al. 1981 in Stix et al. 1988

s = M. Shafiqullah in Stix et al. 1988

t = S. Tamanyu in Stix et al. 1988

Dr = R. Drake in Stix et al. 1988

Do = Doell et al (1968) in Stix et al. 1988

K = D. Krummenacher in Stix et al. 1988

HGS = Heiken et al. 1986

Appendix 2: Densities (ρ) for formations in the Jemez Mountains

Seger 1974 : Gravity model with the following densities

Caldera infill	2.10 g/cm³
Normal surface density	2.45 g/cm³
Normal Granite or Limestone	2.70 g/cm³

Williams 1979 : Gravity model with the following densities

Puye Formation	2.2 g/cm³	
Tschicoma Formation	2.8 g/cm³	
Santa Fe Group	2.4 g/cm³	
El Rito Formation	2.5 g/cm³	(Mesozoic)
Paleozoic rocks	2.6 g/cm³	
Precambrian rocks	2.6 g/cm³	

Dey and Kranz 1988 : Measurements from VC-1 (673 537)

	Depth	Porosity	dry ρ	water saturated ρ
Lower WC-1 tuff	244m	24.5 %	1.75 g/cm³	1.995 g/cm³
Abo Formation	398m	17.1 %	2.35 g/cm³	2.521 g/cm³
Madera Limestone	472m	15.0 %	2.30 g/cm³	2.450 g/cm³
" "	546m	11.9 %	2.40 g/cm³	2.519 g/cm³
" "	648m	0.5 %	2.69 g/cm³	2.695 g/cm³
Sandia Formation	812m	3.9 %	2.54 g/cm³	2.579 g/cm³

Munroe and Sass 1987 : Measurements from VC-1 (673 537)

Banco Bonito Obsidian	2.42 g/cm³, 2.35 g/cm³
Abo Formation	2.57 g/cm³
Madera Limestone	2.56 g/cm³, 2.64 g/cm³, 2.65 g/cm³, 2.55 g/cm³
Sandia Formation	2.50 g/cm³

Musgrave et al. 1989 : Measurements from VC-2a (751 546)

	Depth	ρ
Upper Tuff	34.8m	2.46 g/cm³
Upper Bandelier Tuff	102.1m	2.48 g/cm³
" " " "	186.6m	2.41 g/cm³
" " " "	263.0m	2.13 g/cm³
" " " "	341.0m	2.49 g/cm³
Volcaniclastic Sandstone	356.6m	2.13 g/cm³
Lower Bandelier Tuff	427.5m	2.15 g/cm³
Lower Tuff	500.3m	2.11 g/cm³

Wilt and Vonder Haar 1986 : Gravity model with the following densities

Surface layer of Caldera fill, Lake deposits and other recent alluvium
2.12 g/cm³

The Bandelier Tuff and underlying volcanic and sedimentary units
2.3-2.5 g/cm³ = 2.4 g/cm³

Lower Paleozoic and Upper Precambrian 2.65 g/cm³

Unpublished measurements from VC-2b (753 552)

	Depth	Dry bulk ρ	Grain ρ	Porosity	Water Saturated ρ
Caldera Fill	61.9m	2.320 g/cm^3	2.785 g/cm^3	16.7%	2.487 g/cm^3
Upper Bandelier	186.8m	1.740 g/cm^3	2.723 g/cm^3	36.1%	2.101 g/cm^3
" " "	289.7m	2.499 g/cm^3	2.693 g/cm^3	7.2%	2.571 g/cm^3
Lower Bandelier	457.5m	2.324 g/cm^3	2.627 g/cm^3	11.5%	2.439 g/cm^3
" " "	502.6m	2.029 g/cm^3	2.631 g/cm^3	22.9%	2.258 g/cm^3
Lower Tuff	625.3m	2.101 g/cm^3	2.694 g/cm^3	22.0%	2.321 g/cm^3
Santa Fe Group	765.4m	2.151 g/cm^3	2.667 g/cm^3	19.3%	2.344 g/cm^3
Yeso Formation	854.6m	2.405 g/cm^3	2.779 g/cm^3	13.5%	2.540 g/cm^3
" " "	916.2m	2.094 g/cm^3	2.706 g/cm^3	22.6%	2.320 g/cm^3
Abo Formation	1173.8m	2.647 g/cm^3	2.850 g/cm^3	7.1%	2.718 g/cm^3
Madera Formation	1311.0m	2.659 g/cm^3	2.755 g/cm^3	3.5%	2.685 g/cm^3
Sandia Formation	1525.7m	2.661 g/cm^3	2.738 g/cm^3	2.8%	2.689 g/cm^3
Precambrian	1646.5m	2.622 g/cm^3	2.723 g/cm^3	3.7%	2.659 g/cm^3

Appendix 3. Densities (ρ) for the Breiddalur central volcano: Iceland

Sample	Rock type	Weight in air	Weight in water	Volume	Density	Location
1A	Rhyolitic breccia	55.76g	31.85g	23.91cm^3	2.37g/cm^3	Breiddalur
1B	" " "	27.35g	15.98g	11.37cm^3	2.41g/cm^3	Breiddalur
1C	" " "	15.94g	8.76g	7.18cm^3	2.22g/cm^3	Breiddalur
	" " "				2.33g/cm^3	
2	Rhyolitic tuff	34.31g	20.74g	13.57cm^3	2.53g/cm^3	Breiddalur
3A	Silicified Rhyolite	23.35g	14.63g	8.72cm^3	2.68g/cm^3	Breiddalur
3B	" " " "	23.60g	13.64g	9.96cm^3	2.37g/cm^3	Breiddalur
	" " " "				2.53g/cm^3	
4A	Rhyolite	32.07g	17.78g	14.29cm^3	2.24g/cm^3	Breiddalur
4B	" "	44.23g	25.17g	19.06cm^3	2.32g/cm^3	Breiddalur
4C	" "	38.15g	22.43g	15.72cm^3	2.43g/cm^3	Breiddalur
	" "				2.33g/cm^3	
5	Rhyolite-Pichstone	29.38g	16.40g	12.98cm^3	2.26g/cm^3	Breiddalur
6	Icelandite	28.68g	16.00g	12.68cm^3	2.26g/cm^3	Breiddalur
7	Tholeiitic Icelandite					
		58.36g	34.94g	23.42cm^3	2.49g/cm^3	Breiddalur
8A	Tholeiite	54.59g	36.02g	18.57cm^3	2.94g/cm^3	Breiddalur
8B	" "	48.19g	31.60g	16.59cm^3	2.90g/cm^3	Breiddalur
8C	" "	44.32g	28.75g	15.57cm^3	2.85g/cm^3	Breiddalur
					2.90g/cm^3	
9A	Olivine Tholeiite	62.10g	39.37g	22.73cm^3	2.73g/cm^3	Breiddalur
9B	" " " "	56.99g	37.19g	19.80cm^3	2.88g/cm^3	Breiddalur

Sample	Rock type	Weight in air	Weight in water	Volume	Density	Location
	Olivine Tholeiite				2.81g/cm³	
10	Plagioclase Porphyritic Tholeiite					
		64.17g	40.57g	23.60cm³	2.72g/cm³	Breiddalur
11	Plagioclase Porphyritic Tholeiite					
		47.85g	31.25g	16.60cm³	2.88g/cm³	Breiddalur
12	Lava surface	19.35g	9.93g	9.42cm³	2.05g/cm³	Breiddalur
13	Olivine Tholeiite	42.00g	28.04g	13.96cm³	3.01g/cm³	Breiddalur
14	Olivine Tholeiite with secondary minerals					
		53.12g	33.19g	19.93cm³	2.65g/cm³	Breiddalur
15	Tholeiite	52.21g	34.33g	17.88cm³	2.92g/cm³	
						west of Oxi
16	Plagioclase-porhyritic Tholeiite					
		83.93g	53.77g	30.16cm³	2.78g/cm³	Skali
17	Tholeiite	58.63g	38.61g	20.02cm³	2.93g/cm³	Skali
18	Olivine-Tholeiite	42.85g	28.00g	14.85cm³	2.89g/cm³	Streiti
19	Olivine-Tholeiite	54.02g	34.01g	20.01cm³	2.70g/cm³	
						NE of Skåli
20	Rhyolite	37.35g	21.41g	15.94cm³	2.34g/cm³	
						Kelduskðar - Skåli
21	Icelandite	51.42g	37.24g	19.18cm³	2.94g/cm³	Kelduskðar
22	Porphyritic Tholeiite					
		46.18g	30.40g	15.78cm³	2.93g/cm³	
						Kelduskðar - Skåli

Sample	Rock type	Weight in air	Weight in water	Volume	Density	Location
23	Tholeiite	51.48g	33.45g	18.03cm^3	2.86g/cm^3	North of Skåli
25	Porphyritic Basalt	51.56g	33.72g	17.84cm^3	2.89g/cm^3	Fossårvik
26A	Ryolite & Dacite	35.63g	20.73g	14.90cm^3	2.39g/cm^3	Melhorn
26B	" " " "	18.65g	10.95g	7.70cm^3	2.42g/cm^3	Melhorn
26C	" " " "	12.01g	6.53g	5.48cm^3	2.19g/cm^3	Melhorn
26D	Ryolite & Dacite	19.51g	11.09	8.42cm^3	2.32g/cm^3	Melhorn
					2.33g/cm^3	
27	Acid Tuff	29.89g	15.30g	14.55cm^3	2.05g/cm^3	Melhorn
28	Silicified Pumice or Scooiaecous Rhyolite	19.44g	10.33g	9.11cm^3	2.13g/cm^3	Melhorn
29	Gabbro	76.92g	51.11g	25.81cm^3	2.98g/cm^3	Austushorn
30	Granophyre	42.73g	26.17g	16.56cm^3	2.58g/cm^3	Austushorn
31	Granophyre	37.05g	23.04g	14.01cm^3	2.64g/cm^3	Austushorn
32	Gabbro	49.95g	31.71g	18.24cm^3	2.74g/cm^3	Austushorn

Locations can not be given a grid refence as there is too little information to locate them accurately

Appendix 4. Regional Gravity readings around the Breiddalur area eastern Iceland from Porbergesson et al. 1990.

Loc. = Location code of gravity station
Grid Ref. = Grid reference on U.S. Army Map of Iceland.
BA = Bouguer anomaly in milligals

Loc.	Latitude	Longitude	Grid Ref.	BA
7585	64°51.41'	14°44.41'	123 927	6.2
7586	64°49.34'	14°48.46'	091 888	9.7
7587	64°45.41'	14°56.56'	028 815	5.8
7588	64°41.84'	14°47.53'	098 749	11.1
7589	64°44.74'	14°41.15'	149 803	10.8
7590	64°54.82'	14°52.39'	060 990	11.4
7591	64°55.59'	14°35.87'	190 005	11.1
7592	64°46.66'	14°45.37'	115 838	10.4
7593	64°48.36'	14°33.37'	210 870	6.1
7594	64°46.42'	14°25.24'	275 835	12.6
7600	64°36.48'	14°26.17'	270 652	20.8
7601	64°39.32'	14°16.56'	354 704	21.5
7602	64°42.28'	14°04.64'	439 760	17.8
7603	64°42.16'	14°30.08'	237 755	11.7
7604	64°41.27'	14°21.12'	309 740	18.5
7609	64°52.94'	14°42.53'	138 955	5.1
7610	64°51.99'	14°29.46'	241 938	11.0
7611	64°57.46'	14°19.42'	319 040	13.8
7612	64°54.27'	14°12.70'	372 982	14.1
7613	64°50.55'	14°04.09'	441 914	17.9
7614	64°48.32'	14°17.41'	337 871	17.5
7615	64°58.18'	14°03.38'	445 055	15.3

Appendix 5. Gravity readings in the Breiddalur area eastern Iceland.

Loc. = Location code of gravity station

Grid Ref. = Grid reference on U.S. Army Map of Iceland

g obs. = Gravity in milligals relative to Breiddalsvik base station

g ϕ = Correction for latitude relative to base station in milligals

FAC = Free air correction in milligals

BC = Bouguer correction in milligals

TC = Terrain correction in milligals

BA = Bouguer anomaly in milligals

Reg. = Regional anomaly for Iceland in milligals

A = Anomaly left after adding regional anomaly to bouguer anomaly

Density used in calculations 2.6 g/cm^3

Loc.	Grid Ref.	g obs.	g ϕ	FAC	BC	TC	BA	Reg.	A
Base	469 858	0.000	0.000	0.000	0.000	+1.981	+1.981	-18.0	-16.0
S23	285 899	-17.691	-2.68	+34.100	-12.040	+6.064	+7.753	-13.9	-6.1
S22	289 896	-14.399	-2.53	+30.459	-10.754	+5.110	+7.886	-14.2	-6.3
S21	294 893	-14.233	-2.335	+32.002	-11.299	+4.408	+8.543	-14.5	-6.0
S20	300 890	-12.807	-2.19	+30.058	-10.613	+3.942	+8.390	-14.9	-6.5
S19	304 887	-10.669	-1.955	+26.632	-9.403	+4.813	+9.418	-15.2	-5.8
S18	309 887	-10.739	-1.95	+27.188	-9.599	+3.690	+8.590	-15.5	-6.9
S17	313 885	-11.464	-1.83	+28.885	-10.197	+3.502	+8.896	-15.9	-7.0
S16	316 884	-10.982	-1.80	+28.515	-10.068	+3.361	+9.026	-16.0	-7.0
S15	321 881	-9.307	-1.60	+26.910	-9.501	+3.476	+9.978	-16.4	-6.4
S14	324 880	-9.58	-1.55	+26.601	-9.392	+3.805	+9.884	-16.6	-6.7

Loc.	Grid Ref.	g obs.	$g\phi$	FAC	BC	TC	BA	Reg.	A
S13	327 878	-13.703	-1.40	+22.682	-8.009	+4.863	+4.433	-16.9	-12.5
S12	331 878	-12.945	-1.38	+22.651	-7.998	+4.442	+4.770	-17.0	-12.2
S11	335 877	-11.150	-1.32	+20.800	-7.344	+4.549	+5.535	-17.2	-11.7
S10	340 875	-9.890	-1.23	+18.609	-6.570	+4.660	+5.579	-17.4	-11.8
S09	344 877	-10.057	-1.35	+19.658	-6.941	+3.326	+4.636	-17.5	-12.9
S08	349 875	-7.436	-1.23	+16.418	-5.797	+3.791	+5.746	-17.6	-11.9
S07	354 873	-9.086	-1.09	+19.257	-6.799	+3.473	+5.755	-17.6	-11.8
S06	359 870	-8.809	-0.88	+17.899	-6.320	+3.809	+5.699	-17.6	-11.9
S05	362 867	-9.037	-0.64	+16.757	-5.917	+5.348	+6.511	-17.6	-11.1
S04	366 865	-8.956	-0.53	+16.047	-5.666	+4.996	+5.891	-17.6	-11.7
S03	369 863	-7.937	-0.39	+15.183	-5.361	+5.055	+6.550	-17.6	-11.0
S02	374 867	-3.984	-0.64	+11.974	-4.228	+2.141	+5.263	-17.6	-12.3
S01	375 862	error							
N001	372 892	-4.711	-2.25	+12.838	-4.533	+2.951	+4.295	-17.6	-13.3
N002	364 892	-3.446	-2.25	+16.016	-5.655	+2.934	+7.599	-17.3	-9.7
N003	358 895	-4.999	-2.45	+17.806	-6.287	+3.541	+7.611	-17.0	-9.4
N004	348 897	-5.328	-2.54	+17.066	-6.025	+3.892	+7.065	-16.7	-9.6
N005	337 899	-6.122	-2.71	+20.522	-7.246	+4.923	+9.367	-16.3	-6.9
N006	327 901	-9.845	-2.825	+18.454	-6.516	+5.152	+4.420	-15.9	-11.5
N007	316 903	-9.968	-2.98	+22.713	-8.019	+5.783	+7.529	-15.3	-7.8
N008	305 905	-8.555	-3.07	+25.922	-9.153	+3.387	+8.531	-14.9	-6.4
N009	296 906	-9.938	-3.13	+27.095	-9.567	+2.975	+7.435	-14.5	-7.1
N010	288 913	-12.850	-3.61	+29.687	-10.482	+2.973	+5.718	-13.9	-8.2
N011	282 924	-15.276	-4.20	+33.483	-11.822	+3.240	+5.425	-13.1	-7.7

Loc.	Grid Ref.	g obs.	g ∅	FAC	BC	TC	BA	Reg.	A
N012	275 934	-18.123	-4.905	+40.334	-14.241	+3.613	+6.678	-12.5	-5.8
N013	266 944	-19.440	-5.56	+39.686	-14.012	+4.727	+5.401	-11.7	-6.3
N014	262 948	-18.943	-5.795	+39.840	-14.067	+5.485	+6.520	-11.5	-5.0
V001	263 952	-29.174	-6.02	+54.406	-19.210	+6.357	+6.359	-11.6	-5.2
V002	265 954	-40.931	-6.16	+74.157	-26.183	+6.829	+7.712	-11.6	-3.9
V003	266 957	-55.503	-6.34	+95.141	-33.592	+6.699	+6.405	-11.7	-5.3
V004	266 959	-66.321	-6.49	+113.503	-40.075	+7.307	+7.924	-11.7	-3.8
VS001	261 941	-14.073	-5.35	+31.848	-11.245	+4.620	+5.800	-11.6	-5.8
VS002	254 934	-22.462	-4.93	+43.266	-15.276	+5.093	+5.691	-11.6	-5.9
VS003	253 933	-29.367	-4.85	+52.678	-18.599	+5.314	+5.176	-11.6	-6.4
VS004	251 931	-43.647	-3.61	+72.398	-25.562	+5.218	+4.797	-11.6	-6.8
N015	256 953	-18.139	-6.09	+39.778	-14.045	+6.013	+7.517	-11.5	-4.0
N016	250 955	-18.186	-6.23	+37.341	-13.184	+6.179	+5.920	-11.4	-5.5
N017	247 957	-18.081	-6.375	+39.840	-14.067	+6.274	+7.591	-11.4	-3.8
N018	238 963	-20.131	-6.76	+41.229	-14.557	+7.249	+7.030	-11.3	-4.3
N019	221 972	-24.408	-7.30	+43.173	-15.243	+8.127	+4.349	-11.1	-6.8
N020	212 964	-30.036	-6.79	+48.851	-17.248	+6.005	+0.782	-10.5	-9.7
N021	204 964	-46.000	-6.84	+69.805	-24.647	+5.450	-2.232	-9.9	-12.1
N022	198 967	-60.405	-7.01	+88.229	-31.152	+6.231	-4.107	-9.7	-13.8
SS05	197 972	error							
SS04	194 975	-86.969	-7.54	+131.155	-46.308	+6.001	-3.661	-9.9	-13.6
SS02	193 977	-89.947	-7.67	+134.241	-47.398	+2.949	-7.825	-9.9	-17.7
SS01	191 979	-89.096	-7.83	+135.784	-47.942	+2.627	-6.457	-9.9	-16.4
Oxi1	169 976	-65.851	-7.625	+92.950	-32.819	+3.175	-10.170	-8.2	-18.4
Oxi2	166 968	-70.283	-7.07	+95.666	-33.778	+3.427	-12.038	-7.6	-19.6

Loc.	Grid Ref.	g obs.	$g\phi$	FAC	BC	TC	BA	Reg.	A
Oxi3	159 953	-81.999	-6.16	+108.689	-38.376	+2.534	-15.312	-6.4	-21.7
Oxi4	155 940	-93.458	-5.35	+134.982	-47.659	+1.838	-9.647	-5.3	-15.0
Oxi5	155 924	-102.801	-4.38	+146.554	-51.745	+1.685	-10.687	-5.5	-16.2
Oxi6	154 914	-107.174	-3.78	+153.899	-54.338	+1.333	-10.060	-6.0	-16.1
Oxi7	157 899	-112.243	-2.85	+162.756	-57.466	+0.972	-8.831	-6.6	-15.4
Oxi8	162 892	-108.424	-2.31	+161.058	-56.866	+1.169	-5.373	-6.8	-12.2
Oda1	131 909	-127.624	-3.44	+187.320	-66.139	+0.497	-9.386	-7.0	-16.4
Oda2	139 906	-134.383	-3.22	+196.825	-69.495	+0.880	-9.393	-6.9	-16.3
Oda3	145 898	-131.739	-2.71	+193.832	-68.438	+0.926	-8.129	-7.0	-15.1
Oxi9	167 883	-90.440	-1.77	+132.513	-46.787	+1.988	-4.496	-7.0	-11.5
Oxi10	171 878	-88.426	-1.46	+127.884	-45.153	+2.309	-4.846	-7.1	-11.9
Oxi11	178 880	-86.116	-1.58	+124.582	-43.987	+3.694	-3.407	-6.8	-10.2
Oxi12	185 879	-76.817	-1.49	+108.164	-38.190	+5.219	-3.114	-6.6	-9.7
Oxi13	193 872	-47.180	-1.10	+53.882	-19.024	+8.171	-5.251	-6.6	-11.9
Oxi14	197 875	-46.384	-1.23	+52.215	-18.436	+9.356	-4.479	-6.4	-10.9
Oxi15	206 869	-32.469	-0.88	+29.595	-10.449	+7.887	-6.316	-6.2	-12.5
Oxi16	216 864	-22.758	-0.555	+13.702	-4.838	+7.395	-7.054	-6.9	-14.0
LJBASE	221 863	-21.004	-0.50	+11.418	-4.032	+6.899	-7.219	-7.3	-14.5
Skali13	225 859	-16.494	-0.27	+4.876	-1.722	+7.056	-6.554	-7.7	-14.3
Skali12	229 856	-9.918	-0.07	+3.209	-1.133	+7.145	-0.807	-8.1	-8.9
Skali11	234 856	-14.000	+0.05	+2.006	-0.708	+6.145	-6.507	-8.6	-15.1
Skali10	244 860	-16.331	-0.36	+10.215	-3.607	+6.162	-3.921	-9.7	-13.6
= LJ 20									
Skali9	258 860	-18.503	-0.33	+14.041	-4.958	+5.549	-4.201	-11.2	-15.4
Skali7	259 852	-8.133	+0.20	+0.000	-0.000	+5.587	-2.346	-11.2	-13.5

Loc.	Grid Ref.	g obs.	g ϕ	FAC	BC	TC	BA	Reg.	A
Skali6	266 846	-10.028	+1.72	+6.234	-2.201	+5.369	+1.094	-11.8	-10.7
Skali5	270 835	-12.690	+1.27	+9.505	-3.356	+3.778	-1.493	-12.1	-13.6
Skali4	276 831	-11.251	+1.55	+9.505	-3.356	+3.798	+0.246	-12.8	-12.6
Skali3	284 825	-10.824	+1.92	+8.641	-3.051	+4.417	+1.103	-13.8	-12.7
Skali2	288 818	-11.738	+2.32	+9.042	-3.193	+3.939	+0.370	-14.3	-13.9
Skali1 =									
SW1	293 815	-9.925	+2.56	+5.277	-1.863	+4.410	+0.867	-14.9	-14.0
SW2	308 791	-4.913	+4.06	+1.327	-0.469	+3.362	+3.367	-17.0	-13.6
SW3	321 766	-6.956	+5.63	+5.771	-2.038	+2.646	+5.053	-18.3	-13.2
SW4	338 755	-7.161	+6.32	+8.147	-2.877	+2.603	+7.032	-18.3	-11.3
SW5	372 749	-5.162	+6.73	+3.827	-1.351	+3.931	+7.975	-18.2	-10.2
SW6	393 754	-8.631	+6.41	+4.629	-1.634	+6.195	+6.969	-18.1	-11.1
SW7	428 763	-16.008	+5.89	+12.282	-4.337	+5.545	+3.372	-17.8	-14.4
SW8	461 778	-5.872	+4.96	+5.030	-1.776	+2.422	+4.764	-18.0	-13.2
SW9	469 806	-1.055	+3.26	+1.636	-0.577	+2.259	+5.523	-18.0	-12.5
SW10	444 825	-3.813	+2.03	+4.752	-1.678	+3.047	+4.338	-18.0	-13.7
SW11	411 840	-6.363	+1.07	+11.449	-4.042	+2.283	+4.397	-18.0	-13.6
SW12	409 866	-3.959	-0.58	+10.276	-3.628	+1.438	+3.547	-18.0	-14.5
SW13	429 870	-4.122	-0.82	+10.122	-3.574	+1.703	+3.309	-18.0	-14.7
LJ1	226 866	error							
LJ2	228 869	-31.277	-0.88	+27.342	-9.654	+8.462	-6.007	-8.1	-14.1
LJ3	229 871	-45.000	-1.025	+49.129	-17.347	+8.580	-5.663	-8.2	-13.9
LJ4	230 874	-65.222	-1.23	+81.378	-28.733	+7.440	-6.367	-8.4	-14.8
LJ5	231 877	-79.141	-1.41	+104.029	-36.731	+7.915	-5.338	-8.5	-13.8
LJ6	234 878	-97.111	-1.46	+130.106	-45.939	+8.225	-6.179	-9.0	-15.2

Loc.	Grid Ref.	g obs.	g ϕ	FAC	BC	TC	BA	Reg.	A
LJ7	234 881	-106.154	-1.63	+144.980	-51.191	+8.785	-5.210	-9.0	-14.2
LJ8	233 883	-114.815	-1.72	+158.404	-55.931	+9.021	-5.041	-9.0	-14.0
LJ9	234 886	-131.510	-1.93	+183.216	-64.691	+8.301	-6.614	-9.1	-15.7
LJ10	237 885	-139.115	-1.89	+193.955	-68.483	+7.847	-7.686	-9.4	-17.1
LJ11	239 883	-136.177	-1.77	+189.851	-67.034	+9.058	-6.072	-9.6	-15.7
LJ12	239 880	-106.011	-1.58	+146.276	-51.648	+7.391	-5.572	-9.6	-15.2
LJ13	241 878	-91.278	-1.41	+125.600	-44.348	+7.283	-4.153	-9.8	-14.0
LJ14	243 875	-81.708	-1.23	+112.701	-39.793	+6.270	-3.760	-9.9	-13.7
LJ15	242 873	-74.263	-1.14	+100.789	-35.587	+6.899	-4.302	-9.8	-14.1
LJ16	243 871	-66.444	-1.00	+87.735	-30.978	+7.241	-3.446	-9.8	-13.2
LJ17	244 869	-50.133	-0.94	+62.306	-22.000	+6.732	-4.035	-9.9	-13.9
LJ18	244 867	-41.726	-0.765	+49.407	-17.445	+7.780	-2.749	-9.9	-12.6
LJ19	243 864	-24.881	-0.53	+23.268	-8.216	+6.143	-4.216	-9.6	-13.8

Loc. = Location code of gravity station
Grid Ref. = Grid reference on U.S. Army Map of Iceland
g obs. = Gravity in milligals relative to Breiddalsvik base station
g ϕ = Correction for latitude relative to base station in milligals
FAC = Free air correction in milligals
BC = Bouguer correction in milligals
TC = Terrain correction in milligals
BA = Bouguer anomaly in milligals
Reg. = Regional anomaly for Iceland in milligals
A = Anomaly left after adding regional anomaly to bouguer anomaly
Density used in calculations 2.6 g/cm^3

Appendix 6. Heights and latitudes of gravity stations, Breiddalur area.

Loc.	Grid Ref.	Height	Latitude	A-D (TC)	M (TC)	TC
Base	469 858	+0.0 m	64°47.5¼'	0.000	0.075	1.981
S23	285 899	+110.5 m	64°49.8¼'	0.173	0.174	6.064
S22	289 896	+98.7 m	64°49.7'	0.000	0.173	5.110
S21	294 893	+103.7 m	64°49.5¼'	0.000	0.170	4.408
S20	300 890	+97.4 m	64°49.4'	0.003	0.169	3.942
S19	304 887	+86.3 m	64°49.2'	0.000	0.168	4.813
S18	309 887	+88.1 m	64°49.2'	0.038	0.177	3.690
S17	313 885	+93.6 m	64°49.1'	0.052	0.186	3.502
S16	316 884	+92.4 m	64°49.0¾'	0.007	0.185	3.361
S15	321 881	+87.2 m	64°48.9'	0.000	0.182	3.476
S14	324 880	+86.2 m	64°48.8½'	0.007	0.191	3.805
S13	327 878	+73.5 m	64°48.7¼'	0.017	0.199	4.863
S12	331 878	+73.4 m	64°48.7'	0.020	0.208	4.442
S11	335 877	+67.4 m	64°48.6½'	0.000	0.217	4.549
S10	340 875	+60.3 m	64°48.5¾'	0.003	0.216	4.660
S09	344 877	+63.7 m	64°48.6¾'	0.013	0.217	3.326
S08	349 875	+53.2 m	64°48.5¼'	0.000	0.218	3.791
S07	354 873	+62.4 m	64°48.4½'	0.062	0.215	3.473
S06	359 870	+58.0 m	64°48.2¾'	0.078	0.200	3.809
S05	362 867	+54.3 m	64°48.0¾'	0.118	0.186	5.348
S04	366 865	+52.0 m	64°47.9¾'	0.163	0.179	4.996
S03	369 863	+49.2 m	64°47.8½'	0.082	0.173	5.055
S02	374 867	+38.8 m	64°48.0¾'	0.000	0.198	2.141

Loc.	Grid Ref.	Height	Latitude	A-D (TC)	M (TC)	TC
S01	375 862	error				
N001	372 892	+41.6 m	64°49.4½'	0.000	0.205	2.951
N002	364 892	+51.9 m	64°49.4½'	0.231	0.208	2.934
N003	358 895	+57.7 m	64°49.6½'	0.182	0.211	3.541
N004	348 897	+55.3 m	64°49.7'	0.205	0.213	3.892
N005	337 899	+66.5 m	64°49.8½'	0.413	0.216	4.923
N006	327 901	+59.8 m	64°49.9½'	0.380	0.209	5.152
N007	316 903	+73.6 m	64°50.0¾'	0.316	0.203	5.783
N008	305 905	+84.0 m	64°50.1½'	0.020	0.195	3.387
N009	296 906	+87.8 m	64°50.2'	0.026	0.189	2.975
N010	288 913	+96.2 m	64°50.6'	0.007	0.198	2.973
N011	282 924	+108.5 m	64°51.2½'	0.007	0.207	3.240
N012	275 934	+130.7 m	64°51.7½'	0.007	0.216	3.613
N013	266 944	+128.6 m	64°52.3'	0.004	0.228	4.727
N014	262 948	+129.1 m	64°52.5'	0.001	0.235	5.485
V001	263 952	+176.3 m	64°52.7'	0.491	0.138	6.357
V002	265 954	+240.3 m	64°52.8½'	0.468	0.125	6.829
V003	266 957	+308.3 m	64°52.9¾'	0.268	0.114	6.699
V004	266 959	+367.8 m	64°53.1'	0.364	0.104	7.307
VS001	261 941	+103.2 m	64°52.1½'	0.000	0.239	4.620
VS002	254 934	+140.2 m	64°51.7½'	0.075	0.192	5.093
VS003	253 933	+170.7 m	64°51.6¾'	0.722	0.169	5.314
VS004	251 931	+234.6 m	64°51.6'	1.040	0.138	5.218
N015	256 953	+128.9 m	64°52.7½'	0.007	0.234	6.013
N016	250 955	+121.0 m	64°52.8¾'	0.007	0.231	6.179

Loc.	Grid Ref.	Height	Latitude	A-D (TC)	M (TC)	TC
N017	247 957	+129.1 m	64°53.0'	0.121	0.246	6.274
N018	238 936	+133.6 m	64°53.3½'	0.260	0.260	7.249
N019	221 972	+139.9 m	64°53.8'	0.164	0.274	8.127
N020	212 964	+158.3 m	64°53.3½'	0.092	0.289	6.005
N021	204 964	+226.2 m	64°53.4'	0.116	0.202	5.450
N022	198 967	+285.9 m	64°53.5½'	0.624	0.152	6.231
SS05	197 972	error				
SS04	194 975	+425 m	64°54.0'	2.213	0.107	6.001
SS02	193 977	+435 m	64°54.1½'	0.035	0.099	2.949
SS01	191 979	+440 m	64°54.2½'	0.017	0.091	2.627
Oxi1	169 976	+301.2 m	64°54.0¾'	0.018	0.133	3.175
Oxi2	166 968	+310.0 m	64°53.6'	0.022	0.137	3.427
Oxi3	159 953	+352.2 m	64°52.8½'	0.013	0.098	2.534
Oxi4	155 940	+437.4 m	64°52.1½'	0.003	0.086	1.838
Oxi5	155 924	+474.9 m	64°51.2¾'	0.000	0.114	1.685
Oxi6	154 914	+498.7 m	64°50.7½'	0.000	0.094	1.333
Oxi7	157 899	+527.4 m	64°49.9¾'	0.018	0.091	0.972
Oxi8	162 892	+521.9 m	64°49.5'	0.029	0.091	1.169
Oda1	131 909	+607.0 m	64°50.4½'	0.007	0.085	0.497
Oda2	139 906	+637.8 m	64°50.2¾'	0.000	0.107	0.880
Oda3	145 898	+628.1 m	64°49.8¾'	0.018	0.094	0.926
Oxi9	167 883	+429.4 m	64°49.0½'	0.043	0.130	1.988
Oxi10	171 878	+414.4 m	64°48.7¾'	0.068	0.130	2.309
Oxi11	178 880	+403.7 m	64°48.8¾'	0.074	0.124	3.694
Oxi12	185 879	+350.5 m	64°48.8'	0.107	0.157	5.219

Loc.	Grid Ref.	Height	Latitude	A-D (TC)	M (TC)	TC
Oxi13	193 872	+174.6 m	64°48.4½'	0.277	0.257	8.171
Oxi14	197 875	+169.2 m	64°48.5¾'	0.231	0.257	9.356
Oxi15	206 869	+95.9 m	64°48.2¾'	0.075	0.308	7.887
Oxi16	216 864	+44.4 m	64°48.0'	0.018	0.364	7.395
LJBASE	221 863	+37.0 m	64°47.9½'	0.000	0.343	6.899
Skali13	225 859	+15.8 m	64°47.7½'	0.000	0.367	7.056
Skali12	229 856	+10.4 m	64°47.5¾'	0.013	0.368	7.145
Skali11	234 856	+6.5 m	64°47.4¾'	0.047	0.368	6.145
Skali10	244 860	+33.1 m	64°47.8¼'	0.111	0.322	6.162
= LJ 20						
Skali9	258 860	+45.5 m	64°47.8'	0.064	0.307	5.549
Skali7	259 852	0.0 m	64°47.3½'	0.068	0.332	5.587
Skali6	266 846	+20.2 m	64°46.0½'	0.183	0.307	5.369
Skali5	270 835	+30.8 m	64°46.4½'	0.092	0.282	3.778
Skali4	276 831	+30.8 m	64°46.2'	0.103	0.298	3.798
Skali3	284 825	+28.0 m	64°45.8¾'	0.124	0.298	4.417
Skali2	288 818	+29.3 m	64°45.5¼'	0.009	0.272	3.939
Skali1 =						
SW1	293 815	+17.1 m	64°45.3¼'	0.027	0.228	4.410
SW2	308 791	+4.3 m	64°44.0½'	0.001	0.208	3.362
SW3	321 766	+18.7 m	64°42.7'	0.000	0.155	2.646
SW4	338 755	+26.4 m	64°42.1'	0.007	0.116	2.603
SW5	372 749	+12.4 m	64°41.7½'	0.000	0.088	3.931
SW6	393 754	+15.0 m	64°42.0¼'	0.007	0.095	6.195
SW7	428 763	+39.8 m	64°42.4¾'	0.035	0.073	5.545

Loc.	Grid Ref.	Height	Latitude	A-D (TC)	M (TC)	TC
SW8	461 778	+16.3 m	64°43.2¾'	0.000	0.059	2.422
SW9	469 806	+5.3 m	64°44.7½'	0.026	0.048	2.259
SW10	444 825	+15.4 m	64°45.7¾'	0.004	0.070	3.047
SW11	411 840	+37.1 m	64°46.6½'	0.000	0.101	2.283
SW12	409 866	+33.3 m	64°48.0½'	0.001	0.204	1.438
SW13	429 870	+32.8 m	64°48.2½'	0.013	0.148	1.703
LJ1	226 866	error				
LJ2	228 869	+88.6 m	64°48.2¾'	0.501	0.286	8.462
LJ3	229 871	+159.2 m	64°48.4'	1.166	0.229	8.580
LJ4	230 874	+263.7 m	64°48.5¾'	0.952	0.166	7.440
LJ5	231 877	+337.1 m	64°48.7½'	1.307	0.129	7.915
LJ6	234 878	+421.6 m	64°48.7¾'	2.412	0.130	8.225
LJ7	234 881	+469.8 m	64°48.9½'	2.726	0.103	8.785
LJ8	233 883	+513.3 m	64°49.0'	2.577	0.092	9.021
LJ9	234 886	+593.7 m	64°49.1¾'	1.846	0.100	8.301
LJ10	237 885	+628.5 m	64°49.1½'	0.735	0.100	7.847
LJ11	239 883	+615.2 m	64°49.0½'	1.297	0.100	9.058
LJ12	239 880	+474.0 m	64°48.8¾'	1.164	0.108	7.391
LJ13	241 878	+407.0 m	64°48.7½'	0.735	0.116	7.283
LJ14	243 875	+365.2 m	64°48.5¾'	0.358	0.116	6.270
LJ15	242 873	+326.6 m	64°48.5'	0.358	0.140	6.899
LJ16	243 871	+284.3 m	64°48.3¾'	1.248	0.140	7.241
LJ17	244 869	+201.9 m	64°48.3½'	0.446	0.194	6.732
LJ18	244 867	+160.1 m	64°48.1¾'	1.755	0.194	7.780
LJ19	243 864	+75.4 m	64°47.9¾'	0.231	0.260	6.143